Doctoral theses at NTNU, 2020:405

Håkon J. D. Johnsen

New Approaches to Solar Tracking and Concentration through Numerical Optimization of Lens Arrays

Doctoral thesis

NTNU
Norwegian University of Science and Technology
Thesis for the Degree of Philosophiae Doctor
Faculty of Engineering
Department of Mechanical and Industrial Engineering

NTNU
Norwegian University of Science and Technology

Håkon J. D. Johnsen

New Approaches to Solar Tracking and Concentration through Numerical Optimization of Lens Arrays

Thesis for the Degree of Philosophiae Doctor

Trondheim, December 2020

Norwegian University of Science and Technology
Faculty of Engineering
Department of Mechanical and Industrial Engineering

NTNU
Norwegian University of
Science and Technology

NTNU
Norwegian University of Science and Technology

Thesis for the Degree of Philosophiae Doctor

Faculty of Engineering
Department of Mechanical and Industrial Engineering

ISBN 978-82-471-9743-1 (printed ver.)
ISBN 978-82-471-9791-2 (electronic ver.)
ISSN 1503-8181 (printed ver.)
ISSN 2703-8084 (online ver.)

Doctoral theses at NTNU, 2020:405

Printed by NTNU Grafisk senter

Abstract

Solar concentrators are essential for enabling several solar energy applications, including high-efficiency photovoltaic conversion and high-temperature solar thermal energy. These concentrators require accurate solar tracking, commonly performed by rotating them towards the sun, which adds to the bulk and complexity of the system.

In this thesis, we investigate optically tracking the sun using millimeter-scale translation instead of rotating the complete concentrator — a concept known as tracking integration. We show how the performance of these systems can be pushed beyond the current state of the art through a broad exploration of the design space using a custom sequential ray-tracer in combination with memetic multi-objective optimization algorithms.

We explore two classes of tracking integration: beam-steering lens arrays that consist of an afocal stack of lens arrays, and microtracking concentrators that concentrate sunlight to an array of discrete focal spots where micro-PV cells can convert the solar energy to electricity. Further, we propose possible étendue-squeezing solar concentrator designs that may benefit from tracking integration.

First, we perform a broad exploration of beam-steering lens array configurations for full-day stationary solar tracking. We identify several promising configurations, including one capable of redirecting sunlight into a $< 2^\circ$ divergence half-angle with a 73.4% average yearly efficiency. Second, we identify two microtracking configurations that achieve $> 2000x$ concentration ratio at a two-axis $\pm 60^\circ$tracking range. Finally, we demonstrate a line-focus concentrator with a simulated effective concentration ratio of $218x$ at a $\pm 1^\circ$ acceptance angle that employs étendue squeezing to go beyond the conventional two-dimensional concentration limit. To the best of our knowledge, this is the first demonstration of how a line-focus concentrator can be directly designed as a three-dimensional concentrator to operate beyond the 2D limit (which is $57x$ at the $\pm 1^\circ$ acceptance angle). This concentrator, combined with beam-steering lens arrays, may enable the development of a new class of high-concentration trough-like solar concentrators.

This thesis demonstrates how numerical optimization can be utilized to explore a large design space, develop new concepts for solar tracking and concentration, and contribute to the development of new applications for concentrated sunlight. The method and the obtained results may contribute to the development of low-cost solar tracking and concentration. The optimization problem formulation and optimization algorithms, in general, may also unlock solutions to other yet unexplored problems in nonimaging optics.

Acknowledgements

It is the middle of May 2017. I am in the 4th year of my mechanical engineering studies and the semester is coming to an end. As I wrap up the work for a course, I stumble across a paper — "Wide-angle planar microtracking for quasi-static microcell concentrating photovoltaics" by Jared S. Price and co-authors [5]. The field is unfamiliar, but the well-written paper completely captures my imagination, and I realize that THIS would be interesting to work on! Fast-forward half a year, and this field has become the topic of my Master's thesis and eventually this PhD thesis. I am grateful to all the people who contributed to making this exciting and unexpected journey a reality!

I especially want to thank my supervisor Jan Torgersen for believing in my work and giving me the freedom to pursue this research direction based on my interests and passion. Thank you for doing all the work behind the scenes to make this possible! I also want to thank my co-supervisor, Astrid Aksnes, for being exceptionally helpful and kind. Thank you for always finding time to give feedback despite your busy schedule, and thank you for all your advice — both PhD related and about life in general. Additionally, I want to thank professor Ole Jørgen Nydal for co-supervising the Master's thesis that sparked this research. Thank you for listening to all my wild plans and agreeing to work with me on it!

I appreciate my colleagues at the department for all the time we had together over these three years. With you, being at the office was always a good experience, no matter how deep we all were into our work. I am especially thankful to Gaute Fotland for all the countless deep conversations over coffee on dark winter mornings in our office. Thank you for sharing your wisdom, and for all your efforts to make office life more engaging for all of us!

I want to thank all my good friends in the city for making this such a nice place to live all these years! I am especially thankful to Marie Stavdahl, Åsmund Stavdahl, Ingvild Furnes Lauvås, Nikolai Lauvås, and Oline Lauvås. Thank you for always welcoming me and finding the right balance between giving

me room to work and telling me that it's about time I leave university and join you for dinner!

I am deeply thankful to my family for giving me a safe and nourishing childhood, both in Voss and in Oslo. Hilde, thank you for always finding time for me when I visit. I admire your integrity and your values! Mum, thank you for all your support and encouragement, and for showing that my worth does not rest on any academic achievements. Dad, thank you for sparking my interests in technology, engineering, and computer programming, and for all the deep and good conversations!

Contributions

The work in this thesis was carried out at the Department of Mechanical and Industrial Engineering at NTNU in Trondheim, Norway. The work was supervised by Associate Professor Jan Torgersen and co-supervised by Professor Astrid Aksnes.

The work was carried as part of the Micro and Nanoscale Design group, and was internally financed by the university. Additionally, some work was done in the NorFab cleanrooms. The Research Council of Norway is acknowledged for the support to the Norwegian Micro- and Nano-Fabrication Facility, NorFab, project number 295864.

Publications

The following set of publications constitute this thesis:

Paper 1

H. J. D. Johnsen, J. Torgersen, and A. Aksnes, "Solar tracking using beam-steering lens arrays," in Nonimaging Optics: Efficient Design for Illumination and Solar Concentration XV, 2018.

H.J.D.J. initiated the research into beam-steering lens arrays, developed the sequential ray-tracer, created the phase-space visualizations and optimization method, performed numerical simulations, analyzed the results, and prepared the original draft. J.T. and A.A. supervised the work, reviewed manuscript drafts and contributed to the revision of the paper. The physical proof-of-concept reported in Section 5 of the paper was developed as part of H.J.D.J.'s Master's thesis.

Paper 2

H. J. D. Johnsen, J. Torgersen, and A. Aksnes, "High-concentration wide-angle tracking integration with stacked lens arrays," in 15th International Conference on Concentrator Photovoltaic Systems (CPV-15), 2019.

H.J.D.J. proposed optimizing more advanced microtracking configurations, formulated the optimization problem, performed optimization and simulations, analyzed the results, and prepared the original draft. J.T. and A.A. supervised the work, reviewed manuscript drafts and contributed to the revision of the paper.

Paper 3

H. J. D. Johnsen, A. Aksnes, and J. Torgersen, "Pushing the limits of beam-steering lens arrays," in Nonimaging Optics: Efficient Design for Illumination and Solar Concentration XVI, 2019.

H.J.D.J. initiated the use of multi-objective optimization for beam-steering lens arrays, formulated the optimization problem, performed numerical simulations, analyzed the results, and prepared the original draft. J.T. and A.A. supervised the work, reviewed manuscript drafts and contributed to the revision of the paper.

Paper 4

H. J. D. Johnsen, A. Aksnes, and J. Torgersen, "High-performance stationary solar tracking through multi-objective optimization of beam-steering lens arrays", in Optics Express, 2020.

H.J.D.J. proposed the broad exploration of beam-steering lens array configurations, developed the approach for incorporating manufacturing tolerances in the optimization, performed the large-scale numerical optimization, analyzed the results, and prepared the original manuscript draft. J.T. and A.A. supervised the work, reviewed manuscript drafts and contributed to the revision of the paper.

Paper 5

H. J. D. Johnsen, A. Aksnes, and J. Torgersen, "Beyond the 2D limit: Étendue-squeezing line-focus solar concentrators", in Optics Letters, doc. ID 406280, posted 17 November 2020, in press.

H.J.D.J. proposed the use of étendue-squeezing for line-focus solar concentrators, conceptualized the two design examples, performed numerical optimization, analyzed the results, and prepared the original manuscript draft. J.T. and A.A. supervised the work, reviewed manuscript drafts and contributed to the revision of the paper.

Other dissemination

In addition to the papers listed above, the work was disseminated in the following ways:

- H. J. D. Johnsen, A. Aksnes, and J. Torgersen, "Beam-steering lens arrays and ètendue-squeezing: a pathway towards a new class of solar concentrators?," SPIE Optics + Photonics 2020, 2020. **(Presentation. Recording, Slides)**
- H. J. D. Johnsen, A. Aksnes, and J. Torgersen, "Pushing the limits of beam-steering lens arrays," SPIE Optics + Photonics 2019, 2019. **(Presentation. Recording, Slides)**
- H. J. D. Johnsen, J. Torgersen, and A. Aksnes, "Design and fabrication of beam steering lens arrays through raytracing and maskless grayscale lithography," 10th Annual Workshop of the Norwegian PhD Network on Nanotechnology for Microsystems, 2019. (**Presentation**)
- H. J. D. Johnsen, A. Aksnes, and J. Torgersen, "High-Concentration Wide-Angle Tracking Integration with Stacked Lens Arrays," The 15th International Conference on Concentrator Photovoltaics (CPV-15), 2019. **(Presentation. Slides)**

- H. J. D. Johnsen, J. Torgersen, and A. Aksnes, "Tracking-Integrated Solar Energy Using Stacked Lens Arrays," Norwegian Solar Cell Conference (NSCC) 2019, 2019. **(Poster)**
- H. J. D. Johnsen, J. Torgersen, and A. Aksnes, "Beam-steering lens arrays for solar tracking," First NTNU Young Researcher Clean Energy Symposium, 2019. **(Presentation)**
- H. J. D. Johnsen, J. Torgersen, and A. Aksnes, "Beam-steering lens arrays for solar tracking," NTNU Nano Symposium 2018, 2018. **(Presentation)**
- H. J. D. Johnsen, J. Torgersen, and A. Aksnes, "Solar tracking using beam-steering lens arrays," SPIE Optics + Photonics 2018, 2018. **(Presentation. Recording)**
- H. J. D. Johnsen, "Interview: Håkon J. Dugstad Johnsen – Beam steering lens array for solar cooking," SunPod podcast, 2018. **(Podcast Interview)**
- H. J. D. Johnsen, J. Torgersen, and O. J. Nydal, "Beam Steering Lens Array for Solar Cooking," The 10th International SolarZentrum Conference for food quality, solar cooking, drying, farming, and gardening, 2018. **(Invited Presentation)**
- H. J. D. Johnsen, J. Torgersen, and O. J. Nydal, "Beam Steering Lens Array for Solar Cooking," Consolfood 2018, 2018. **(Presentation. Slides)**

Contents

List of Abbreviations

BSLA	Beam-steering lens array
BFGS	Broyden–Fletcher–Goldfarb–Shanno algorithm
CPV	Concentrator photovoltaics
CSP	Concentrated solar power
LED	Light-emitting diode
MLA	Micro-lens array
MOEA/D	Multi-objective evolutionary algorithm based on decomposition
NA	Numerical aperture
NSGA	Non-dominated sorting genetic algorithm
PMMA	Poly(methyl methacrylate)
PV	Photovoltaics
RMS	Root mean square
SLSQP	Sequential least squares programming algorithm
SMS	Simultaneous multiple surface method
SMS3D	Three-dimensional simultaneous multiple surface method

1 Introduction

In recent years, solar energy deployment has grown rapidly with the advent of low-cost photovoltaics (PV) technology. Conventional PV systems utilize sunlight without concentration, but several additional applications and benefits can be enabled by introducing optical concentration to the sunlight. However, solar concentration introduces the additional complexity that concentrating optics needs to track the sun's movement across the sky. In traditional concentrators, solar tracking is implemented by rotating the entire optical system to face the sun, with the mechanical bulk and complexity that this entails.

In recent years there has been increasing research into developing alternative approaches to solar tracking. One approach is using arrays of micro-optical systems for active integrated tracking. These micro-optical systems can be designed to track the sun's movement across the sky using micro-movements or tunable optical properties, providing concentrated sunlight without extensive external tracking systems as illustrated in Figure 1.1. This thesis investigates the development, achievable performance, and potential use cases of these tracking-integrated systems, with a focus on a variant known as beam-steering lens arrays.

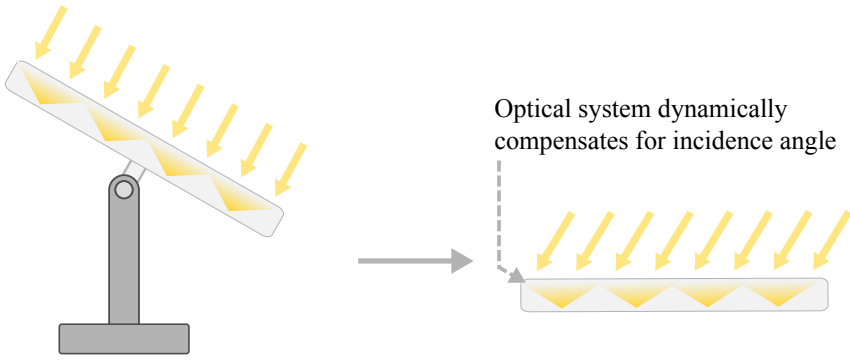

Fig. 1.1.: Tracking integration performs solar tracking as part of the optical design, reducing or eliminating the need for rotating the concentrator to face the sun.

1.1 Research objectives, methods and scope

The overall aim of this thesis was to investigate the potential of performing solar tracking using tracking-integrated designs, with a focus on beam-steering lens arrays. This involved the following set of objectives:

1. Developing a design method capable of designing beam-steering lens arrays and related tracking-integrated optical systems.

2. Exploring the design space of tracking-integrated optics, and identifying potentially promising designs.

3. Investigating new approaches to solar concentration enabled by the addition of tracking integration.

In addition to these objectives, some work was carried out towards proof-of-concept fabrication using grayscale lithography, to physically demonstrate the developments from the thesis. This fabrication effort has not yet reached the level of journal publication, and is therefore not included in this thesis.

1.2 Thesis overview

This thesis is written as a collection of 5 research papers reporting on different aspects of the work towards achieving the objectives listed in Section 1.1. These papers are listed in Section 5, and their full text is included in Appendix A. Objective 1 is covered by Papers 1, 2, and 4. Objective 2 is covered by Papers 3 and 4. Objective 3 is covered by Paper 5.

The following chapters cover the background for the work in this thesis, an outline of the methods used, and a brief report and discussion of the most important results. The full-text version of each paper then follows in the appendix of the thesis.

2 Background

This chapter briefly introduces the basics of solar concentration, tracking integration, and numerical optimization, laying the groundwork for the work carried out as part of this thesis.

2.1 Solar concentration

The power of concentrated sunlight has been known for millennia [6]. It was not until the 1960s and 1970s that a more rigorous research field was established, researching how the concentrating optics can be designed to achieve ideal or close to ideal energy transfer — a field known as Nonimaging Optics [7, 8]. This field brought a deeper understanding of how the fundamental limits of optical concentration could be achieved, and illuminated the deep connections between geometrical optics and thermodynamics [9].

The use of concentrated sunlight enables multiple use cases that are not achievable with non-concentrated sunlight, including electricity conversion with high-efficiency multi-junction solar cells [10], high-temperature thermal energy [11], direct catalysis of chemical reactions [12], or solar lighting [13].

Mirrors or lenses are used to optically concentrate the sunlight for these applications. These concentrators depend upon being accurately aimed towards the sun to enable high optical concentration. The amount of concentration in air is fundamentally limited by Equation 2.1, where θ represents acceptance half-angle of the concentrator [7].

$$C_{max} = \left(\frac{1}{\sin\theta}\right)^2 \tag{2.1}$$

The acceptance angle must at a minimum be wide enough for the divergence half-angle of sunlight, at $\theta \approx 0.27°$[14, p. 49]. This gives a maximum concentration ratio of $C_{max} \approx 45\,000$. In most practical applications, the achievable concentration ratio is much lower, due to tolerances for tracking errors and imperfect optics. The decline in concentration ratio with increased acceptance angle means that accurate solar tracking is necessary for high-concentration applications.

For some applications, especially thermal applications, it can be beneficial to concentrate sunlight to a line-focus. This enables heat extraction through a heat-transfer fluid circulated through a receiver tube as illustrated in Figure 2.1, and allows the use of simplified one-axis solar tracking about the axis of this receiver tube.

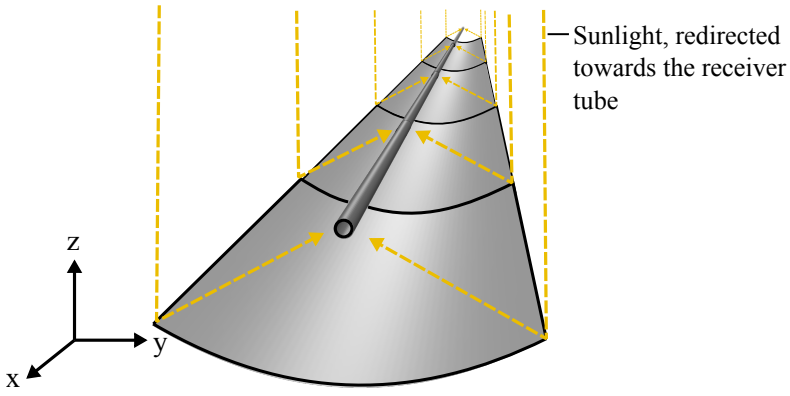

Fig. 2.1.: Example of a line-focus concentrator, in the form of a parabolic trough. The reflector concentrates sunlight towards the receiver tube, where a heat-transfer fluid is used to extract the heat.

Line-focus concentrators are commonly designed by extruding two-dimensional concentrator geometries, known as linear concentrators. The translationally symmetric two-dimensional profile of these linear concentrators means that their solar concentration is limited by the 2D concentration limit [7]:

$$C_{max,2D} = \frac{1}{\sin \theta_{max}}. \tag{2.2}$$

For a solar divergence half-angle of $\theta = 0.27°$, the limit is approximately 212x, with commercial systems operating at a fraction of this limit [15].

It has been shown that the concentration ratio of linear primary concentrators can be boosted beyond the 2D concentration limit by introducing three-dimensional secondary concentrators close to the line-focus to break the translational symmetry, reaching concentration ratios of 300x with one-axis polar tracking [16], or >1000x with two-axis tracking [17, 18]. These secondary concentrators achieve their increased concentration ratio by using three-dimensional concentrators to break the line-focus into a set of small point- or line-foci. Therefore, they are primarily useful for discrete receivers such as PV cells, not tubular receivers commonly used for concentrated solar power (CSP) applications. It has also been shown that the 2D limit can be surpassed using nominally linear concentrators where the translational symmetry is broken by ridges in the concentrator, but these have focused on relatively large acceptance angles suitable for stationary solar concentration[19, 20, 21].

2.2 Tracking integration

Conventional solar concentrators are rotated to follow the sun's apparent movement across the sky — either to point directly towards the sun using a dual-axis solar tracker, or to align its normal vector in the same plane as the sun and the axis of rotation using a single-axis solar tracker. Rotating the system to face the sun enables the possibility of high optical concentration.

At the same time, it also ensures that the projected area of the concentrator, as seen from the sun, is as large as possible — maximizing the conversion per concentrator area as further discussed in Chapter 2.6. Still, the rotation motion also has drawbacks, including mechanical bulk and complexity, sensitivity to wind loads, and difficulties being mounted on locations such as rooftops [22].

Recent developments in solar tracking and concentration have demonstrated how solar tracking can be performed optically instead of rotating the concentrator to follow the sun. In this manner, large mechanical structures for solar tracking and concentration can be replaced by small trackers integrated into a planar form factor. This development has mainly been carried out within the field of concentrator photovoltaics (CPV) [23]. Less work has been carried out to implement similar techniques for other solar energy fields such as concentrated solar power (CSP). This tracking integration enables the implementation of solar concentration in form factors not traditionally suitable for such concentration.

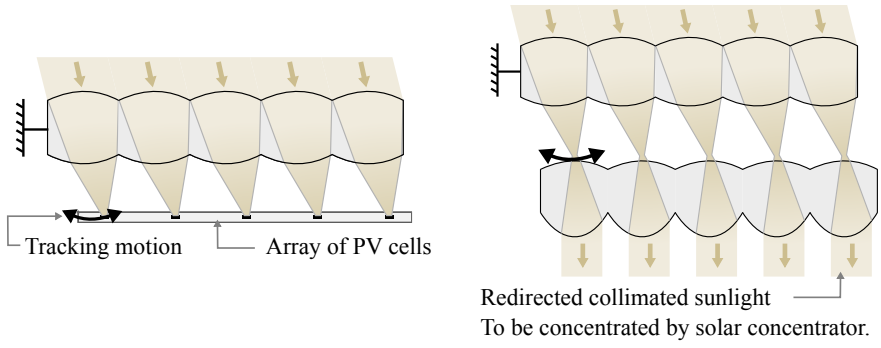

Fig. 2.2.: Lens-arrays can be used to achieve tracking integration, both in the form of (a) microtracking solar concentrators, useful for CPV applications, as well as (b) beam-steering lens arrays useful for CSP applications.

Tracking-integration for CPV applications commonly takes the form of what is known as microtracking concentrators. These concentrators split the light into many parallel paths, and each path performs tracking using micro-movements while also concentrating the sunlight to many discrete focal spots, as illustrated in Figure 2.2a. For other applications such as CSP applications, the

receiver cannot be made small to correspond to each of the individual lenslets. The tracking system can then instead be designed to emit collimated light for concentration by a larger concentrator, as illustrated in Figure 2.2b. The general concept is known as beam-steering, and the specific approach using movable lens arrays shown in Figure 2.2b, is known as beam-steering lens arrays[1].

2.3 Microtracking for CPV applications

When designing tracking-integrated concentrators for CPV applications, the individual PV cells can be made small enough to directly use the individual focal points from the lenslets in a lens array, as illustrated in Figure 2.2a. These designs are known as microtracking concentrators. Early implementations of this technique were developed by Kotsidas et al. in 2010 [22], first using lenses designed with the simultaneous multiple surface (SMS) method, and later using gradient index lenses [28]. At around the same time, Sweatt et al. demonstrated a microtracking system designed for correcting coarse external tracking [29]. Hallas et al. demonstrated a microtracking concept where instead of using PV cells at each focal point, the light was coupled into a planar light guide [30].

Duerr et al. showed how the performance of microtracking concentrators could be improved by using two lens arrays that could move relative to each other [31, 32], and Price et al. showed how a catadioptric pair of lens arrays could be used to achieve higher tracking range [5].

In 2018, Ito et al. demonstrated how an objective function could be formulated to design microtracking CPV systems optimized for average yearly efficiency [33], allowing the system to be designed without explicitly choosing a specific tracking range.

[1]The same idea has previously been described using several different terms, including "beam steering with decentered microlens arrays"[24], "beam-deflecting microlens array telescopes" [25], "beam-scanning MLA system"[26], and "beam-steering array optics"[27]. In this thesis, we consistently use the term "beam-steering lens arrays" (BSLA) as a general descriptive term for the concept.

Microtracking concentrators are currently being commercialized by the company Insolight [34].

Some work has also been carried out to implement passive solar tracking using related techniques, for instance, using phase-changing materials that locally react to the concentrated sunlight to actuate a coupling feature [35] or to modulate the transparency of the material [36].

2.4 Beam-steering

Instead of concentrating the sunlight to many small discrete focal spots, another way to implement tracking integration is the concept of beam-steering, where collimated sunlight is emitted and can be concentrated by a separate concentrator.

Several possible approaches to beam-steering of sunlight have been reported in the literature in recent years. Some of the proposed concepts include microfluidic prism arrays actuated using electrowetting [37], microfluidic beam-steering arrays [38], rotating prism arrays [39], rotating Fresnel-like lenses [40], and beam-steering lens arrays [27].

In this thesis, we have focused on beam-steering lens arrays. These systems benefit from relying on well-known geometrical optics and can likely be made compatible with high-volume manufacturing processes such as injection molding or roll-to-roll processes.

2.5 Beam-steering lens arrays

A beam-steering lens array consists of a set of lens arrays arranged in an afocal configuration, enabling beam-steering by relative lateral translation between the lens arrays, as illustrated in Figure 2.2b [1][2]. The concept was originally

[2] Portions of the description of beam-steering lens arrays in this section have been published in Paper 4 of this thesis [4]

proposed for steering of laser beams [41, 24, 26]. In 2012, Lin et al. proposed utilizing the same concept for single-axis solar tracking, while also proposing a design method based on the Simultaneous Multiple Surface (SMS) method [27]. In the Masters thesis leading up to this work, we extended the concept to two-axis solar tracking for solar cooking applications [42].

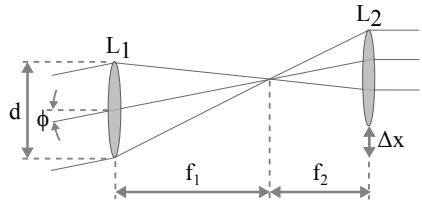

Fig. 2.3.: Paraxial working principle of a simple beam-steering lens array, showing one of the lens pairs. These lens pairs are then laid out next to each other in a complete lens array.

Figure 2.3 shows the paraxial working principle of a basic beam-steering lens array with a pair of lens arrays stacked in an afocal configuration. The lens arrays are separated by their combined focal lengths $f_1 + f_2$. The system can track incoming sunlight at an angle ϕ by translating the last lens array a distance Δx such that it is always aligned with the image of the sun from the first lens array:

$$\Delta x \quad = \quad f_1 \tan \phi. \tag{2.3}$$

In order for all rays to reach the correct lenslet in the array L_2, the second focal length must be smaller than the first. This leads to an angular magnification factor M:

$$M = \frac{f_1}{f_2} \quad = \quad 1 + 2\frac{f_1}{d} \tan \phi_{max}, \tag{2.4}$$

where ϕ_{max} is the highest supported angle of incidence for the beam-steering lens array.

As discussed in Section 2.1, sunlight has an inherent divergence half-angle of approximately $\theta \approx 0.27°$. The divergence is magnified by this angular magnification factor M after passing through a beam-steering lens array. The resulting magnified divergence half-angle limits the maximum achievable concentration of a concentrator placed behind the beam-steering lens array, in following the concentration limit of Equation 2.1. To allow high concentration ratios, it is therefore desirable that the angular magnification of the system is low. This leads to a trade-off between the tracking range ϕ_{max}, and divergence angle θ for this simple paraxial model of a beam-steering lens array.

It has been shown that this magnification factor can be eliminated in laser beam-steering systems by introducing an additional paraxial field lens to the system, where all three lens arrays have the same focal length f[24]. This shows the importance of design choices such as the number and order of surfaces when designing a beam-steering lens array.

While utilizing the same underlying principle, there are significant differences between earlier systems for steering of laser beams [41, 24, 26] and a system designed for solar tracking:

- In solar tracking, the beam-steering system receives sunlight from varying directions and emits it in a fixed direction. The earlier proposed laser systems [41, 24, 26] work in reverse, receiving the beam from a fixed direction and emitting in a variable direction.

- In laser systems, the lens arrays usually work in the diffractive regime, and additional phase-shifting optics are required to enable continuous beam-steering [24]. For solar tracking covering larger areas, the individual lenslets can be made large enough so that the geometrical optical approximation is appropriate, and the separate lenslets can be considered individually.

- The steering range used in previously proposed laser systems is $5°$ to $15°$[43, 26, 44], allowing design considerations based mainly on the paraxial approximation. For stationary solar tracking, much larger steering angles are required, and the paraxial approximation presented in this section is no longer sufficient

- In solar tracking, the system must be able to handle broadband sunlight, requiring chromatic aberration to be taken into account.

This thesis therefore covers a further investigation into the achievable performance of beam-steering lens arrays designed for solar tracking applications.

2.6 Projection effects

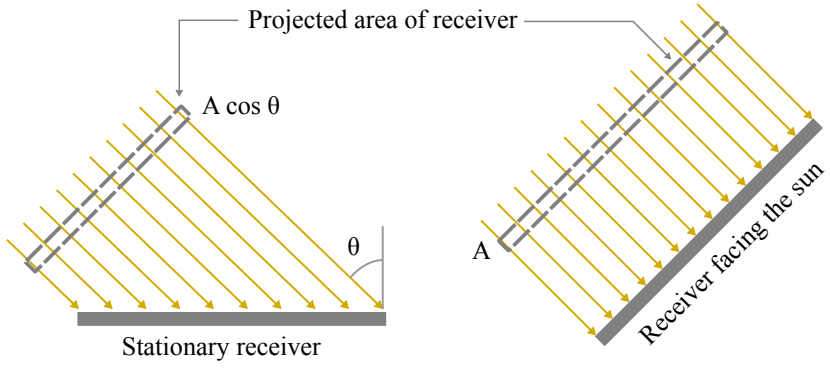

Fig. 2.4.: Projection effect of a stationary solar receiver. When sunlight comes from an angle θ, a receiver with area A has a projected area of only $A \cdot \cos\theta$, causing the receiver to intercept less sunlight than when facing the sun.

One significant drawback with tracking-integrated systems compared to externally tracked systems is the cosine projection effect, as illustrated in Figure 2.4. An optimally tilted stationary receiver intercepts only on the order of 60%-80% of the daily solar irradiation compared to a receiver under two-axis external solar tracking, depending on location and local conditions [45]. If the ultimate objective is to maximize energy conversion per concentrator surface area, the concentrator should therefore be rotated to follow the sun. On the other hand, conversion per land area can be higher with a stationary concentrator because there is a reduced need to place the modules far apart to prevent partial shading from the neighboring modules [5]. For this reason, tracking integration is most useful in places where conversion per area is an important factor or where conventional external solar tracking has an impractical form factor, for instance, rooftop-mounted solar energy [5]. Another use for tracking integration is to achieve dual-axis tracking using a simplified

single-axis external tracker [32]. If a receiver is placed on a single-axis polar-aligned external tracker, it intercepts 96%-99% of the sunlight compared to a receiver under two-axis external tracking [45].

2.7 Designing tracking-integrated systems

Several powerful design methods have been developed in the field of Nonimaging Optics, including the edge ray principle, the SMS and SMS3D method, and the flow-line method [7]. These methods have primarily focused on the design of static optical systems, and are based on finding static optics that couple a predetermined set of incoming and outgoing ray-bundles.

A tracking-integrated system, on the other hand, is dynamic. It is designed to change its behavior depending on its orientation relative to the sun. Some work has focused on extending existing nonimaging methods for this new application. For instance, Lin et al. used a method based on the SMS method for designing their beam-steering lens arrays [27]. Duerr et al. developed a tailored design method using Fermat's principle to derive a set of differential equations for a wide-angle lens used as a microtracking concentrator [32].

Alternatively, the tracking-integrated systems can be designed using numerical optimization, as demonstrated by a number of micro-tracing designs [5, 33, 34, 30]. Numerical optimization has higher computational demand than analytic methods, but it enables the design of more complex systems without first needing to derive an analytic design method for the specific problem. It is also straightforward to integrate additional effects into the design process, including chromatic aberration, behavior under expected manufacturing errors, and appropriate weighting of performance across a large field of view.

Numerical optimization involves parameterizing the optical system's design by a set of parameters $\mathbf{x}$, and defining an objective function $f(\mathbf{x})$ that evaluates the optical system and gives it a score based on a predefined set of requirements and goals. Often this score is formulated so that a lower number represents a better system. In other words, it is a minimization problem. An additional set of constraints often needs to be fulfilled: $c_i(\mathbf{x}) \geq 0$. In an

optical system, this can for instance be the requirement that all lenses have a positive thickness. Formally, this optimization problem can then be written as [46][3]:

$$\min\ f(\mathbf{x}) \tag{2.5}$$

$$\text{such that } c_i(\mathbf{x}) \geq 0 \tag{2.6}$$

This optimization problem is then passed to an optimization algorithm that systematically tries different values for the parameters $\mathbf{x}$, searching for the parameters that give the best objective function value. Since $f(\mathbf{x})$ can be evaluated for millions of different values of $\mathbf{x}$ during this search, numerical optimization is a computationally expensive design method, and it is essential that the evaluation is as efficient as possible.

2.8 Ray-tracing and ray-sampling

In order to implement an objective function that gives a score to a specific design, it is necessary to simulate this optical system's performance. In geometrical optical design-problems, like the ones described in this thesis, this is commonly done using ray-tracing: Tracing many discrete rays through the system and inferring the whole system's performance based on the behavior of these rays. There is then a trade-off between the accuracy of the simulation and the computational requirements: Tracing a larger number of rays gives a more accurate estimate of the performance but also increases the computational load.

Objective functions in nonimaging optics, including those used in this thesis, can often be considered a form of numerical integration. The objective function integrates some figure of merit across the parameters of the irradiation.

[3] In the classical formulation of nonlinear optimization problems, they may include a set of equality constraints $c_j(\mathbf{x}) = 0$ in addition to the inequality constraints presented here. Such equality constraints were not used in the optimization problems in this thesis.

An objective function based on a random sampling of rays through the system can therefore be considered as a form of Monte-Carlo integration. For well-behaved numerical integration problems, it has been shown that the error of Monte-Carlo integration can be reduced if the integration points are sampled from a low-discrepancy sequence instead of being truly random. This process is known as Quasi-Monte Carlo integration [47].

Quasi-Monte Carlo methods have been shown to have significantly improved performance compared to conventional Monte-Carlo methods for many different integration problems [47]. They have also been shown to give significantly reduced errors when simulating optical devices [48].

2.9 Memetic optimization

The numerical optimization of nonimaging systems is challenged by the fact that most nonimaging optical problems are multimodal [7] — they contain several local optima in addition to the global optimum.

Classical gradient-based local optimization algorithms are highly efficient at finding a local optimum, but this local optimum is not necessarily the global optimum for the optimization problem as illustrated in Figure 2.5. Conversely, population-based heuristic optimization algorithms such as evolutionary or genetic algorithms have been shown to be less sensitive to local optima and search a wider region in the design landscape, but they are usually not very good at finding the exact location of an optimum as illustrated in Figure 2.5b.

A class of heuristic optimization algorithm known as memetic algorithms can be used to create a hybrid of these two classes of optimization algorithms: It uses local gradient-based algorithms for refining the individuals in the population used by the population-based algorithm [49], as illustrated in Figure 2.5c. Different memetic optimization algorithms have successfully been broadly applied to many different engineering problems [50].

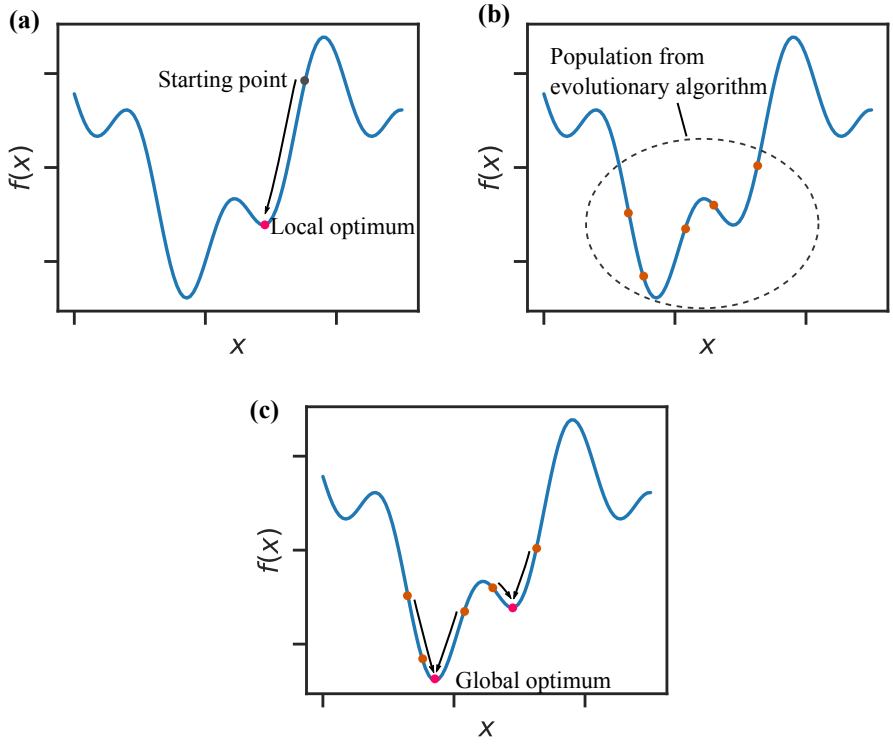

Fig. 2.5.: Conceptual illustration of memetic optimization with a single-variable objective function. (a) Local gradient-based optimization algorithms efficiently find a local optimum from a given starting point, but it is not necessarily the global optimum. (b) Population-based algorithms such as genetic or evolutionary algorithms search a broader region in the decision space and finds several points that may be near the global optimum. (c) Using a memetic algorithm, the population-based algorithm finds a number of good points, which are continuously refined using local search, increasing the likelihood that the global optimum will be found.

2.10 Objective function formulation

The optimization problem shown in Equation 2.5 is based on a single-valued objective function $f(\mathbf{x})$, which evaluates the behavior of the optical system $\mathbf{x}$, and gives it a single numerical score to represent how well it achieves the design objective. However, the design of an optical system often involves the simultaneous optimization of several different objectives. In the case of tracking integration, these objectives may include:

- Maximizing the optical efficiency
- Maximizing the concentration ratio (or minimizing the divergence of the outgoing light in the case of beam-steering systems)
- Maximizing the tracking range
- Minimizing the mechanical complexity of the design

Therefore, the formulation of an optimization problem involves finding a way to combine these objectives into the single-valued objective function $f(\mathbf{x})$ — a process known as scalarizing the problem. Several approaches have been used to achieve this. A common choice is to use a predetermined tracking range and concentration ratio, and optimizing the system for maximum efficiency under these conditions. This approach was used, for instance, by Price et al. [5]. Another popular way to scalarize an optimization problem with multiple objectives is to use a sum scalarization [51]:

$$f(\mathbf{x}) = \sum_{i=1}^{m} w_i f_i(\mathbf{x}) \tag{2.7}$$

where $f_i(\mathbf{x})$ is the individual objectives and w_i is a set of weights determining how they should be weighted in the scalarized objective function.

While maximizing the tracking range and maximizing the optical efficiency are two distinct objectives, they both affect the yearly cumulative solar energy collected by the system. Ito et al. therefore elegantly showed how these

two objectives can be combined into the single objective of maximizing this collected cumulative solar energy [33], which they defined as:

$$E_{\text{annual}} = \sum_{\theta_i=0^\circ}^{90^\circ} E\left(\theta_i\right) \cdot \eta_{opt}\left(\theta_i\right) \tag{2.8}$$

where θ_i is incidence angle, $E\left(\theta_i\right)$ is yearly cumulative solar radiation incident at the incidence angle θ_i, and $\eta_{opt}\left(\theta_i\right)$ is the optical efficiency at incidence angle θ_i.

With this objective formulation, it is no longer necessary to choose a predetermined tracking range. Instead, the optimization algorithm can select the optimum trade-off between tracking range and optical efficiency with the ultimate objective of maximizing the yearly cumulative solar energy collected.

2.11 Multi-objective optimization

As an alternative to scalarizing the optimization problem, it is possible to use algorithms that directly work on multiple objectives, known as multi-objective optimization algorithms. These algorithms do not look for a single optimal solution, but instead look for a set of solutions that represent different levels of trade-off between the multiple objectives in the optimization problem. This set of solutions is known as the Pareto front of the problem, as illustrated in Figure 2.6. In this case, the objective function becomes vector-valued:

$$\min \mathbf{f}\left(\mathbf{x}\right) = \left(f_1\left(\mathbf{x}\right), f_2\left(\mathbf{x}\right), \cdots\right) \tag{2.9}$$

$$\text{such that } c_i\left(\mathbf{x}\right) \geq 0 \tag{2.10}$$

Multi-objective optimization problems are often solved using evolutionary or genetic algorithms, such as the NSGA II algorithm [52] or the MOEA/D

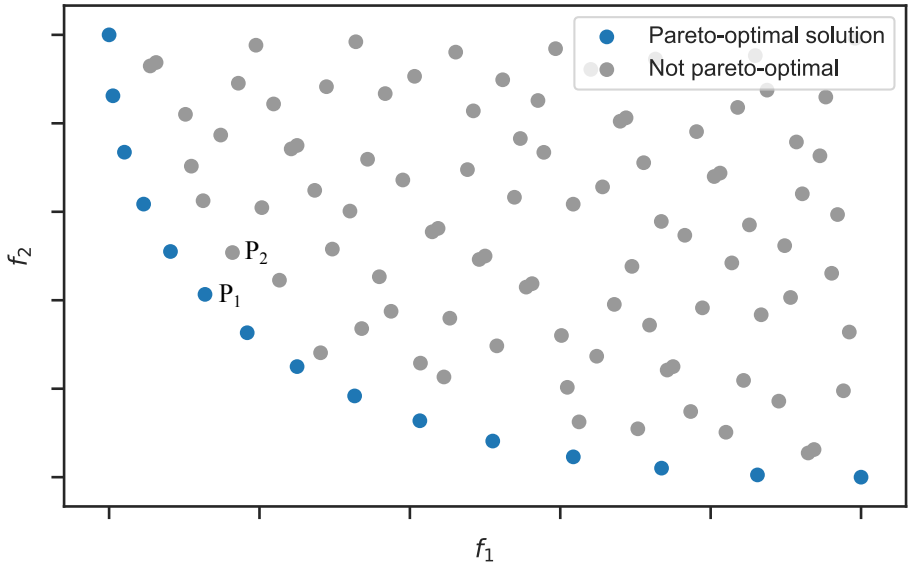

Fig. 2.6.: In multi-objective optimization, the algorithm tries to identify the set of Pareto-optimal solutions — solutions where no other solution exists that improves on all the objectives simultaneously. As an example, P_2 is not a Pareto optimal solution, because P_1 has a better value for both objectives. Conversely, P_1 is Pareto optimal — none of the other solutions are superior in both objectives. The set of Pareto optimal solutions map out the trade-off between the objectives of the optimization problem.

algorithm [53]. In the same way as with single-objective optimization, it is possible to combine these algorithms with local search algorithms to create hybrid memetic algorithms [54].

2.12 Étendue Squeezing

Many well-known designs in non-imaging optics are either translationally or rotationally symmetric. This simplifies the design of the systems, but it can also introduce additional limitations that are a consequence of these symmetries and not of the design problem itself. One way to utilize freeform surfaces to go beyond these limitations is the concept of étendue squeezing [55], as introduced by Miñano and Benitez in 2005 [56].

Étendue squeezing is a way to achieve a lens with a different field of view along the x-axis and y-axis, achieved by squeezing the angular extent along one axis while expanding it along the other axis so that the total étendue is conserved [55]. This type of lens solves the same nominal problem as an anamorphic lens in conventional imaging optics [57]. However, while an anamorphic lens achieves this squeezing of the field of view by changing the entrance pupil's shape, an étendue-squeezing lens uses a set of parallel optical paths to obtain an entrance pupil as large as the lens itself, to facilitate the efficient transfer of energy.

A simple form of étendue squeezing lens is created when both object and image is at infinity, and is illustrated in Figure 2.7. This lens uses many afocal pairs of lens surfaces to compress an optical beam in one axis while expanding it in the other axis, as illustrated in Figure 2.7a. If the ratio of compression and expansion is 1:N where N is an integer, the lens pairs can be tessellated so that they fill the complete front and back surface of a lens array, as shown in Figure 2.7b [58]. This specific type of étendue squeezing is known as an étendue-squeezing lens array, and was described by José Blen in his 2007 PhD dissertation [59]. The étendue-squeezing lens array trades angular extent along one axis against angular extent along the other axis by a factor N, known as the squeeze factor of the optics [58]. The idea has been demonstrated for applications such as changing the aspect ratio of a collimated beam from an LED source [58].

As part of this thesis, we investigate whether this étendue squeezing principle also may be used for solar concentration, specifically in combination with tracking integration.

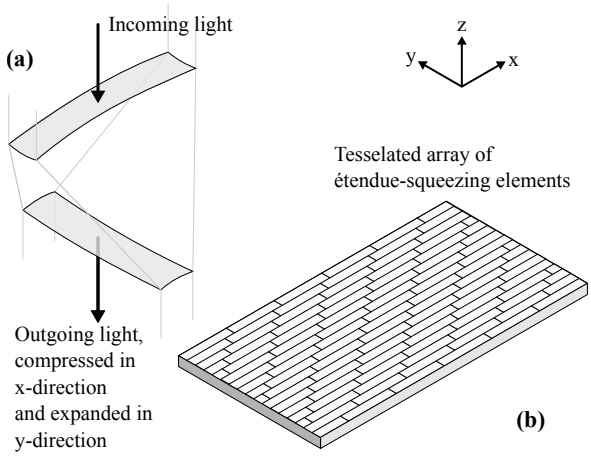

Fig. 2.7.: (a) Principle of étendue-squeezing using an afocal lens pair. (b) The lens-pairs can be tessellated into a complete étendue-squeezing lens array.

3 Research methods

The primary research method in this thesis has been the numerical simulation and optimization of optical systems to fulfill the goals outlined in Section 1.1. This involved the development of a sequential ray-tracer explicitly designed for simulating tracking-integrated systems, which was used to optimize beam-steering lens arrays, microtracking concentrators, and a new type of solar concentrator based on étendue squeezing.

3.1 Custom Python-based ray-tracer

Several commercial software packages exist for the simulation and design of optical systems, and these have previously been used to design tracking-integrated and microtracking systems. For instance, LightTools was used to design the microtracking concentrators by Ito et al. [33], while Zemax OpticStudio was used to the design microtracking concentrators by Price et al. [5] and Hallas et al. [60]. We acquired Zemax OpticStudio for the work performed in this thesis, but we found that it did not fulfill all our requirements for performing a broad exploration of the design landscape for tracking-integration, mainly due to limitations in the formulation of objective functions and optimization algorithms. We therefore developed a custom Python-based ray-tracer to allow for greater flexibility.

The ray-tracer is a sequential ray-tracer designed specifically for optimizing tracking-integrated optical designs. It is written as a Python library, and compiled using the LLVM-based Numba just-in-time compiler [61], enabling high-performance ray-tracing despite being written in an interpreted programming language.

By having the architecture of a Python library, this ray-tracer opens up new possibilities compared to the use of commercial optical design software, including:

- The use of a prototyping-friendly high-level language makes it possible to experiment with various objective functions defined using the full expressiveness of this language, without the overhead of interprocess communication between the language and another commercial software package.

- By not relying on limited software licenses, it became possible to be flexible regarding the computational environment, and to perform large-scale optimization using computational resources from Google Compute Engine.

- It became possible to take advantage of the existing scientific computing ecosystem available from the Python programming language, including several optimization libraries with different optimization algorithms that have previously been shown to work well for optical design problems[62].

- The flexibility of the implementation made it possible to implement efficient objective functions based on quasi-Monte Carlo methods as described in Chapter 2.8, where the extra integration dimensions from the movable optical surfaces are included in the Quasi-Monte Carlo integration.

We emphasized ensuring numerical stability in the ray-tracer and making the objective functions smooth and differentiable to enable the use of gradient-based optimization algorithms. The gradients were estimated using finite differences, as is also commonly done in commercial optical design software.

In numerous other scientific domains, it has been shown that superior accuracy and performance can be achieved if gradients are estimated explicitly as part of the simulation, instead of using numerical finite differences. This is known as differentiable programming, and is usually implemented using automatic differentiation[63]. Due to limitations in the combination

of Python and Numba, it was not straightforward to use automatic differentiation with the ray-tracer implemented as part of this thesis. Therefore, significant further performance improvements may be expected if this ray-tracer is re-implemented using an architecture that enables automatic differentiation.

3.2 Formulation of the optimization problem

In the initial optimization of beam-steering lens arrays for this thesis, we defined our objective function as a sum scalarization between efficiency and divergence of the outgoing light, and optimized the systems for a fixed tracking range. Formally, this objective function could be written as:

$$\min\ f(\mathbf{x}) = \sum_{i=1}^{m} \left(w_1 \frac{1}{\eta_i(\mathbf{x})} + w_2 \left(\delta\theta_i(\mathbf{x})\right)^2 \right) \tag{3.1}$$

$$\text{such that } g_j(\mathbf{x}) \leq 0 \tag{3.2}$$

where w_1 and w_2 are relative weights applied to the efficiency and divergence. $\eta_i(\mathbf{x})$ is the simulated efficiency for a ray-traced grid of rays with incidence angle number i and optical system described by $\mathbf{x}$. $\delta\theta_i(\mathbf{x})$ is the corresponding RMS divergence half-angle for field number i. m separate incidence angles are evaluated across the tracking range of the BSLA. $g_j(\mathbf{x})$ is a set of inequality constraints ensuring manufacturability, such as minimum and maximum thickness, and maximum lens curvature. When optimizing microtracking concentrators, we used the same objective function but replaced RMS divergence half-angle with RMS spot size.

A drawback of this optimization problem was that the tracking range had to be specified, and an explicit weighting between efficiency and divergence had to be selected. In order to improve the optimization and enable a broad exploration of beam-steering lens array configurations, we reformulated the optimization problem using an approach inspired by Ito et al.'s formulation

as described in Chapter 2.10. We defined an average yearly efficiency of the beam-steering lens array:

$$\overline{\eta}\left(\mathbf{x}, \theta_{max}\right) = \frac{E_{out}\left(\mathbf{x}, \theta_{max}\right)}{E_{in}}, \tag{3.3}$$

where E_{in} is the yearly direct irradiation received by the beam-steering lens array surface, and $E_{out}\left(\mathbf{x}, \theta_{max}\right)$ is the yearly irradiation successfully redirected by the beam-steering lens array within the permitted exit cone $\pm\theta_{max}$.

Using this average yearly efficiency, we defined the following multi-objective optimization problem:

$$\min \mathbf{f}\left(\mathbf{x}, \theta_{max}\right) = \left(-\overline{\eta}\left(\mathbf{x}, \theta_{max}\right), \theta_{max}\right) \tag{3.4}$$

$$\text{such that } g_j\left(\mathbf{x}\right) \leq 0, \tag{3.5}$$

where θ_{max} is the allowed divergence of outgoing sunlight, and $\mathbf{x}$ is a set of free variables specifying the optical system. $\overline{\eta}\left(\mathbf{x}, \theta_{max}\right)$ is the average yearly optical efficiency of the optical system subject to θ_{max}. The two components of $\mathbf{f}$ represent the two objectives: Maximizing the average yearly efficiency (minimizing $-\overline{\eta}$), while also minimizing the allowed divergence (minimizing θ_{max}).

We then used memetic multi-objective optimization algorithms to solve this multi-objective optimization problem, and mapped out the trade-off between average yearly efficiency and permitted divergence half-angle for a broad selection of beam-steering lens arrays.

3.3 Generating beam-steering lens array configurations

As outlined in Section 1.1, one of the main objectives of this thesis was to explore the design space of tracking-integrated optics. This was carried out by optimizing a large number of beam-steering lens array systems using the multi-objective optimization problem and algorithm described above.

In order to optimize a beam-steering lens array, a configuration needs to be selected — the number and types of lens arrays comprising the system, as well as the permitted movements between these lens arrays. Previously proposed beam-steering lens array designs have utilized both single-sided [27] and double-sided [1] lens arrays, with relative lateral [64] or curved [27] tracking motion, and with both two [27], and three [25] lens arrays stacked together. In order to readily specify, compare, and evaluate different classes of designs, we specified a set of symbols as reported in Table 3.1 to represent beam-steering lens array configurations. We then used these symbols to generate a full set of beam-steering lens arrays for optimization.

The symbols from Table 3.1 can be used to classify both existing and new beam-steering lens array configurations. For instance:

- The example beam-steering lens array in Figure 2.2b: ◆⤸◆
- Lin et al., 2012 [27]: ◀⤸▶
- Watson, 1993 [24] (for steering of laser beams): ◆↓◆ and ◆↓◆▤◆
- Johnsen et al., 2018 [1]: ◆⤸◆ and ◀⤸◆⤸◆

Using the presented symbols for specifying beam-steering lens arrays, we performed a comprehensive optimization of all possible combinations of the symbols with a maximum of 1 air-gap. This lead to a total of 52 configurations, of which 40 contains at least 1 movable surface and are candidates for optimization. These configurations cover the range from complex configurations such as ◀▶⤸◀▶, to simple configurations such as ◀▶. Optimizing across

Tab. 3.1.: Symbols used classifying different beam-steering lens array configurations.

Symbol	Meaning
◀	Single-sided lens array with the flat side on the right.
▶	Single-sided lens array with the flat side on the left.
◆	Double-sided lens array
◀▶	A pair of single-sided lens arrays placed back-to-back, with index-matched lubricating oil between them supporting relative lateral translation between the lens arrays.
↓	Air-gap between lens arrays supporting a flat, lateral tracking trajectory.
⤸	Air-gap between lens arrays supporting a curved tracking trajectory.
▤	Air-gap between two surfaces, but no relative movement between the surfaces.

this span can therefore give insight into the trade-off between minimizing complexity and maximizing system performance.

3.4 Optimization of microtracking concentrators

We did an initial exploration of the achievable performance of different microtracking solar concentrators for CPV applications. This was done before adopting the multi-objective design method described in Chapter 3.2, and we therefore used a sum-scalarization to optimize for concentration ratio and optical efficiency.

We optimized the three configurations sketched in Figure 3.1. The first configuration was chosen because it has already been shown by Price et al. to have good performance [5], and the two additional configurations were chosen to see how the concentration can be increased if we let the system have higher complexity. We optimized each configuration for a fixed tracking range of $\pm 60°$.

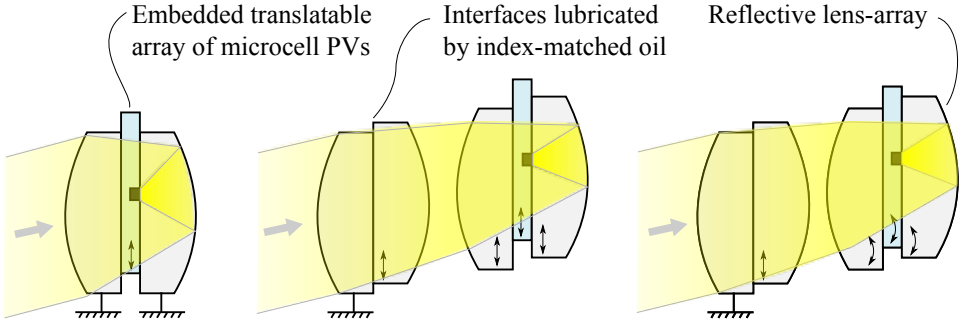

Fig. 3.1.: Conceptual illustration of the three different CPV-configurations that were optimized: Simple catadioptric (a), flat tracking trajectory (b), and curved tracking trajectory (c). In each configuration, the lenslets are assumed to be arranged in hexagonally packed lens arrays.

3.5 Optimization of étendue-squeezing solar concentrators

Beam-steering lens arrays are designed to emit collimated light, for concentration by a separate solar concentrator. To allow for sufficient concentration

despite the divergence half-angle introduced by the beam-steering lens arrays, this concentrator would typically be a three-dimensional concentrator due to the much higher achievable concentration ratios compared to two-dimensional concentrators, as discussed in Chapter 2.1. For instance, in the solar cooker developed in the master's thesis leading up to this PhD thesis, an off-axis parabolic concentrator with a point-focus was used [42].

However, as further described in Chapter 2.1, line-focus concentrators have the benefit that they are compatible with tubular receivers, which can simplify the heat extraction through heat-transfer fluids. We therefore investigated whether it would be possible to design a three-dimensional solar concentrator that focuses sunlight to a line-focus without being limited by the two-dimensional concentration limit. Such a concentrator could then be combined with a beam-steering lens array to create a tracking-integrated line-focus concentrator for solar thermal applications.

We used the concept of étendue squeezing combined with numerical optimization to create two design examples of line-focus concentrators: One concentrator consisting of only a double-sided lens array, and one concentrator using an additional secondary reflector. Both designs were based on the étendue squeezing lens array described in Chapter 2.12. The goal was to achieve a concentration ratio higher than the two-dimensional concentration limit, which applies to conventional line-focus concentrators. The étendue-squeezing lens array was modified by optimizing each lens pair individually to redirect sunlight towards the focal line of the concentrator. Both designs were constructed with an étendue squeezing factor of $N = 7$ (the ratio of the short to the long side of the individual rectangular facets is 1:7). The factor 7 was chosen as an example, to be high enough to allow for a significant concentration boost, while low enough to allow for practical implementation. The lens arrays are assumed to be made from PMMA, and illuminated using the AM1.5D solar spectrum and a top-hat $\pm 1^\circ$ angular distribution. This angular distribution was chosen as an example, to demonstrate the possibility of designing for some tolerance to tracking errors.

4 Main Results

The full set of results from this thesis are reported in the full-text papers listed in Appendix A. In this chapter we report on the most important results from these papers.

4.1 Beam-steering lens arrays

The beam-steering lens array optimization of this thesis culminate in a broad exploration of possible beam-steering lens array configurations for stationary solar tracking applications[1]. The main result from this exploration is shown in Figure 4.1, which summarizes the expected average yearly efficiency of each beam-steering lens array configuration depending on the required divergence half-angle of the outgoing sunlight.

Each line represents a specific beam-steering lens array configuration specified using the symbols from Chapter 3.3, and each point along the line represents a specific design optimized for the particular trade-off between efficiency and divergence half-angle. In order for the comparison to not unrealistically favor highly complex designs that are overly sensitive to manufacturing errors, the presented results are optimized for as-built performance with a set of manufacturing tolerances, as reported in Paper 4.

Due to the number of optimized configurations, only the best-performing configurations are shown in Figure 4.1. The full set is available in the appendix of Paper 4.

[1]The beam-steering lens array results presented in this section are based on the published results from Papers 1, 3, and 4 of this thesis [1, 3, 4].

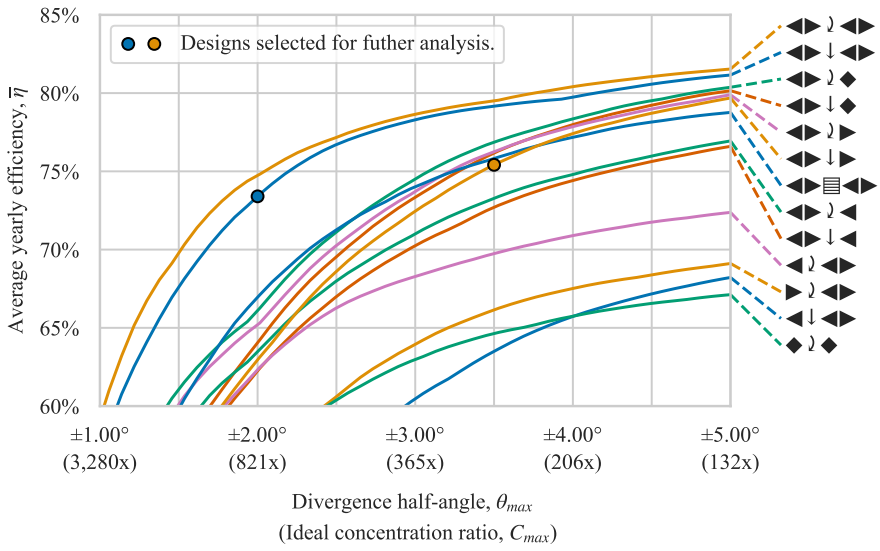

Fig. 4.1.: Set of the best performing optimized configurations, mapping out the trade-off between efficiency and divergence half-angle. The value in brackets below the divergence half-angle represents the ideal geometric concentration at this divergence half-angle, according to Equation 2.1.

From the set of designs reported in Figure 4.1, we chose to highlight two designs representing different trade-offs between efficiency, divergence, and complexity. The first result is a ◀▶↓◀▶ configuration optimized for a divergence half-angle of $\pm 2°$, which achieves 73.4% average yearly efficiency. This represents a configuration with high complexity, low divergence, and high efficiency. The result is highlighted with a blue circle in the Pareto fronts in Figure 4.1, and a ray-traced drawing of the system can be seen in Figure 4.2.

The second result is a ◀▶↓▶ configuration optimized for $\pm 3.5°$ divergence half-angle, which achieves 75.4% average yearly efficiency. This is an example of a system where a lower mechanical complexity is traded for a higher permitted divergence half-angle. The result is highlighted with a brown circle in the Pareto front in Figure 4.1, and a ray-traced drawing of the system can be seen in Figure 4.3. A 3D model of the two highlighted designs is shown in Figure 4.4.

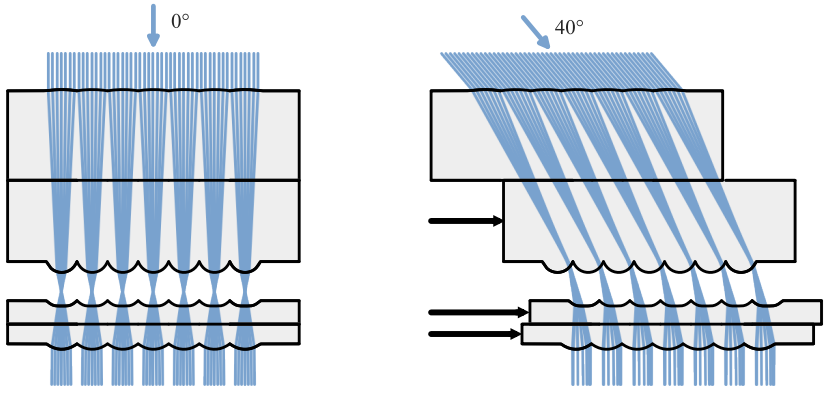

Fig. 4.2.: Beam-steering lens array with ◀▶↓◀▶ configuration optimized for $2°$ divergence half-angle (● in Figure 4.1), drawn at $0°$ and $40°$ angles of incidence respectively. The black arrows indicate tracking motion. The drawing shows a 2-dimensional slice of the optimized system, which consists of hexagonally packed three-dimensional lens arrays.

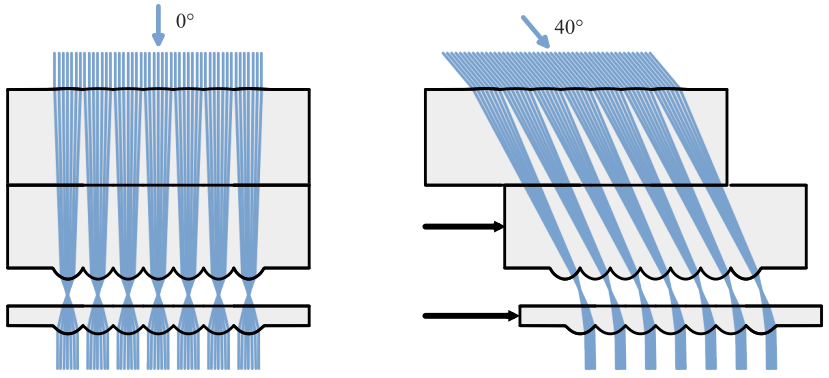

Fig. 4.3.: Simplified beam-steering lens array with ◀▶↓▶ configuration optimized for $3.5°$ divergence half-angle (● in Figure 4.1), drawn at $0°$ and $40°$ angles of incidence respectively. The black arrows indicate tracking motion. The drawing shows a 2-dimensional slice of the optimized system, which consists of hexagonally packed three-dimensional lens arrays.

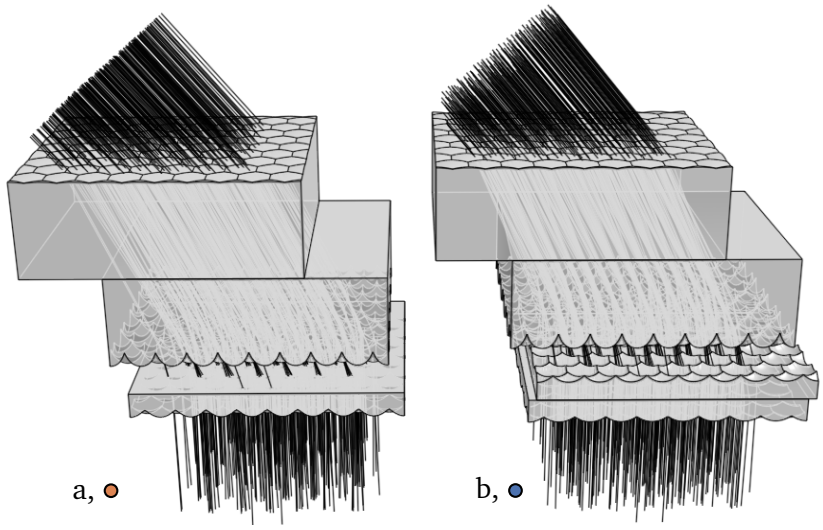

Fig. 4.4.: Ray-traced 3D-model of the two selected beam-steering lens arrays, both shown at a $40°$ angle of incidence. (a) ◀▶↓▶ configuration optimized for a permitted divergence of $3.5°$, (b) ◀▶↓◀▶ configuration optimized for a permitted divergence of $2.0°$.

4.2 Microtracking solar concentrators

As described in Section 3.4, we optimized three configurations of microtracking solar concentrators. A ray-traced drawing of the resulting designs are shown in Figure 4.5[2]. Simulated efficiency and concentration ratio across the $\pm 60^\circ$ field of view are shown in Figure 4.6.

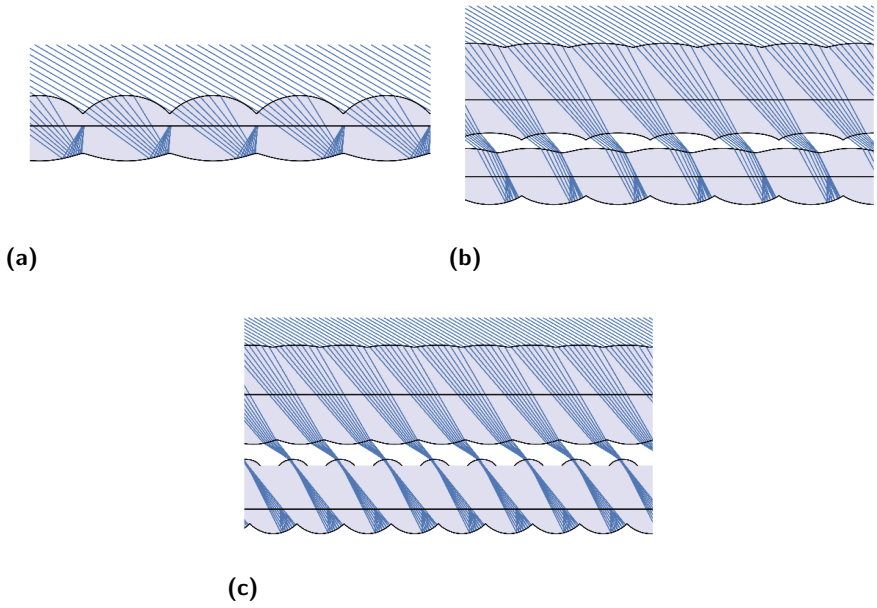

Fig. 4.5.: Ray-traced drawing of the three optimized microtracking CPV concentrators, each shown at 60° angle of incidence.

The simulated performance of the simple catadioptric configuration gives a geometric concentration ratio >400x and optical efficiency >90%. This is comparable to the results published by Price et al [5], and the small variations may be caused in part because our work assumes a circular receiver when estimating concentration ratio. The lowest concentration ratio across the field of view is increased from approximately 400x to approximately 2000x when adding an additional pair of lens arrays to the system in the configuration shown in Figure 3.1b. The lowest concentration ratio is further increased

[2]The microtracking concentrator results presented in this section are based on the published results from Paper 2 of this thesis [2].

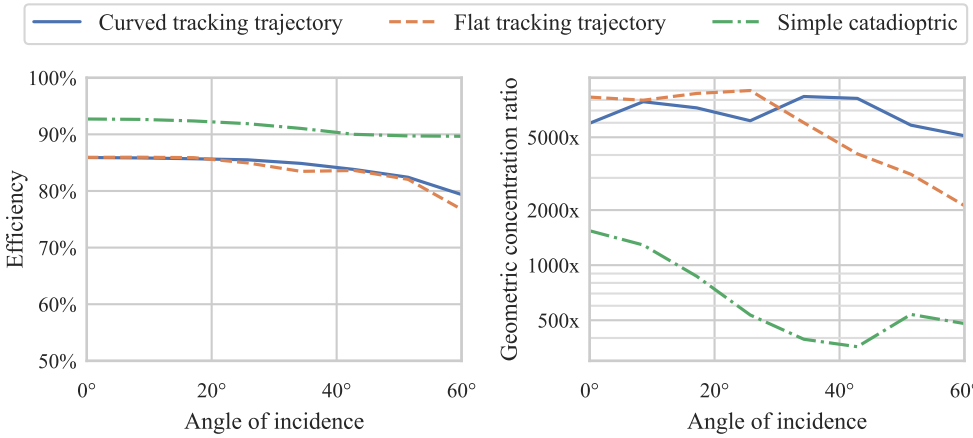

Fig. 4.6.: Simulated optical efficiency and concentration across tracking range for the optimized CPV configurations. The geometric concentration ratio is defined as the geometric concentration ratio that would lead to a 90% intercept factor at that specific angle of incidence.

to approximately 5000x if the lens arrays are allowed to follow a curved tracking trajectory, as illustrated in Figure 3.1c. The significantly increased concentration ratio comes at the cost of reduced optical efficiency due to reflection losses and the additional mechanical complexity with several lens arrays moving relative to each other. In order to reduce the burden of this additional mechanical complexity, all the lens arrays are constrained to move proportionally to each other. They may therefore share the same mechanical actuator.

4.3 Étendue-squeezing line-focus solar concentrators

As described in Chapter 3.5, we optimized two solar concentrators based on the étendue squeezing principle. Both design examples were optimized for $\pm 1^\circ$ acceptance angle. At this designed acceptance angle, the 2D concentration limit is 57.3x, while the 3D concentration limit is 3 283x according to Equations 2.1 and 2.2. The first design example is a single double-sided lens array, for operation similar to a linear Fresnel lens. A ray-traced 3D model of the concentrator is shown in Figure 4.7, and a 2D drawing is shown in Figure 4.8.

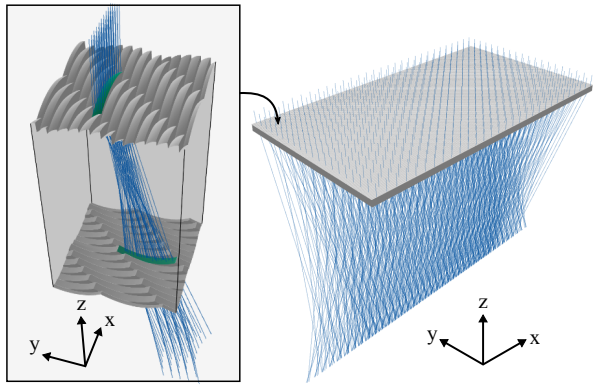

Fig. 4.7.: A solar concentrator utilizing étendue-squeezing, consisting of an array of tessellated étendue-squeezing lens pairs. Each lens-pair squeezes the beam in the x-direction and expands it in the y-direction, while redirecting the sunlight towards the common focal line. The cutout shows one such lens-pair highlighted in green, and demonstrates how the lens-pairs are tessellated into a complete double-sided lens array.

The concentrator has a numerical aperture of $NA = 0.32$ $(f/1.47)$ and achieves 79.1% efficiency at 95x geometric concentration ratio under $\pm 1^\circ$ illumination, leading to an effective optical concentration of $C_{eff} = 0.791 \cdot 95 \approx 75.1$. The intensity across the focal line of the concentrator is shown in Figure 4.9. This design demonstrates that it is possible to surpass the 2D concentration limit, but the concentration ratio of this example design is still only about 31% higher than the 2D limit. The low numerical aperture of the

resulting concentrator indicates that the concentration can be increased by a high numerical aperture secondary concentrator, leading us to the next design example.

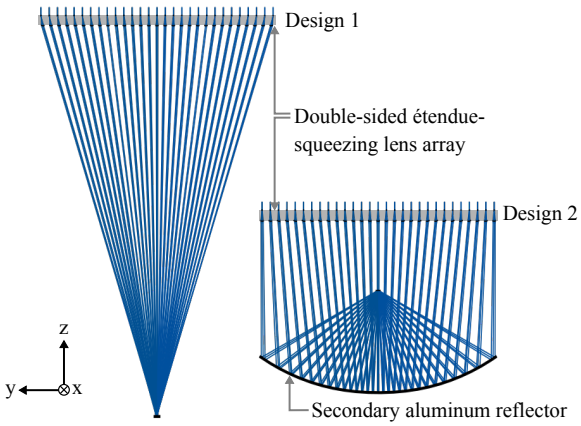

Fig. 4.8.: Ray-traced drawing of the two design examples. Only a subset of the lens-pairs are drawn and traced, to reduce clutter in the drawing. In reality, the lens-pairs are tessellated to fill the entire front and back surface of the lens array, as shown in Figure 4.7.

The second design example combines the étendue-squeezing lens array with a reflective secondary concentrator assumed to be made from aluminum. The geometry of this reflective secondary is designed so that the resulting concentrator is approximately aplanatic, a condition that has previously been shown to generate concentrators with performance very close to the fundamental concentration limit [65, 66]. The concentrator has a numerical aperture of $NA = 0.89$ and achieves 78.0% efficiency at a 280x geometric concentration ratio under $\pm 1^{\circ}$illumination. This leads to an effective optical concentration of $C_{eff} = 0.780 \cdot 280 \approx 218$. The intensity across the focal line of the concentrator is shown in Figure 4.9.

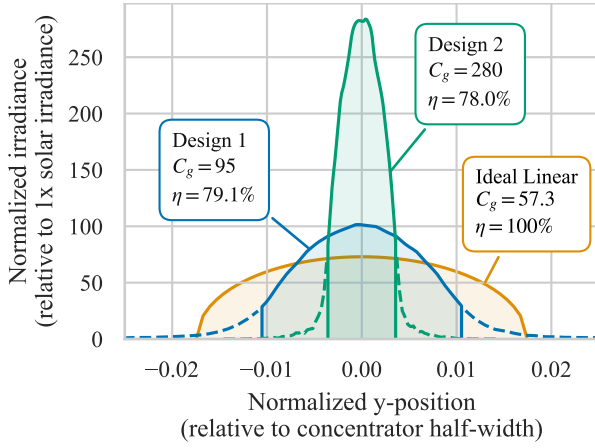

Fig. 4.9.: Intensity profile across the focal line for the two concentrators, under 1 sun AM1.5D illumination with a $\pm 1^\circ$ top-hat angular distribution. Both concentrators go beyond the 2D concentration limit. The non-uniform intensity profile of the ideal linear concentrator is caused by the circular $\pm 1^\circ$ angular distribution of the illumination and assuming an ideal imaging concentrator, as further discussed in the supplemental document to Paper 5 of this thesis.

List of papers

5

5.1 Paper 1

Title	Solar tracking using beam-steering lens arrays
Authors	Håkon J. D. Johnsen, Jan Torgersen, Astrid Aksnes
DOI	10.1117/12.2320046
Type	Conference Paper
Publisher	Proceedings of SPIE

This paper gives a thorough introduction to how beam-steering lens arrays can be used to achieve solar tracking, and describes how the beam-steering lens array concept can be viewed from a phase-space perspective. This phase-space perspective was also used to develop an optimization method where the focusing and collimating lens are designed separately.

Using an optimization method based on the phase-space representation of the optical system, we developed two examples of beam-steering lens array designs. One using two lens arrays and achieving a simulated $> 60\%$ efficiency across a two-axis $\pm 40°$ tracking range, and a divergence of the outgoing beam of less than $\pm 1.7°$. The second design used three lens arrays, and achieved a simulated $> 70\%$ efficiency across the two-axis $\pm 40°$ field of view, with a divergence of the outgoing beam of less than $\pm 0.65°$.

The paper also reports on the physical proof-of-concept developed as part of the master's thesis leading up to this work [42].

Limitations and implications for further work

The use of phase-space optics to divide the optimization problem into smaller sub-problems was initiated before the development of the Python-based ray-tracer, and mainly as a consequence of limitations in Zemax OpticStudio making it difficult to optimize the complete system without dividing the problem into sub-problems. While this phase-space approach provides useful insights into the behavior of the optical system, it turned out to not be necessary for optimization once the in-house ray-tracer had been developed. In the work following this publication, the optical system was therefore treated more like a black box, optimizing the complete system simultaneously.

The $\pm 40^{\circ}$ tracking range permits 5.3 hours of stationary solar tracking, which is useful for demonstrating the idea but likely not sufficient for a practical implementation.

5.2 Paper 2

Title	High-concentration wide-angle tracking integration with stacked lens arrays
Authors	Håkon J. D. Johnsen, Jan Torgersen, Astrid Aksnes
DOI	10.1063/1.5124204
Type	Conference Paper
Publisher	AIP Conference Proceedings

The paper reports on the use of a numerical optimization-based design method which is used to optimize microtracking concentrators with much higher concentration ratios than what has previously been reported in the literature. One of the optimized configurations achieved an approximately 5000x concentration ratio across a two-axis $\pm 60°$ tracking range, and another achieved $> \ 2000x$ concentration across the same tracking range. This work shows that there is still a large unexplored region in the design space of microtracking solar concentrators, and that significantly improved concentration is achievable using more complex optical designs.

Limitations and implications for further work

The design of microtracking concentrators is a trade-off between performance and complexity. This paper explored designs towards the more complex end of that spectrum, and most likely at a complexity level where the results are not directly applicable for practical systems. Still, the results demonstrate that there is room for improving the performance of microtracking concentrators, and may motivate a search for other designs that find an appropriate balance between complexity and performance.

This work was carried out before developing the objective function listed in Chapter 3.2, and the system was therefore optimized with an explicitly chosen tracking range of $\pm 60°$ and a simple sum-scalarization to combine the efficiency and concentration objectives. The simulation results also assume ideal

systems with no manufacturing errors, and the optimization may therefore have favored designs that are more sensitive to such errors.

Additionally, the optimized systems are reported with a geometric concentration ratio varying as a function of incidence angle. This can be useful to see how the performance of the optics varies as a function of angle of incidence. However, in a practical microtracking concentrator for CPV applications, the PV cell is not going to change its size across the tracking range. It may therefore have been more relevant to report on the performance of the concentrator under a fixed geometric concentration ratio.

5.3 Paper 3

Title	Pushing the limits of beam-steering lens arrays
Authors	Håkon J. D. Johnsen, Astrid Aksnes, Jan Torgersen
DOI	10.1117/12.2528751
Type	Conference Paper
Publisher	Proceedings of SPIE

This paper explores how beam-steering lens arrays can be optimized specifically for stationary solar tracking using multi-objective optimization. It introduces the notion of optimizing a stationary tracking-integrated system for average yearly efficiency, and formulates a bi-objective optimization problem where the objectives are to maximize this average yearly efficiency while minimizing divergence half-angle of the redirected sunlight, as outlined in Section 3.2. The paper introduces the notation from Chapter 3.3 for describing beam-steering lens array configurations, and compares the beam-steering lens array configurations reported in Paper 1 to two new configurations with improved performance. One example configuration consists of four single-sided lens arrays that can track the sun with a yearly average efficiency of 74.4% into an exit-cone with divergence half-angle less than $\pm 1^\circ$. Another, simplified system consists of three single-sided lens arrays achieving 74.6% efficiency and a divergence half-angle of less than $\pm 2.2^\circ$, and might be relevant for low or medium concentration applications. These results demonstrate the multi-objective optimization based design method, and how the notation from Chapter 3.3 can be used to specify and optimize new beam-steering lens array configurations.

Limitations and implications for further work

The simulations in this paper did not take into account manufacturing errors, and therefore does not necessarily reflect the performance of physical implementation of the design. Additionally, only 4 different beam-steering lens array configurations were optimized, and it therefore did not constitute a thorough exploration of the design space.

5.4 Paper 4

Title	High-performance stationary solar tracking through multi-objective optimization of beam-steering lens arrays
Authors	Håkon J. D. Johnsen, Astrid Aksnes, Jan Torgersen
DOI	10.1364/OE.396477
Type	Journal Paper
Publisher	Optics Express

This paper uses the design method introduced in Paper 3 to optimize a large number of beam-steering lens array configurations. Additionally, it introduces a way to incorporate position and slope errors into the optimization, in order to optimize for designs that are more tolerant to such errors.

Using this approach, the paper reports on screening the full set of beam-steering lens array configurations that can be represented using the symbols introduced in Section 3.3 and with a maximum of one air-gap. Two designs from this optimization are highlighted in the paper, as well as in Section 4.1 of this thesis. One design with a ◀▶↓◀▶ configuration achieving 73.4% average yearly efficiency with a $< 2^\circ$ divergence half-angle, as well as a simplified design with a ◀▶↓▶ configuration achieving 75.4% efficiency with a $< 3.5^\circ$ divergence half-angle. These designs indicate the potential use of beam-steering lens arrays for stationary solar tracking. The higher divergence half-angles compared to Paper 3 are a result of assuming a certain set of manufacturing error in the optimization and simulation. The paper discusses and explores how this encourages the optimization algorithm to find designs less sensitive to such errors.

Limitations and implications for further work

The magnitude of the error distribution during simulation and optimization in this paper were selected to demonstrate the principle, but do not necessarily represent the manufacturing and tracking errors of a specific implementation. Before creating a physical implementation of these designs, the lens arrays

should be re-optimized with the expected tolerances for the selected manufacturing process and mechanical actuator.

The optimization performed in this paper assumes rotationally symmetric lens profiles packed hexagonally in a lens array. The expected angular distribution of sunlight reaching a stationary receiver is far from rotationally symmetric. Therefore, it may be beneficial to utilize freeform surfaces that can utilize this lack of symmetry for increased performance.

Additionally, this paper only explores the use of beam-steering lens arrays for stationary solar tracking. As outlined in Chapter 2.6, another possible application for beam-steering lens arrays is on a single-axis external tracker, to track across the second axis and use concentrating optics that utilize two-axis tracking. This may have been especially useful for the type of étendue-squeezing concentrator also explored in this thesis, and will be relevant for future exploration.

The beam-steering lens arrays in this paper are simulated as scale-independent geometrical optical systems, and no specific dimensions were selected for the simulation. Therefore, the designs can be arbitrarily scaled up or down for a physical implementation, as long as the size of the lenslets is large enough that diffractive effects are negligible. Several factors would affect the choice of dimensions for a physical implementation of the concept. Important factors to consider will be that larger lenslets lead to lower sensitivity to positioning errors (in absolute terms), including position errors caused by different thermal expansion of the different lens arrays in the stack. On the other hand, thinner lenslets lead to reduced material usage and reduced volume absorption losses in the resulting system. An evaluation of these different aspects was not carried out in this paper, and is left for further work.

5.5 Paper 5

Title	Beyond the 2D limit: Étendue-squeezing line-focus solar concentrators
Authors	Håkon J. D. Johnsen, Astrid Aksnes, Jan Torgersen
DOI	10.1364/OL.406280
Type	Journal Paper
Status	In Press at Optics Letters. Accepted November 17th, 2020.

This paper investigates the possibility of using étendue squeezing to develop a line-focus solar concentrator capable of concentrating beyond the 2D concentration limit. It provides a quick introduction to étendue squeezing and describes how the concept can be used for solar energy applications. The paper uses numerical optimization to design and simulate two design examples to demonstrate the principle, and the resulting designs are reported in Chapter 4.3.

Limitations and implications for further work

While demonstrating that étendue-squeezing can achieve high line-focus solar concentration, the demonstrated concentration is still quite far from the three-dimensional concentration limit. The different parameters selected in the two example designs were selected without much exploration, in order to demonstrate the concept. To further investigate the feasibility of this concept, a much more thorough exploration of the design space should be carried out.

The two-axis tracking may come from a stationary beam-steering lens array like the ones explored in Papers 3 and 4. However, the $\pm 1^\circ$ angular distribution assumed during optimization of these étendue-squeezing concentrators is smaller than what would be expected from such a stationary beam-steering lens array. Therefore, further work would be needed to explore étendue-squeezing solar concentrators designed for the larger divergence half-angles from stationary beam-steering lens arrays.

Alternatively, the two-axis tracking may come from a combination of one-axis external tracking and one-axis tracking from a beam-steering lens array, where the beam-steering lens array's reduced tracking requirements may improve tracking performance compared to what is reported in Papers 3 and 4. Optimization and simulation of a complete system combining these two approaches are left for further work.

6 Conclusions and further work

This thesis has investigated the achievable performance when using lens arrays to implement solar tracking and concentration. This includes a thorough screening of the performance of different beam-steering lens array configurations, an exploration of new microtracking configurations, and the development of a line-focus solar concentrator based on étendue-squeezing lens arrays. These developments were enabled by the development of a sequential ray-tracer designed specifically for tracking integrated optics, as well as the adoption of memetic and multi-objective optimization algorithms. Together, these results demonstrate how numerical optimization can be used to develop a broad range of lens-arrays suitable for solar tracking and concentration.

The presented results may not necessarily compete with conventional approaches for tracking & concentrating sunlight in their current form. Still, they demonstrate that there are unexplored regions in the design space of optical systems for tracking integration and solar concentration. With further development, it may be possible to identify designs that appropriately balance the trade-off between optical performance and complexity.

The work in this thesis has identified several promising directions for further research:

Single-axis external tracking All the tracking-integrated systems optimized during this work have been assumed to be stationary systems performing two-axis solar tracking. For several applications, it might be beneficial to still use a single-axis external tracker. As discussed in Chapter 2.6, this eliminates most of the cosine projection losses compared to a stationary system, while it can be implemented with significantly reduced mechanical bulk and complexity

compared to a dual-axis external tracker. Therefore, an important direction for further work would be to explore the same design methods used in this thesis, but applied to single-axis tracking.

Freeform surfaces All the beam-steering lens arrays and microtracking concentrators optimized in this thesis used rotationally symmetric lens profiles. The angular distribution of incident irradiation is not rotationally symmetric — whether it is a stationary orientation or on a one-axis external tracker. Therefore, there may be benefits of further exploring the design space of optical profiles that are not rotationally symmetrical.

Combining beam-steering lens arrays and étendue-squeezing The results from this thesis indicate that there may be a promising path towards combining beam-steering lens arrays and étendue-squeezing solar concentrators. Further work is needed to explore the potential of this approach. This would include the development of beam-steering lens arrays for one-axis external tracking as described above, as well as the combination of these beam-steering lens arrays with étendue-squeezing concentrators. An important question would be whether it is possible to design such a combined system while keeping the complexity and number of optical surfaces sufficiently low.

Applying optimization approaches to other design problems in nonimaging optics The numerical optimization in this thesis introduces several concepts that, as far as we know, have not previously been applied to optimization problems in nonimaging optics. This includes multi-objective optimization, memetic optimization, and the stochastic approach used to optimize for tolerance to manufacturing errors. These developments may therefore be of interest for identifying promising solutions to other design problems in nonimaging optics.

Physical proof-of-concept All the work in this thesis has been based on numerical simulation and optimization. The simulation is based on well understood geometrical optics, but there are still open questions regarding how well

they will perform under real-world conditions, manufacturing tolerances, and manufacturing constraints. The development of a physical demonstration of the concepts developed in this thesis will therefore be of interest.

In summary, this thesis has developed numerical optimization-based design methods suitable for designing tracking-integrated optical systems, and used this to explore the design space of beam-steering lens arrays, microtracking concentrators, and étendue-squeezing solar concentrators. These results may contribute towards the development of low-cost utilization of concentrated sunlight for both CPV and CSP applications, and the design method may be of interest for the broader field of nonimaging optics.

Bibliography

[1] Håkon J. D. Johnsen, Jan Torgersen, and Astrid Aksnes. Solar tracking using beam-steering lens arrays. *Proc. SPIE*, 10758:1075805, 2018.

[2] Håkon J. D. Johnsen, Jan Torgersen, and Astrid Aksnes. High-concentration wide-angle tracking integration with stacked lens arrays. *AIP Conference Proceedings*, 2149(1):070005, 2019.

[3] Håkon J. D. Johnsen, Astrid Aksnes, and Jan Torgersen. Pushing the limits of beam-steering lens arrays. *Proc. SPIE*, 11120:111200B, 2019.

[4] Håkon J. D. Johnsen, Astrid Aksnes, and Jan Torgersen. High-performance stationary solar tracking through multi-objective optimization of beam-steering lens arrays. *Optics Express*, 2020.

[5] Jared S. Price, Xing Sheng, Bram M. Meulblok, John A. Rogers, and Noel C. Giebink. Wide-angle planar microtracking for quasi-static microcell concentrating photovoltaics. *Nature Communications*, 6:6223, 2015.

[6] John William Humphrey, John Peter Oleson, Andrew Neil Sherwood, and Milo Nikolic. *Greek and Roman Technology: A Sourcebook : Annotated Translations of Greek and Latin Texts and Documents*. Psychology Press, 1998.

[7] Roland Winston, Juan C Minano, Pablo G Benitez, With contributions by Narkis Shatz and John C. Bortz, and John C Bortz. *Nonimaging Optics*. Elsevier Science, 2005.

[8] Julio Chaves. *Introduction to Nonimaging Optics, Second Edition*. CRC Press, 2015.

[9] Roland Winston, Lun Jiang, and Davoud Masoumi. Searching for a better way to concentrate light. *Proc. SPIE*, page 1, 2020.

[10] Carlos Algora and Ignacio Rey-Stolle. *Handbook of Concentrator Photovoltaic Technology*. Wiley, Chichester, West Sussex, United Kingdom, 1st edition edition, 2016.

[11] Ricardo Guerrero-Lemus and José Manuel Martínez-Duart. Concentrated Solar Power. In *Renewable Energies and CO2 : Cost Analysis, Environmental Impacts and Technological Trends- 2012 Edition*, pages 135–151. Springer London, London, 2013.

[12] Eugene A. Katz, Iris Visoly-Fisher, Daniel Feuermann, Reshef Tenne, and Jeffrey M. Gordon. Concentrated Sunlight for Materials Synthesis and Diagnostics. *Advanced Materials*, 30(41):1800444, 2018.

[13] R Núñez, I Antón, and G Sala. Proof-of-concept of a building-integrated hybrid concentrator photovoltaics-lighting system. *Lighting Research & Technology*, 50(7):1082–1090, 2018.

[14] Soteris A. Kalogirou. *Solar Energy Engineering: Processes and Systems*. Academic, 2013.

[15] G. K. Manikandan, S. Iniyan, and Ranko Goic. Enhancing the optical and thermal efficiency of a parabolic trough collector – A review. *Applied Energy*, 235:1524–1540, 2019.

[16] M. Brunotte, A. Goetzberger, and U. Blieske. Two-stage concentrator permitting concentration factors up to 300x with one-axis tracking. *Solar Energy*, 56(3):285–300, 1996.

[17] Brian Wheelwright, Roger Angel, and Blake Coughenour. Freeform lens design to achieve 1000X solar concentration with a parabolic trough reflector. In *Classical Optics 2014*, page ITh1A.2. Optical Society of America, 2014.

[18] Thomas Cooper, Gianluca Ambrosetti, Andrea Pedretti, and Aldo Steinfeld. Theory and design of line-to-point focus solar concentrators with tracking secondary optics. *Applied Optics*, 52(35):8586–8616, 2013.

[19] Mats Rönnelid and Björn Karlsson. Optical acceptance function of modified compound parabolic concentrators with linear corrugated reflectors. *Applied Optics*, 37(22):5222–5226, 1998.

[20] John C. Bortz, Narkis E. Shatz, and Roland Winston. Performance limitations of translationally symmetric nonimaging devices. *Proc. SPIE*, 4446:201–220, 2001.

[21] Johan Nilsson, Ralf Leutz, and Björn Karlsson. Micro-structured reflector surfaces for a stationary asymmetric parabolic solar concentrator. *Solar Energy Materials and Solar Cells*, 91(6):525–533, 2007.

[22] Panagiotis Kotsidas, Eleni Chatzi, and Vijay Modi. Stationary nonimaging lenses for solar concentration. *Applied Optics*, 49(27):5183–5191, 2010.

[23] Harry Apostoleris, Marco Stefancich, and Matteo Chiesa. Tracking-integrated systems for concentrating photovoltaics. *Nature Energy*, 1:16018, 2016.

[24] Edward A. Watson. Analysis of beam steering with decentered microlens arrays. *Proc. SPIE*, 32(11):2665–2670, 1993.

[25] Jacques Duparré, Daniela Radtke, and Peter Dannberg. Implementation of field lens arrays in beam-deflecting microlens array telescopes. *Applied Optics*, 43(25):4854–4861, 2004.

[26] Ata Akatay, Caglar Ataman, and Hakan Urey. High-resolution beam steering using microlens arrays. *Optics Letters*, 31(19):2861–2863, 2006.

[27] Wang Lin, Pablo Benitez, and Juan Carlos Miñano. Beam-steering array optics designs with the SMS method. *Proc. SPIE*, 8485:848505, 2012.

[28] Panagiotis Kotsidas, Vijay Modi, and Jeffrey M. Gordon. Nominally stationary high-concentration solar optics by gradient-index lenses. *Optics Express*, 19(3):2325–2334, 2011.

[29] W. C. Sweatt, B. H. Jared, G. N. Nielson, M. Okandan, A. Filatov, M. B. Sinclair, J. L. Cruz-Campa, and A. L. Lentine. Micro-optics for high-efficiency optical performance and simplified tracking for concentrated photovoltaics (CPV). *Proc. SPIE*, 7652:765210–765210–8, 2010.

[30] Justin M. Hallas, Katherine A. Baker, Jason H. Karp, Eric J. Tremblay, and Joseph E. Ford. Two-axis solar tracking accomplished through small lateral translations. *Applied Optics*, 51(25):6117, 2012.

[31] Fabian Duerr, Youri Meuret, and Hugo Thienpont. Tracking integration in concentrating photovoltaics using laterally moving optics. *Optics Express*, 19(103):A207–A218, 2011.

[32] Fabian Duerr, Youri Meuret, and Hugo Thienpont. Tailored free-form optics with movement to integrate tracking in concentrating photovoltaics. *Optics Express*, 21(103):A401–A411, 2013.

[33] Atsushi Ito, Daisuke Sato, and Noboru Yamada. Optical design and demonstration of microtracking CPV module with bi-convex aspheric lens array. *Optics Express*, 26(18):A879–A891, 2018.

[34] Gaël Nardin, Alvaro F. Aguilar, Laetitia Anglade, Mathilde Duchemin, Florian Gerlich, Mathieu Ackermann, Laurent Coulot, Delphine Petri, Jacques Levrat, Antonin Faes, Jonathan Champliaud, Nicolas Badel, Julien Brossard, Gabriel Christmann, Matthieu Despeisse, Stephen Askins, Norman Jost, César Domínguez, and Ignacio Antón. Towards industrialization of planar microtracking photovoltaic panels. *AIP Conference Proceedings*, 2149(1):040001, 2019.

[35] E. J. Tremblay, D. Loterie, and C. Moser. Thermal phase change actuator for self-tracking solar concentration. *Optics Express*, 20(106):A964–A976, 2012.

[36] H.N. Apostoleris, M. Chiesa, and M. Stefancich. Self-tracking concentrator based on switchable transparency and rejected-ray recycling. *Proc. SPIE*, 9572, 2015.

[37] Vinayak Narasimhan, Dongyue Jiang, and Sung-Yong Park. Design and optical analyses of an arrayed microfluidic tunable prism panel for enhancing solar energy collection. *Applied Energy*, 162:450–459, 2016.

[38] Leo D. DiDomenico. Towards doubling solar harvests using wide-angle, broad-band microfluidic beam steering arrays. *Optics Express*, 23(24):A1398–A1417, 2015.

[39] Noel León, Carlos Ramírez, and Héctor García. Rotating Prism Array for Solar Tracking. *Energy Procedia*, 57:265–274, 2014.

[40] R. Campbell and M. Machado. LOW cost CPV = Embedded CPV with internal tracker. In *2010 35th IEEE Photovoltaic Specialists Conference*, pages 003003–003007. IEEE, 2010.

[41] Kevin M. Flood, Bill Cassarly, Christina Sigg, and J.Michael Finlan. Continuous wide angle beam steering using translation of binary microlens arrays and a liquid crystal phased array. *Proc. SPIE*, 1211:296–304, 1990.

[42] Håkon J. D. Johnsen. Novel Low Cost Solar Thermal Energy Concepts for Developing Countries. *NTNU*, 2017.

[43] J. Bourderionnet, M. Rungenhagen, D. Dolfi, and H. D. Tholl. Continuous laser beam steering with micro-optical arrays: Experimental results. *Proc. SPIE*, 7113:71130Z, 2008.

[44] Jie Xiang, Nan Wu, Jian Zhang, and Liying Wu. Design of driving and control system based on Voice Coil Actuation for linear motion of microlens array. *Proc. SPIE*, 7133:713330, 2009.

[45] Thomas Huld, Tomáš Cebecauer, Marcel Šúri, and Ewan D. Dunlop. Analysis of one-axis tracking strategies for PV systems in Europe. *Progress in Photovoltaics: Research and Applications*, 18(3):183–194, 2010.

[46] Jorge Nocedal and Stephen Wright. *Numerical Optimization*. Springer, New York, 2nd edition edition, 2006.

[47] William J. Morokoff and Russel E. Caflisch. Quasi-Monte Carlo Integration. *Journal of Computational Physics*, 122:218–230, 1995.

[48] Shuhei Yoshida, Shuma Horiuchi, Zenta Ushiyama, and Manabu Yamamoto. Application and evaluation of quasi-Monte Carlo method in illumination optical systems. *Optics Express*, 20(9):9692–9697, 2012.

[49] Pablo Moscato et al. On evolution, search, optimization, genetic algorithms and martial arts: Towards memetic algorithms. *Caltech concurrent computation program, C3P Report*, 826:1989, 1989.

[50] Xianshun Chen, Yew-Soon Ong, Meng-Hiot Lim, and Kay Chen Tan. A Multi-Facet Survey on Memetic Computation. *IEEE Transactions on Evolutionary Computation*, 15(5):591–607, 2011.

[51] Panos M. Pardalos, Antanas Žilinskas, and Julius Žilinskas. *Non-Convex Multi-Objective Optimization*. Springer Optimization and Its Applications. Springer International Publishing, 2017.

[52] K. Deb, A. Pratap, S. Agarwal, and T. Meyarivan. A fast and elitist multiobjective genetic algorithm: NSGA-II. *IEEE Transactions on Evolutionary Computation*, 6(2):182–197, 2002.

[53] Q. Zhang and H. Li. MOEA/D: A Multiobjective Evolutionary Algorithm Based on Decomposition. *IEEE Transactions on Evolutionary Computation*, 11(6):712–731, 2007.

[54] Chi-Keong Goh, Yew Soon Ong, and Kay Chen Tan, editors. *Multi-Objective Memetic Algorithms*. Studies in Computational Intelligence. Springer-Verlag, Berlin Heidelberg, 2009.

[55] Juan C. Minano, Pablo Benitez, Yupin Sun, William A. Parkyn, Roberto Alvarez, and Waqidi Falicoff. Etendue-squeezing illumination optics, 2009.

[56] P Benítez, JC Miñano, et al. étendue squeezing optics: Beating the angle-space compromise of symmetrical systems. In *International Nonimaging Optics Workshop*, 2005.

[57] Ian Powell. Variable anamorphic lens for a 35-mm SLR. *Applied Optics*, 22(20):3249–3257, 1983.

[58] Pablo Benítez, Juan C. Miñano, and José Blen. Squeezing the Étendue. In *Illumination Engineering*, pages 71–99. John Wiley & Sons, Ltd, 2013.

[59] José Blen. *Design of Multiple Free-Form Optical Surfaces in Three Dimensions*. PhD thesis, Universidad Politécnica de Madrid, 2007.

[60] Justin M. Hallas, Jason H. Karp, Eric J. Tremblay, and Joseph E. Ford. Lateral translation micro-tracking of planar micro-optic solar concentrator. *Proc. SPIE*, page 776904, 2010.

[61] Siu Kwan Lam, Antoine Pitrou, and Stanley Seibert. Numba: A LLVM-based Python JIT Compiler. In *Proceedings of the Second Workshop on the LLVM Compiler Infrastructure in HPC*, LLVM '15, pages 7:1–7:6, New York, NY, USA, 2015. ACM.

[62] Furkan E. Sahin. Open-source optimization algorithms for optical design. *Optik*, 178:1016–1022, 2019.

[63] Atilim Gunes Baydin, Barak A. Pearlmutter, Alexey Andreyevich Radul, and Jeffrey Mark Siskind. Automatic differentiation in machine learning: A survey. *arXiv:1502.05767 [cs, stat]*, 2018.

[64] E.A. Watson, D.T. Miller, and K.J. Barnard. Analysis of fill factor improvement using microlens arrays. *Proc. SPIE*, 3276:123–134, 1998.

[65] Jeffrey M. Gordon. Aplanatic optics for solar concentration. *Optics Express*, 18(101):A41–A52, 2010.

[66] Emerson T. A. Gomes, Naum Fraidenraich, Olga C. Vilela, Carlos A. A. Oliveira, and Jeffrey M. Gordon. Aplanats and analytic modeling of their optical properties for linear solar concentrators with tubular receivers. *Solar Energy*, 191:697–706, 2019.

Full-text papers

A

Paper 1: Solar tracking using beam-steering lens arrays

Solar tracking using beam-steering lens arrays

Håkon J. D. Johnsen*[a], Jan Torgersen[a], and Astrid Aksnes[b]

[a]Department of Mechanical and Industrial Engineering, Norwegian University of Science and Technology, Trondheim, Norway
[b]Department of Electronic Systems, Norwegian University of Science and Technology, Trondheim, Norway

ABSTRACT

Conventional tracking solar concentrators track sunlight by rotating the concentrator optics to face the sun, which adds to the cost and bulk of the system. Beam-steering lens arrays, in contrast, allow solar tracking without bulk rotation of the optics. It consists of lens arrays stacked in an afocal configuration, and tracking is implemented by relative translation between these lens arrays. In this work, we present a phase-space methodology for analyzing and optimizing the performance of the beam-steering, and for revealing optical aberrations in the system. Using this methodology, we develop a beam-steering lens array with a simulated ≈70% efficiency across a two-axis ±40° tracking range, and a divergence of the outgoing beam of less than ±0.65°. We also present a functional small-scale prototype and demonstrate the feasibility of the concept for solar tracking. Beam-steering lens arrays can be placed in front of conventional concentrator optics and operated with little or no external tracking. This may enable low-cost robust concentrated solar power systems, and could also find other applications such as solar lighting and steerable illumination.

Keywords: beam-steering, lens arrays, solar tracking, micro-tracking, phase space

1. INTRODUCTION

Solar concentrators can provide highly concentrated solar power for applications such as concentrator photovoltaics, solar thermal energy, or solar lighting.[1] However, the concentrators require accurate solar tracking in order to achieve high concentration.[2] This tracking has traditionally been performed *external* to the concentrating optics, by mounting the concentrating optics to an external tracking system. The tracking system rotates the concentrating optics to keep it facing the sun, which introduces complicating factors including wind loads, the challenge of balancing the center of mass, and more complicated mechanical structures.[3]

As an alternative to external tracking, several studies[3–8] have recently considered *integrated* tracking, where an optical system tracks sunlight without being rotated towards the sun. Lin et al.[5] proposed a tracking-integrated beam-steering concept that emits collimated light, which can be used directly or passed on to a separate concentrator system as conceptually illustrated in Figure 1.

In this work, the beam-steering concept proposed by Lin et al is explored further, and we adopt the term beam-steering lens array (BSLA) for describing this type of concept.[†] First, the concept of BSLA for solar tracking is introduced, and discussed both from the perspective of paraxial optics and from the perspective of phase-space optics. Then, an optimization-based method is developed for designing BSLAs utilizing insights from phase-space optics. To demonstrate the feasibility of BSLA for large-range two-axis solar tracking, two different BSLA concepts are optimized using this design method. Finally, a physical proof-of-concept of a BSLA is presented.

* E-mail: hakon.j.d.johnsen@ntnu.no

[†]Related beam-steering concepts based on decentered lens arrays have previously been described using several different terms, including "beam steering with decentered microlens arrays",[9] "beam-deflecting microlens array telescopes",[10] "beam-scanning MLA system",[11] and "beam-steering array optics".[5] In this work, we choose to use "beam-steering lens arrays" (BSLA) as a general descriptive term for the concept of using decentered lens arrays for beam-steering.

Nonimaging Optics: Efficient Design for Illumination and Solar Concentration XV,
edited by Roland Winston, Eli Yablonovitch, Proc. of SPIE Vol. 10758, 1075805
 · doi: 10.1117/12.2320046

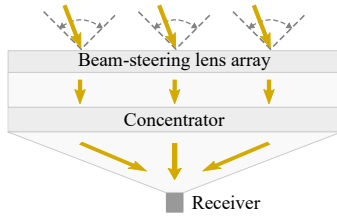

Figure 1: Conceptual illustration of how a beam-steering lens array can be combined with conventional concentrator optics.

2. BEAM-STEERING LENS ARRAYS

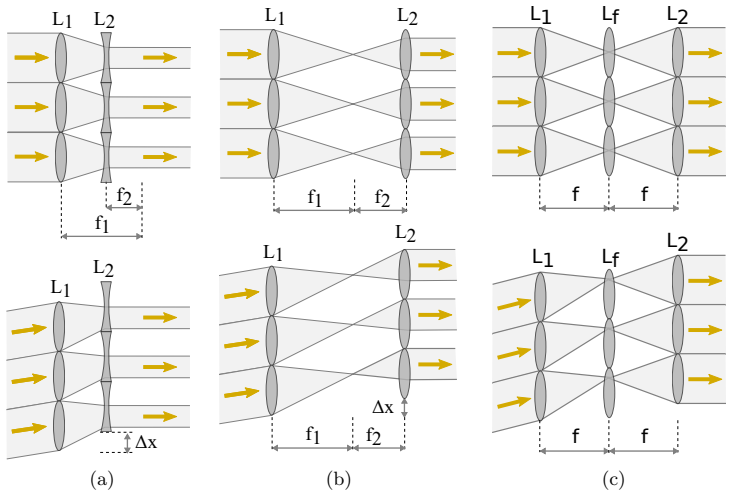

Figure 2: Paraxial beam-steering lens array principle using (a) Galilean configuration, (b) Keplerian configuration, and (c) Keplerian configuration including a field lens.

A basic BSLA consists of a pair of lens arrays arranged in an afocal configuration, allowing beam-steering by relative lateral translation of the two lens arrays as illustrated in Figure 2. This concept has previously been proposed for steering of laser beams.[9,11] Despite utilizing the same idea, there are some important differences between these laser applications and applications for solar energy:

- For laser beam-steering, a BSLA receives a beam parallel to its optical axis and emits it at an angle. For solar energy applications, the BSLA must be operated in reverse, receiving a beam at an angle, and emitting it parallel to the optical axis, as first proposed by Lin et al.[5]
- When used for solar energy, the BSLA must be orders of magnitude larger than when used for laser beam steering. This naturally also leads to larger lenslets.
- The coherence of laser light means that additional optics are required in order to allow for continuous laser beam steering.[11] This is not necessary for solar tracking, due to the reduced coherence of sunlight.

- The beam-steering range for laser beam-steering is typically on the order of 5° to 15°.[11–13] For solar tracking, much larger beam-steering angles are required.

Because of the large differences from previous laser applications, there is a need to re-think the concept and develop new design methods, which is the target of this work.

The idea behind this approach to beam-steering can be described both from the perspective of paraxial optics and from the perspective of phase-space optics.

2.1 Paraxial optics

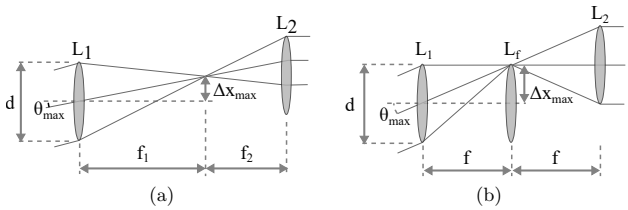

Figure 3: Geometry of a BSLA lenslet (a) without and (b) with a field lens, at maximum steering angle.

Figure 2a and Figure 2b show basic beam-steering lens arrays in Keplerian and Galilean configurations. The lens arrays are separated by their combined focal lengths $f_1 + f_2$. The BSLA can track incoming sunlight at an incidence angle θ by translating the last lens array a distance Δx such that the second lens array is always aligned with the focused image of the sun from the first lens array:

$$\Delta x \quad = \quad f_1 \cdot \tan\theta. \tag{1}$$

In order for all rays to reach the correct lens in the array L_2, the second focal length must be smaller than the first, as illustrated in Figure 3a. This leads to an angular magnification factor M:

$$M = \frac{f_1}{f_2} \quad = \quad 1 + 2\frac{f_1}{d}\tan\theta_{max}. \tag{2}$$

Sunlight has an inherent divergence of $\pm 0.27°$.[14] In order to limit the increase of divergence behind the BSLA and allow concentrators with high concentration factors, it is desirable that the angular magnification of the system is low. With two paraxial lenses, we therefore face a trade-off between the tracking range θ_{max}, and the additional divergence caused by angular magnification.

One approach to reduce this angular magnification is to add a field lens L_f to the BSLA in the Keplerian configuration, as shown in Figure 2c. With this approach, identical focal lengths f and an angular magnification of unity can be achieved.[9] However, with a field lens, the maximum tracking angle is limited to $\theta_{max} = \arctan\frac{d}{2f}$ as illustrated in Figure 3b.

2.2 Phase-space optics

A phase-space approach can be used to develop visual insight into the behavior and performance of a BSLA, and provides understandings that are useful in reducing the complexity of the design of such a system.

The trajectory of a ray in a geometrical optical system is determined by its position and direction. These parameters can be represented together in optical phase space, a space consisting of the linear dimensions as well as direction cosines of the optical ray. Phase-space optics is used to prove a number of important results in nonimaging optics,[2] and is also useful in visualizing the performance and aberrations of optical systems.[15]

For three-dimensional systems, four parameters are required to describe a ray-bundle crossing a surface - two directional parameters and two physical parameters. The phase-space representation of a three-dimensional optical system is therefore not very easy to visualize. However, much information about the system can be extracted from the two-dimensional counterpart, where ray-bundles crossing a surface can be described using only two parameters.[15]

Figure 4 shows the optical behavior of a paraxial BSLA from a phase-space perspective. At each indicated surface, ray-bundles from the whole tracking range are plotted in two-dimensional phase-space with their position x, and direction $p = n \cdot \sin\theta$. This illustrates the different transformations performed by the system: The lenses are used to convert a collimated beam with an angular offset into a focused ray-bundle with translational offset. This focused ray-bundle can then easily be tracked mechanically before being transformed back into a collimated beam.

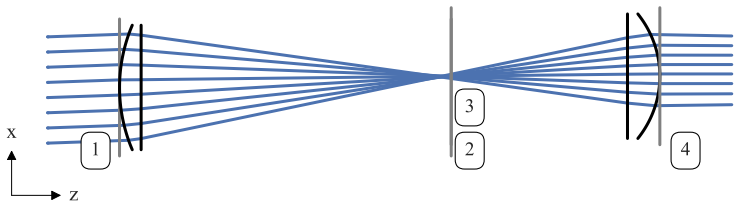

(a)

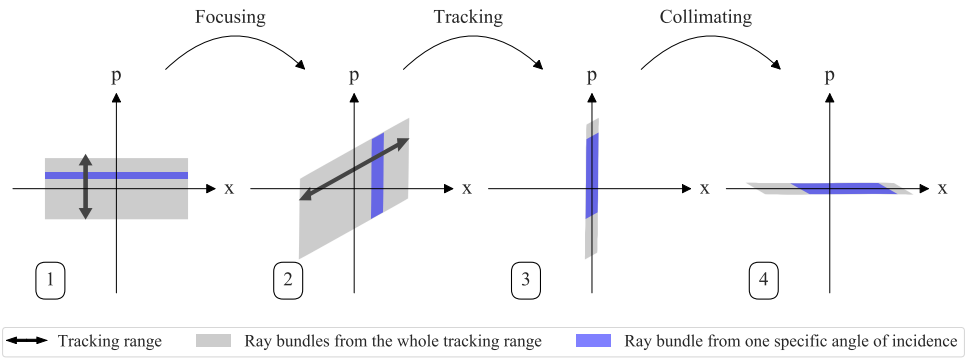

(b)

Figure 4: (a) Simple two-dimensional BSLA without field lens. (b) Sketch of the phase-space transformations performed by a two-dimensional paraxial BSLA. An incoming collimated ray bundle has a certain offset in direction p. The focusing lens transforms the rays into a focused bundle with a certain offset in position x. The tracker performs a coordinate transformation to center this position. Finally, the collimating lens transforms the rays into a centered collimated beam.

Figure 4 indicates that the phase-space transformation performed by the focusing lens has very different requirements from the phase-space transformation performed by the collimating lens:

- The focusing transformation is heavily overdetermined. From each separate tracking angle, the focusing lens should transform the incoming ray-bundle into a ray-bundle with a consistent phase-space geometry. The design problem is therefore very similar to design problems in conventional imaging optics, with one

important relaxation: the focused wavefronts should be *consistent*, but not necessarily *spherical*. This difference is further discussed and illustrated below.

- The collimating transformation should transform a single ray-bundle into a narrow collimated ray-bundle. This is a variant of the bundle-coupling problem of Nonimaging Optics, and well known design methods such as the Simultaneous Multiple Surface (SMS) method can give optimal or close to optimal solutions to this problem.[2]

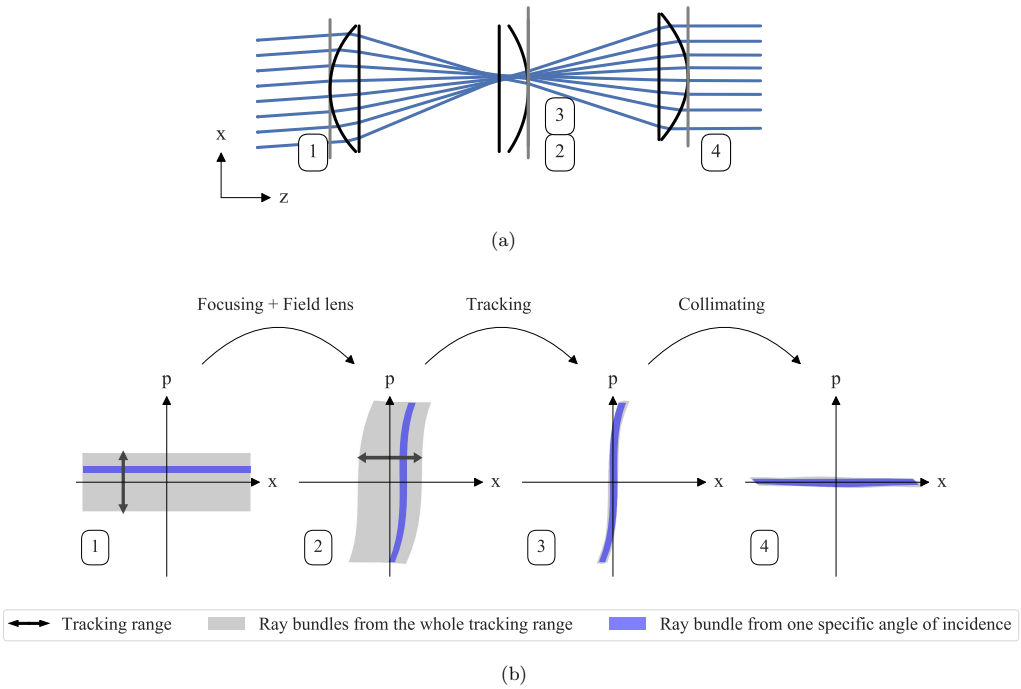

Figure 5: (a) Simple two-dimensional BSLA with field lens. (b) Phase-space transformations by this BSLA. The two first lenses are spherical, which is visible in the spherical aberration at surface 2 and 3. This spherical aberration is corrected by the final lens, which is aspherical.

Figure 5 shows phase-space plots of a real BSLA with a field lens, illustrating the difference between the focusing (and field) lens in a BSLA and a conventional imaging system. For illustration purposes, the focusing and field lenses in this system are spherical, leading to significant spherical aberration. This spherical aberration is visible as curved shapes in the second and third phase-space plots of Figure 5, and the lenses would therefore work poorly as an imaging system. As part of a BSLA however, the collimating lens is able to compensate for the spherical aberration. This is the major distinction between an imaging lens and the focusing lens in a BSLA: The performance of an imaging system depends on how well rays from a single field of the input, p, are mapped onto a position, x. In other words, it depends on the edges to be vertical in phase-space plot 2 of Figure 5. The performance of a BSLA on the other hand, does not require focusing to a perfect point. Instead, performance depends on the size of the total phase-space area to be collimated by the collimating lens. This area can be reduced by making ray-bundles from all the different incidence angles overlap as much as possible after tracking, as they do in phase-space plot 3 of Figure 5.

It is possible to estimate the performance of a BSLA directly without its collimating lens, by utilizing the properties of the phase-space transformations. Assuming that the collimating transformation can be solved with close to optimal performance, BSLA-performance can be predicted by evaluating the total occupied area in phase-space by all ray-bundles after tracking. The evaluated area is the etèndue of the ray-bundles,[15] and assuming optimal etèndue-conserving collimation, this directly gives the etèndue and the divergence of the collimated beam. This concept will be used for subdividing and simplifying the optimization problem for designing a BSLA.

3. OPTIMIZATION OF BEAM-STEERING LENS ARRAY

An optimization approach is developed for designing a three-dimensional BSLA. Optimization methods are more computationally expensive and less stable than direct solution methods, but they have the benefit that they readily handle overdetermined problems with the complexities of real-world systems such as wavelength dependent effects and manufacturing constraints.

3.1 Practical considerations

In order to implement a BSLA with high efficiency over a large two-axis field of view, some modifications must be done to the basic principles in Figure 2:

- The field lens in Figure 2c improves performance, but limits the tracking range to $\theta_{max} = \arctan \frac{d}{f}$. It can either be removed, or it can be allowed to move as part of the tracking motion in order not to limit the system's tracking range.
- For wide field of view, field curvature becomes significant, and planar tracking is not sufficient. Tracking is therefore allowed to follow a curved trajectory.
- For tight packing in a lens array, close-packed hexagonal lenses are used instead of circular lenses.
- The wide field of view and limited number of optical surfaces introduce large aberrations, which are compensated for by using thick lenses and allowing each lens surface to have an aspherical profile.

3.2 Formulation of optimization problem

We will consider three main performance indicators for quantifying and evaluating the performance of a complete BSLA:

- Maximizing tracking range
- Maximizing efficiency
- Minimizing divergence

The design of a BSLA can be considered a multi-objective optimization problem, where a solution must be found that provides a reasonable trade-off between these three performance indicators. Improving one of these indicators can be done at the cost of lower performance in the other indicators. For example increasing the tracking range will increase the off-axis optical aberrations, leading to increased divergence of the outgoing rays. Increasing the efficiency on the other hand imposes additional constraints on the system, leaving fewer degrees of freedom for handling the optical aberrations and decreasing divergence. Multi-objective optimization algorithms can be used to find a set of Pareto optimal solutions for these types of problems,[16] quantifying these trade-offs and allowing the designer to make an informed choice among the set of solutions. However, in order to limit the scope of this work, the optimization problem is reduced to a single-objective optimization problem in the following way:

- A sum scalarization[16] is performed to combine the efficiency and divergence into a single objective function.
- The racking range is fixed to a single value. In the design examples in this work, the value of $\pm 40°$ is chosen as an example of a relatively wide tracking range.

A sum scalarization allows optimization using simpler single-objective optimization algorithms, and a solution to the scalarized problem is also a solution to the original multi-objective problem.[16] However, this approach has the drawback that it gives only a single solution and therefore no information about the trade-off between the different performance indicators. The result is the following optimization problem

$$\min f(\mathbf{x}) = \sum_{i=1}^{m} \left(w_1 \frac{1}{\eta_i(\mathbf{x})} + w_2 \left(\delta\theta_i(\mathbf{x})\right)^2 \right) \tag{3}$$

$$\text{such that } g_j(\mathbf{x}) \leq 0 \tag{4}$$

where w_1 and w_2 are relative weights applied to the efficiency and divergence. $\eta_i(\mathbf{x})$ is the simulated efficiency for a ray-traced grid of rays with incidence angle number i and optical system described by $\mathbf{x}$. $\delta\theta_i(\mathbf{x})$ is the corresponding RMS divergence half-angle for field number i. m separate incidence angles are evaluated across the tracking range of the BSLA. $g_j(\mathbf{x})$ is a set of inequality constraints ensuring manufacturability, such as minimum and maximum thickness, and maximum lens curvature.

3.2.1 Separation of optimization procedure using phase-space optics

The optimization problem in Equations 3 and 4 can in theory be solved directly for the complete system, using ray-tracing simulations and a suitable optimization algorithm. However, it is a non-linear non-convex optimization problem with many variables, with no guarantee of finding the global minimum.

In order to reduce the complexity of the optimization problem and to increase the chance of finding a global minimum, the phase-space analysis from Section 2.2 can be utilized to subdivide the optimization problem. This gives the following final design process:

1. *Optimize focusing lens (and field lens, if included).* The optimization problem in Equations 3 and 4 is solved. $\eta_i(\mathbf{x})$ and $\delta\theta_i(\mathbf{x})$ are estimated by evaluating the volume in phase-space occupied by the set of bundles focused by the focusing (and field) lens. $\mathbf{x}$ contains only parameters varying the geometry of the focusing (and field) lens. The analysis in Section 2.2 considered only two-dimensional systems, but this volume estimate is readily extended to three-dimensional systems by assuming rotational symmetry of the collimating lens.

2. *Optimize a collimating lens for the optimized focusing lens.* The same optimization problem in Equations 3 and 4 is solved, but now $\eta_i(\mathbf{x})$ and $\delta\theta_i(\mathbf{x})$ are evaluated directly from ray-tracing results of the complete system, and $\mathbf{x}$ contains only parameters for the geometry of the collimating lens. This step might also be performed using a direct method such as the SMS method, bypassing the need for optimization in this step.

3. *Refine the complete system* by performing an optimization step where $\mathbf{x}$ contains all parameters for the complete system. This allows for any final improvements that were not achieved when optimizing separately due to inaccuracies in the phase-space model. For instance, the phase-space evaluation assumes a rotationally symmetric system, while the lenses are actually hexagonal when closely packed in an array. Some small additional improvements can therefore be gained by this final optimization step, and step 1 and 2 can be considered as a way to get a good initial starting point for this final optimization step.

4. DESIGN EXAMPLE

4.1 Methods

Two different systems were optimized using the optimization procedure outlined in Sections 3.2 & 3.2.1.

- One BSLA with three lens arrays: A focusing lens, a movable field lens, and a collimating lens. This was chosen in order to demonstrate how the benefits of a field lens can be extended to large tracking ranges when the field lens is allowed to move.

- One BSLA with only two lens arrays: A focusing lens and a collimating lens. This was chosen in order to demonstrate a BSLA without the mechanical complexity of the movable field lens.

Both BSLAs were simulated across the AM1.5D solar spectrum,[17] with Poly(methyl methacrylate) (PMMA) as lens material, using a custom sequential three-dimensional ray-tracer. The ray-tracer was written in Python and accelerated using Numba.[18] Optimization was performed using a combination of the Differential Evolution, Basinhopping and L-BFGS-B-algorithms available from SciPy.[19]

Table 1: Constraints used in optimization of BSLA. The dimensions of the system are scalable with the arbitrary scaling factor k.

Parameter	Constraint
Semi-diameter of lenses	$1.0 \cdot k$
Minimum thickness at thinnest point of lens	$0.5 \cdot k$
Maximum thickness at thickest point of lens	$2.0 \cdot k$
Minimum air gap between lenses	$0.05 \cdot k$
Maximum air gap between lenses	$2.0 \cdot k$
Minimum radius of curvature on lens	$0.7 \cdot k$
Maximum aspect ratio of single surface	0.5

Fresnel reflections and dispersion were taken into account, while material absorption was ignored*. Hexagonal lenses were used for all simulations to allow for close packing in a lens array. The divergence of outgoing light was estimated as a combination of divergence due to optical aberrations, and divergence due to magnification of the inherent divergence of sunlight.

The constraints from Table 1 were used to ensure reasonable, manufacturable designs. For the design with a field lens, the lateral translation of the two lens arrays were constrained to be proportional to each other, allowing linked control sharing the same mechanical actuator.

Plots of efficiency and divergence half-angle are created using ray-tracing of 80 000 random rays per incidence angle, with random wavelengths according to the AM1.5D spectrum and random directions within the 0.27° divergence half-angle of sunlight. The plotted divergence half-angle is defined as the half-angle encircling 90% of the transmitted energy. The plotted efficiency takes into account Fresnel reflections, but does not consider material absorption or cosine projection loss.

4.2 Results and discussion

The resulting optimized design with a field lens is shown in Figure 6a, and the system without a field lens is shown in Figure 6b. The simulated optical performance under solar irradiation is shown in Figure 7. The system with a field lens has lower optical efficiency at low angles of incidence, due to the increased number of optical surfaces. However, at high incidence angles, it still surpasses the efficiency of the system without a field lens.

The additional divergence introduced by the BSLA requires the use of concentrator optics with higher acceptance angle, decreasing the maximum achievable concentration ratio. However, the results in Figure 7 show that by including a field lens, this final divergence half-angle can be kept at less than 0.65° across the tracking range, which will still permit approximately 7800x concentration from an ideal concentrator.[2]

With increased angle of incidence, intensity of sunlight received by a flat stationary receiver decreases due to the cosine projection effect. Even if the lens design is improved with a higher acceptance angle, power will therefore be low for high angles of incidence, and some amount of external tracking might be required for

*Material absorption depends on the physical dimensions of the BSLA, which are not fixed in these design examples

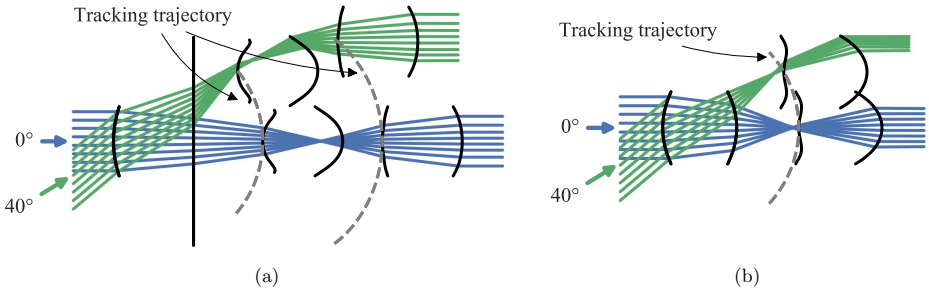

Figure 6: Ray-traced sketch of optimized system (a) with, and (b) without field lens.

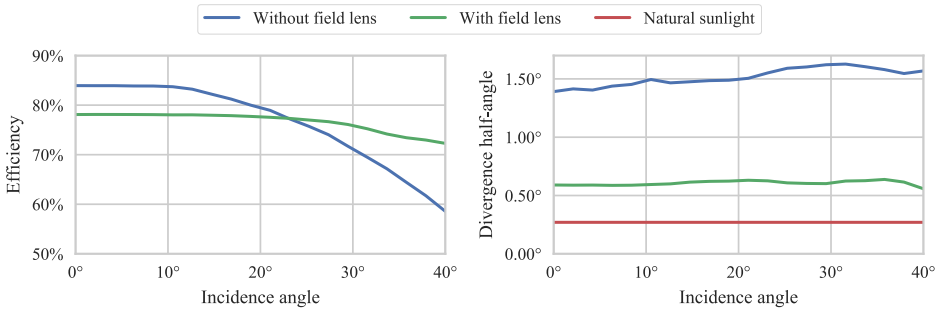

Figure 7: Simulated optical performance with and without field lens. Using a field lens reduces divergence significantly at the cost of increased mechanical complexity. Inherent divergence of natural sunlight is included for reference.

efficient full-day operation. Yet, we conclude that the use of beam-steering lens arrays still significantly reduces the requirements for this external tracking.

Figure 8 shows two-dimensional phase-space plots of the optimized systems. The phase-space plots are generated at the focal point after tracking. As discussed in Section 2.2, performance of the focusing transformation depends on how well the ray-bundles from one specific wavelength and angle of incidence overlap with all other ray bundles. For the BSLA without field lens (Figure 8b) we can see that the optimization algorithm has chosen a focusing lens where the shape of the total occupied area in phase-space is strongly nonlinear, but this is not a problem for the collimating lens. We can also see that ray-bundles from different wavelengths don't overlap very well, indicating significant chromatic aberration. For the BSLA with field lens, in Figure 8a, we see that the field lens is able to significantly improve the overlap of the ray-bundles, especially the overlap in momentum. In addition, the ray-bundles for different wavelengths overlap more. This leads to the reduced divergence after collimation and improved performance.

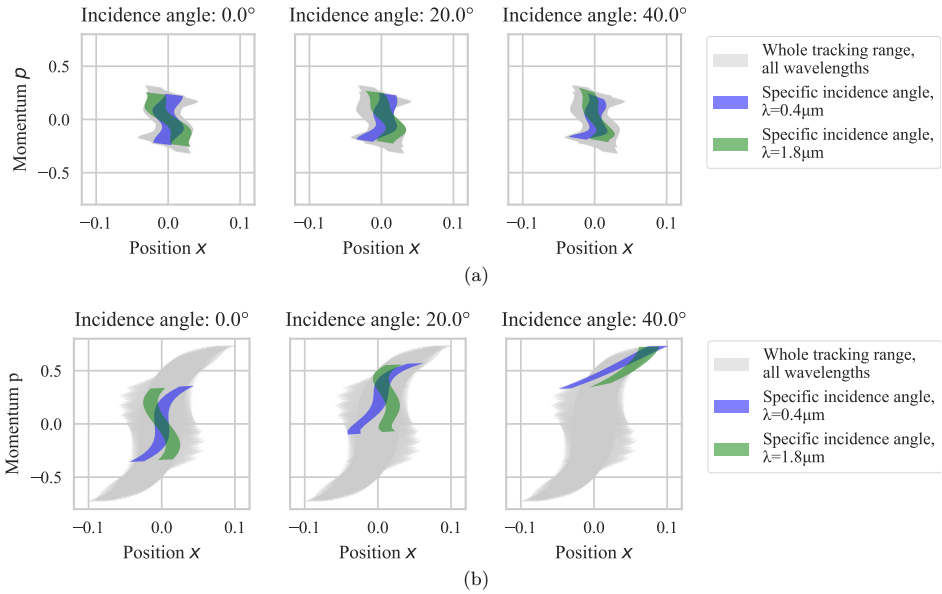

Figure 8: Two-dimensional phase-space plots at focal point. For system (a) with, and (b) without field lens.

5. PROOF-OF-CONCEPT

A physical and functional proof-of-concept with automatic tracking has been created using a previously optimized BSLA design. The design was created using an earlier optimization technique, with lower performance.[20] Despite this lower performance, the proof-of-concept serves to demonstrate the feasibility of creating a complete, functional BSLA. As an example use case for this proof-of-concept, the BSLA has been attached to an off-axis parabolic reflector that illuminates a target from the underside. This specific configuration is a scaled-down version of a solar cooking concept using BSLA.

5.1 Manufacturing and testing methods

Compression molds for the lens arrays were machined in aluminum on an in-house Computer Numerical Control (CNC) milling machine, due to the lack of access to high-precision optical manufacturing equipment. These molds were used for compression molding of PMMA plates.

The tracking motion is actuated using SG-92R micro servos and controlled from an Arduino Nano development board. The system uses a combination of open- and closed-loop control, and both control loops have been implemented with low-cost photocells: Approximate solar position is detected using a set of four inclined photocells, each inclined ±40° from the front plane about their respective axes. The four photocells sense different relative brightness values due to their different angle towards the sun and the cosine projection loss. From this data, the incidence angle of the sunlight can be inferred. The microcontroller orients the BSLA to this approximate angle. Secondly, the tracking is fine-tuned by diverting a small section of the input aperture to a set of photocells that measure tracking error, and a closed control loop is implemented in order to minimize this tracking error.

An image analysis setup was used for testing the optical performance of the completed BSLA, as reported in earlier work.[20]

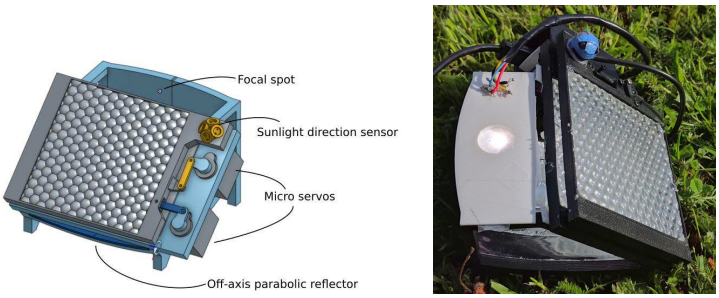

(a) (b)

Figure 9: (a) 3D model of Proof-of-concept with concentrator (b) Video of proof-of-concept tested outside in the sun. http://dx.doi.org/10.1117/12.2320046.1

5.2 Results

A 3D model of the proof-of-concept attached to a concentrator is shown in Figure 9a, and the device is shown outside in the sun in Figure 9b.

Figure 10 shows the measured optical performance of the proof-of-concept BSLA, compared to simulated values. The results show ≈ 10% reduced efficiency compared to the simulated values, and approximately a doubling of divergence compared to simulation. The high divergence is likely a result of a waviness in the surface of the lens array, due to the low precision of the mold manufacturing process. With improved mold manufacturing and corresponding increased surface quality, future prototypes are expected to better follow the predicted performance.

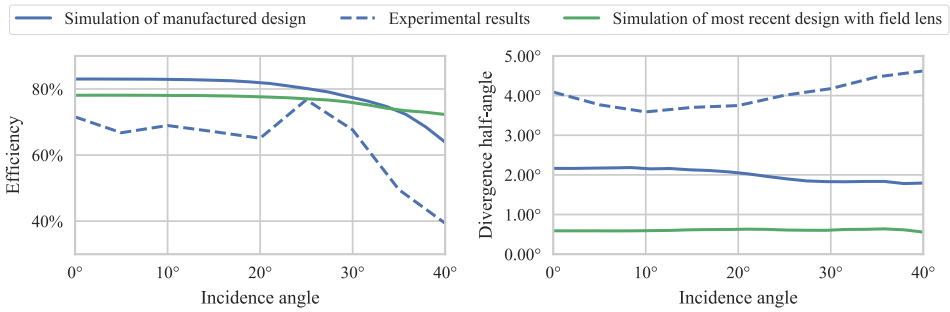

Figure 10: Simulated and measured efficiency and divergence of the proof-of-concept over its field of view.

6. OUTLOOK AND CONCLUSIONS

We have shown that beam-steering lens arrays can be used to track and redirect sunlight with low losses over a two-axis ±40˚ tracking range, and we have presented an optimization-based design method for designing such systems. We have also demonstrated a physical proof-of-concept, demonstrating its practicality in the real world. Further work will involve exploration of the solution space, by mapping the trade-off between tracking range, efficiency, and divergence, as well as the impact of the selected manufacturing constraints. We are also planning to create a new proof-of-concept according to updated BSLA designs, and with improved manufacturing methods.

Beam-steering lens arrays can be made from common low-cost materials such as PMMA, and they can be compatible with high-volume production techniques such as injection molding or hot embossing. They may therefore foster the development of low-cost, small-scale solar energy systems for a number of applications including solar cooking, small-scale solar thermal processing, solar water heating, concentrator photovoltaics and solar lighting.

REFERENCES

[1] Xie, W. T., Dai, Y. J., Wang, R. Z., and Sumathy, K., "Concentrated solar energy applications using Fresnel lenses: A review," *Renewable and Sustainable Energy Reviews* **15**, 2588–2606 (Aug. 2011).

[2] Winston, R., Minano, J. C., Benitez, P. G., contributions by Narkis Shatz and John C. Bortz, W., and Bortz, J. C., [*Nonimaging Optics*], Saint Louis : Elsevier Science, Saint Louis (2005).

[3] Apostoleris, H., Stefancich, M., and Chiesa, M., "Tracking-integrated systems for concentrating photovoltaics," *Nature Energy* **1**, 16018 (Mar. 2016).

[4] Grede, A. J., Price, J. S., and Giebink, N. C., "Fundamental and practical limits of planar tracking solar concentrators," *Optics Express* **24**, A1635–A1646 (Dec. 2016).

[5] Lin, W., Benitez, P., and Miñano, J. C., "Beam-steering array optics designs with the SMS method," *Proc. SPIE* **8485**, 848505–848505–7 (2012).

[6] Campbell, R. and Machado, M., "LOW cost CPV = Embedded CPV with internal tracker," in [*2010 35th IEEE Photovoltaic Specialists Conference (PVSC)*], 003003–003007 (June 2010).

[7] Duerr, F., Meuret, Y., and Thienpont, H., "Tailored free-form optics with movement to integrate tracking in concentrating photovoltaics," *Optics Express* **21**, A401–A411 (May 2013).

[8] Hallas, J. M., Baker, K. A., Karp, J. H., Tremblay, E. J., and Ford, J. E., "Two-axis solar tracking accomplished through small lateral translations," *Applied Optics* **51**, 6117 (Sept. 2012).

[9] Watson, E. A., "Analysis of beam steering with decentered microlens arrays," *Optical Engineering* **32**(11), 2665–2670 (1993).

[10] Duparré, J., Radtke, D., and Dannberg, P., "Implementation of field lens arrays in beam-deflecting microlens array telescopes," *Applied Optics* **43**, 4854–4861 (Sept. 2004).

[11] Akatay, A., Ataman, C., and Urey, H., "High-resolution beam steering using microlens arrays," *Optics Letters* **31**, 2861–2863 (Oct. 2006).

[12] Bourderionnet, J., Rungenhagen, M., Dolfi, D., and Tholl, H. D., "Continuous laser beam steering with micro-optical arrays: Experimental results," *Proc. SPIE* **7113**, 71130Z, International Society for Optics and Photonics (Oct. 2008).

[13] Xiang, J., Wu, N., Zhang, J., and Wu, L., "Design of driving and control system based on Voice Coil Actuation for linear motion of micro-lens array," *Proc. SPIE* **7133**, 713330, International Society for Optics and Photonics (Jan. 2009).

[14] Kalogirou, S. A., [*Solar Energy Engineering: Processes and Systems*], Academic Press (Oct. 2013).

[15] Herkommer, A. M., "Phase space optics: An alternate approach to freeform optical systems," *Proc. SPIE* **53**, 031304 (Dec. 2013).

[16] Pardalos, P. M., Žilinskas, A., and Žilinskas, J., [*Non-Convex Multi-Objective Optimization*], Springer Optimization and Its Applications, Springer International Publishing (2017).

[17] Renewable Resource Data Center, "Solar Spectral Irradiance: Air Mass 1.5." https://rredc.nrel.gov/solar/spectra/am1.5/.

[18] Lam, S. K., Pitrou, A., and Seibert, S., "Numba: A LLVM-based Python JIT Compiler," in [*Proceedings of the Second Workshop on the LLVM Compiler Infrastructure in HPC*], *LLVM '15*, 7:1–7:6, ACM, New York, NY, USA (2015).

[19] Jones, E., Oliphant, T., Peterson, P., and others, "SciPy: Open source scientific tools for Python," (2001).

[20] Johnsen, H. J. D., "Novel Low Cost Solar Thermal Energy Concepts for Developing Countries," *NTNU* (2017).

Paper 2: High-concentration wide-angle tracking integration with stacked lens arrays

High-Concentration Wide-Angle Tracking Integration with Stacked Lens Arrays

Håkon Jarand Dugstad Johnsen[1, a)], Jan Torgersen[1], and Astrid Aksnes[2]

[1] *Norwegian University of Science and Technology, Department of Mechanical and Industrial Engineering, Richard Birkelands Vei 2b, Trondheim, Norway*
[2] *Norwegian University of Science and Technology, Department of Electronic Systems, O.S. Bragstads plass 2b, Trondheim, Norway*

[a)] Corresponding author: hakon.j.d.johnsen@ntnu.no

Abstract. Tracking-integration can reduce or eliminate the need for external solar tracking in CPV (concentrator photovoltaics). Previous research has shown how tracking-integrated systems can achieve high concentration ratios, wide tracking ranges, and compatibility with low-cost high-volume manufacturing methods. However, to our knowledge, no existing concept has demonstrated high performance in all of these objectives at the same time. We show how a numerical optimization-based design method can be used to develop high-performance tracking-integrated configurations. We then present a configuration maintaining an approximately 5000x geometric concentration ratio across a two-axis ±60° tracking range, while also being compatible with low-cost manufacturing processes. By significantly increasing the achievable concentration ratio of low-cost tracking integrated systems, these systems may improve the competitiveness for concentrator photovoltaics. This can also lead to new applications such as high efficiency rooftop-mountable or vehicle-mountable CPV.

INTRODUCTION

Concentrator photovoltaics (CPV) promises improved efficiency compared to flat-panel Silicon photovoltaics [1], but this requires highly accurate solar tracking. Solar tracking is usually implemented using an external dual-axis tracking system, which adds to the bulk and cost of the installation. The large mechanical size can also make these trackers unsuitable for small-scale installations such as rooftop or vehicle-mountable CPV.

Tracking-integrated concentrator-schemes have been proposed as a way to mitigate this problem by reducing or removing the need for external solar trackers [2]. Kotsidas et al. proposed a system where an array of solar cells is moved relative to a stationary lens array in order to track the sun [3], and Hallas et al. proposed a similar system where an array of waveguide coupling features are moved relative to a stationary lens array [4]. Duerr et al. proposed a system where a pair of lens arrays are moved relative to each other to concentrate sunlight onto a moving lens array [5]. Price et al. proposed a system where a catadioptric optical stack creates a very flat image plane, and solar tracking is implementing by moving an array of microcells in this image plane [6].

In this work, we present an optimization-based design method for designing tracking-integrated CPV systems, and use this method to combine the novel catadioptric stack proposed by Price et al. with the idea of relative motion between lens arrays as proposed by Duerr et al. These new configurations achieve concentration ratios on the order of 5000x across a ±60° tracking range.

DESIGN METHOD

A tracking-integrated CPV concentrator should concentrate incident solar radiation with (1) the highest possible efficiency, (2) across the largest possible tracking range, and (3) onto the smallest possible surface of a PV cell. The

15th International Conference on Concentrator Photovoltaic Systems (CPV-15)
AIP Conf. Proc. 2149, 070005-1–070005-6; https://doi.org/10.1063/1.5124204
Published by AIP Publishing. 978-0-7354-1894-3/$30.00

design of a tracking-integrated CPV concentrator can therefore be considered a multi-objective optimization problem where the goal is to find a design that optimizes these three objectives.

We have chosen a design method based on numerical optimization. The objective function is scalarized using a sum scalarization of the efficiency and concentration ratio objectives:

$$\min f(x) = \sum_{i=1}^{m} (w_1 \frac{1}{\eta_i(x)} + w_2 \left(r_i(x)\right)^2 \quad (1)$$

$$\text{such that } g_j(x) \leq 0, \quad (2)$$

where $\eta_i(x)$ is the simulated optical efficiency for a grid of rays with incidence angle number i and optical system described by the parameters x. $r_i(x)$ is the RMS radius of the rays in field number i relative to the position of the PV cell for this angle of incidence. w_1 and w_2 are relative hand-tuned weights applied to optical efficiency and RMS radius. $g_j(x)$ is a set of constraints ensuring manufacturability of the design.

A set of constraints were selected as shown in Table 1. These constraints were chosen as example values in order to demonstrate how manufacturing requirements can be taken into account in the optimization process. When choosing a manufacturing method, these constraints should be updated to match the requirements of the specific process. All lenses were assumed to be made from PMMA as an example of an injection-moldable thermoplastic with good optical properties, and reflective lens arrays were assumed to be silver coated. We have chosen a fixed two-axis tracking range of ±60° for the optimization.

TABLE 1. Constraints used when optimizing the different CPV configurations. The dimensions of the system are scalable with the arbitrary scaling factor k.

Parameter	Value
Semi-diameter of lenses	$1.0 \cdot k$
Minimum thickness at thinnest point of lens	$0.4 \cdot k$
Maximum thickness at thickest point of lens	$2.5 \cdot k$
Minimum air gap between lenses	$0.05 \cdot k$
Maximum air gap between lenses	$4 \cdot k$
Minimum radius of curvature on the lens	$0.5 \cdot k$
Maximum aspect ratio of a single surface	0.5

A custom-built three-dimensional sequential ray-tracer was used to simulate the optical system, as reported in a previous publication [7]. The ray-tracer takes into account reflection losses and chromatic aberration in the PMMA lens arrays. The material is assumed to be non-absorptive, because absorption losses depend on system dimensions which were not fixed in this work. The surface profile is aspheric and rotationally symmetric, and modelled as an even polynomial with 4 terms. The lenses were assumed to be hexagonally packed in a lens array.

The numerical optimization problem was solved using memetic optimization, a class of optimization algorithms that combine evolutionary algorithms and their ability to search a large design space for an approximate global minimum, with the ability of local gradient-based algorithms to quickly and accurately identify a local minimum. We implemented a memetic optimization algorithm based on Qin et al.'s local search chains [8]. The differential evolution solver from SciPy [9] was extended to evolve the population using local search chains based on SciPy's SLSQP optimization algorithm in parallel to the differential evolution algorithm.

Three different configurations were optimized:

- **Simple catadioptric**: A catadioptric stack with an embedded translatable array of microcell PV, as conceptually illustrated in Fig. 1a and first proposed by Price et al. [6]
- **Flat tracking trajectory**: A catadioptric stack similar to *simple catadioptric*, but all lens arrays are allowed to move laterally relative to each other, and an additional pair of lens arrays are added to the front, as conceptually illustrated in Fig. 1b.
- **Curved tracking trajectory**: A catadioptric stack similar to *flat tracking trajectory*, but the lens arrays are allowed to follow a curved tracking trajectory at the air gap between the two pairs of lens arrays as illustrated in Fig. 1c.

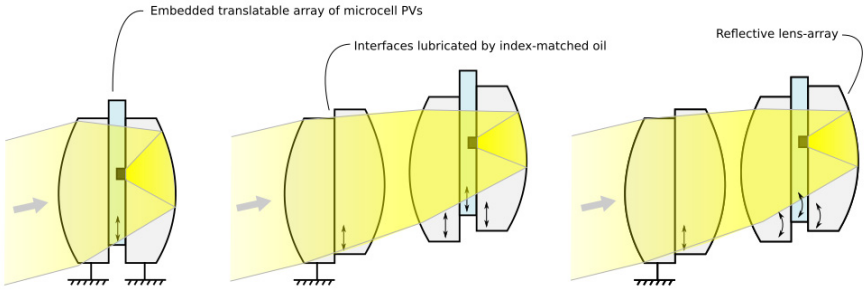

FIGURE 1. Conceptual illustration of the three different CPV-configurations that were optimized: Simple catadioptric (a), flat tracking trajectory (b), and curved tracking trajectory (c). In each configuration, the lens stacks are assumed to be arranged in a hexagonally packed lens array.

OPTIMIZATION RESULTS

Figure 2-4 show ray-traced drawings of the optimized CPV-designs after 9000 iterations of differential evolution.

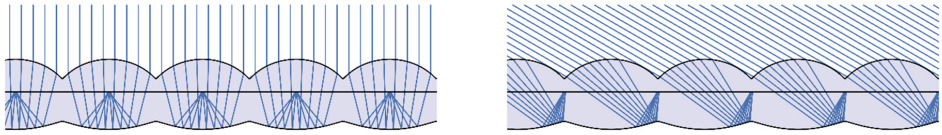

FIGURE 2. Optimized simple catadioptric CPV-system at 0° (a), and 60° (b) angle of incidence.

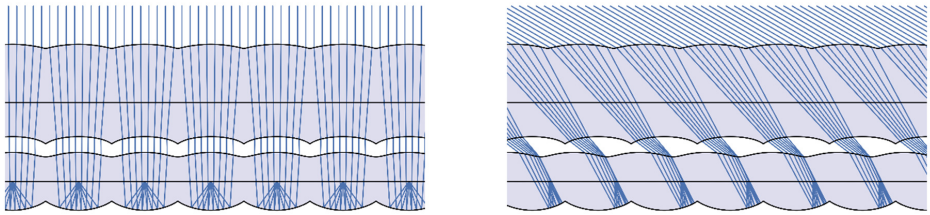

FIGURE 3. Optimized CPV-system with flat tracking trajectory at 0° (a), and 60° (b) angle of incidence.

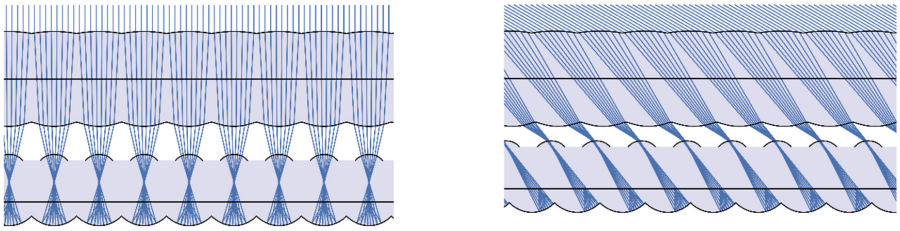

(a) (b)

FIGURE 4. Optimized CPV-system with curved tracking trajectory at 0° (a), and 60° (b) angle of incidence.

A more comprehensive Monte-Carlo simulation was performed on the optimized systems, quantifying optical efficiency and geometric concentration ratio as a function of angle of incidence. We define optical efficiency $\eta = \frac{P_{in}}{P_{out}}$ where P_{in} is total energy in the rays entering the system for a specific angle of incidence, and P_{out} is the energy in the rays arriving on the receiver plane. We define geometric concentration ratio as $C_{geo} = \frac{A_{in}}{A_{out}}$ where A_{in} is the hexagonal area of a lenslet, and A_{out} is defined as the smallest area of a circular receiver intercepting 90% of the transmitted energy for the given angle of incidence. This definition allows quantifying how the concentrating abilities of the system varies with angle of incidence. In a physical implementation, a fixed receiver size A_{out} would be chosen.

For each angle of incidence, 100 000 rays were sampled with random wavelengths according to the AM1.5D solar spectrum, random directions within the 0.27° divergence half-angle of sunlight, and random positions within the hexagonal aperture of the first lens. The results from this Monte-Carlo simulation are shown in Fig. 5.

The simulated performance of the *simple catadioptric* configuration gives a geometric concentration ratio >400x and optical efficiency >90%. This is comparable to the results published by Price et al [6], and the small variations are mainly because our work assumes a circular receiver when estimating concentration ratio.

The geometric concentration ratio is increased from approximately 400x to approximately 2000x when adding an additional pair of lens arrays to the system in the configuration shown in Fig. 1b. The concentration ratio is further increased to approximately 5000x if the lens arrays are allowed to follow a curved tracking trajectory as illustrated in Fig. 1c. The improved concentration ratio comes at the cost of reduced optical efficiency due to reflection losses, but these reflection losses can possibly be reduced without significant added cost using anti-reflective coatings or anti-reflective surface nanostructures [10].

The improved concentration ratio also introduces additional mechanical complexity with several lens arrays moving relative to each other. However, the translation of the different lens arrays is constrained to be proportional to each other so that they can share the same mechanical actuators, and the increased complexity might be justified by the significant improvement to concentration ratio. The designs are compatible with high-volume manufacturing techniques, such as injection molding or hot embossing by being relatively thin and made from commonly available thermoplastics such as PMMA.

The reported concentration ratios are very high, and much higher than in conventional CPV systems. We believe that the very high simulated concentration ratio is explained by a combination of factors. First, the concentration happens inside a dielectric, which inherently increases the thermodynamic limit to concentration by a factor n^2 where n is the refractive index of the dielectric. Second, the largest contributor to optical power in the system is the reflective lens array, which does not suffer for chromatic aberration unlike refractive lenses. Third, the system is assumed to be able to track the sun exactly, with an acceptance angle just large enough to fit the angular extent of the solar disc. This final assumption is made because each module can track the sun individually using a closed control loop, eliminating tracking errors from mounting the module to an external tracer, as well as tracking errors due to flexing of this external tracker.

Manufacturing tolerances are not taken into account in these simulations. It is likely that this will limit somewhat the ratio achieved in a physical implementation. The reported concentration ratios may also be too high for a PV cell to handle. However, we believe that this work demonstrates how it is possible to design tracking-integrated optical

systems where optical aberrations are not the limiting factor to system performance, and that it can motivate a further search towards tracking-integrated configurations with an optimal trade-off between performance and complexity.

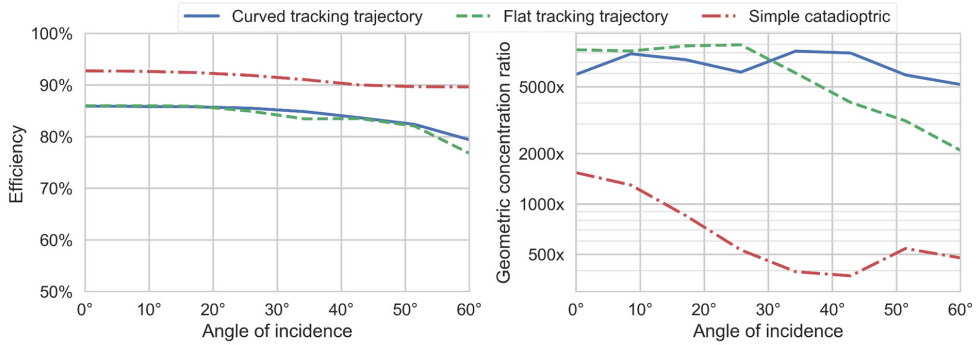

FIGURE 5. Simulated optical efficiency and geometric concentration ratio across tracking range for the optimized CPV configurations. The performance is simulated using Monte Carlo ray-tracking, taking into account reflection losses, chromatic aberration in the PMMA lens arrays, and the angular divergence of sunlight. The material is assumed to be non-absorptive.

CONCLUSIONS

We have presented an optimization-based design method for tracking-integrated CPV concentrator, and demonstrated how this method can be used to develop new and improved concentrators. Using this design method, we demonstrated new configurations for tracking-integrated CPV concentrators with improved optical performance, including a concentrating achieving a geometric concentration ratio of 5000x across a two-axis ±60° tracking range.

By significantly increasing the achievable concentration ratio of low-cost tracking integrated systems, these systems may improve the competitiveness for concentrator photovoltaics, and can also motivate the further search for new and promising concentrator configurations. The improved performance might enable new applications such as high efficiency rooftop-mountable or vehicle-mountable CPV. The presented design method can take into account the requirements of a specific application and manufacturing method, and can therefore be used to develop tailored CPV solutions optimized for specific use-cases and applications.

REFERENCES

1. M. A. Green, Y. Hishikawa, E. D. Dunlop, D. H. Levi, J. Hohl-Ebinger, M. Yoshita, and A. W. Y. Ho-Baillie, "Solar cell efficiency tables (Version 53)," Prog. Photovolt. Res. Appl. **27**, 3–12 (2019).
2. H. Apostoleris, M. Stefancich, and M. Chiesa, "Tracking-integrated systems for concentrating photovoltaics," Nat. Energy **1**, 16018 (2016).
3. P. Kotsidas, E. Chatzi, and V. Modi, "Stationary nonimaging lenses for solar concentration," Appl. Opt. **49**, 5183–5191 (2010).
4. J. M. Hallas, K. A. Baker, J. H. Karp, E. J. Tremblay, and J. E. Ford, "Two-axis solar tracking accomplished through small lateral translations," Appl. Opt. **51**, 6117 (2012).
5. F. Duerr, Y. Meuret, and H. Thienpont, "Tailored free-form optics with movement to integrate tracking in concentrating photovoltaics," Opt. Express **21**, A401–A411 (2013).
6. J. S. Price, X. Sheng, B. M. Meulblok, J. A. Rogers, and N. C. Giebink, "Wide-angle planar microtracking for quasi-static microcell concentrating photovoltaics," Nat. Commun. **6**, 6223 (2015).
7. H. J. D. Johnsen, J. Torgersen, and A. Aksnes, "Solar tracking using beam-steering lens arrays," in *Nonimaging Optics: Efficient Design for Illumination and Solar Concentration XV* (International Society for Optics and Photonics, 2018), Vol. 10758, p. 1075805.

8. A. K. Qin, K. Tang, H. Pan, and S. Xia, "Self-adaptive differential evolution with local search chains for real-parameter single-objective optimization," in *2014 IEEE Congress on Evolutionary Computation (CEC)* (IEEE, 2014), pp. 467–474.
9. E. Jones, T. Oliphant, P. Peterson, and others, "SciPy: Open source scientific tools for Python," (2001).
10. C.-J. Ting, M.-C. Huang, H.-Y. Tsai, C.-P. Chou, and C.-C. Fu, "Low cost fabrication of the large-area anti-reflection films from polymer by nanoimprint/hot-embossing technology," Nanotechnology **19**, 205301 (2008).

Paper 3: Pushing the limits of beam-steering lens arrays

Pushing the limits of beam-steering lens arrays

Håkon J. D. Johnsen*[a], Astrid Aksnes[b], and Jan Torgersen[a]

[a]Department of Mechanical and Industrial Engineering, Norwegian University of Science and Technology, Trondheim, Norway
[b]Department of Electronic Systems, Norwegian University of Science and Technology, Trondheim, Norway

ABSTRACT

An essential part of a concentrated solar power system is the solar tracker. Tracking is usually implemented by rotating the entire optical system to follow the sun, adding to the bulk and complexity of the system. Beam-steering lens arrays, on the other hand, enable solar tracking using millimeter-scale relative translation between a set of lens arrays stacked in an afocal configuration. We present an approach for designing and comparing beam-steering lens arrays based on multi-objective optimization, where the objective is to maximize efficiency, minimize divergence, and minimize cost/complexity. We then use this approach to develop new configurations with improved performance compared to previously reported results. As an example of a design suitable for high-concentration applications, we present a system consisting of four single-sided lens arrays that can track the sun with a yearly average efficiency of 74.4% into an exit-cone with divergence half-angle less than ±1°. We also present a simplified system consisting of three single-sided lens arrays, which can be implemented with less mechanical complexity and potentially lower cost. This simplified system achieves 74.6% efficiency and a divergence half-angle of less than ±2.2°, and might be relevant for low or medium concentration applications. We believe that these results demonstrate the previously untapped potential of beam-steering lens arrays. If such designs are successfully manufactured, they may become an attractive alternative to conventional external solar trackers for a range of solar energy applications.

Keywords: beam-steering, lens arrays, solar tracking, micro-tracking

Paper 3

1 INTRODUCTION

Solar concentrators can provide highly concentrated solar power for applications such as concentrator photovoltaics, solar thermal energy, or solar lighting.[1] The concentrators require accurate solar tracking in order to achieve high concentration,[2] which is usually performed by rotating the concentrator to face the sun. Recent work, however, has considered the use of tracking-integrated systems, which can track the sun without being rotated by an external solar tracker.[3]

One approach to tracking-integration is the concept of beam-steering, where a tracking-integrated system emits collimated light, which can then be concentrated in a separate concentrator, as conceptually illustrated in Figure 1a. This approach enables the same beam-steering system to be used for several different applications and allows the design of the concentrator optics to be independent of the design of the tracking optics. Several beam-steering concepts have been proposed for solar tracking, including electrowetting to change the angle of the interface between two liquids with different refractive indices,[4] microfluidic beam-steering arrays,[5] rotating prism arrays,[6] liquid crystals controlled by electric fields,[7] rotating off-axis Fresnel lenses,[8] and beam-steering lens arrays.[9,10]

A beam-steering lens array consists of a set of lens arrays stacked in an afocal configuration that can redirect sunlight by relative movement between these lens arrays, as first proposed for solar tracking by Lin et al.[9] The core principle is illustrated in Figure 1b.

In this work, we investigate the achievable performance of beam-steering lens arrays. We develop a new approach for comparing different beam-steering lens array configurations and use it to optimize new configurations with improved performance compared to previously reported results.

* E-mail: hakon.j.d.johnsen@ntnu.no

Nonimaging Optics: Efficient Design for Illumination and Solar Concentration XVI, edited by Roland Winston, Eli Yablonovitch, Proc. of SPIE Vol. 11120, 111200B · © 2019 SPIE
CCC code: 0277-786X/19/$21 · doi: 10.1117/12.2528751

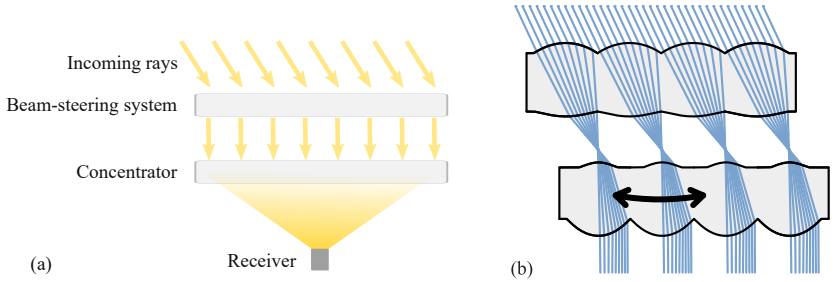

Figure 1: (a) Conceptual illustration of how a beam-steering system can be combined with conventional concentrator optics. (b) Example of a beam-steering lens array: An afocal stack of lens arrays, which redirects sunlight utilizing relative movement between these lens arrays.

2 CLASSIFYING DIFFERENT CONFIGURATIONS

With the development of new types of beam-steering lens arrays, we believe that it will be useful to have a way of classifying different designs. Previous beam-steering lens array designs have utilized both single-sided[9] and double-sided[10] lens arrays, with relative lateral[11] or curved[9] tracking motion, and with both two,[9] and three[12] lens arrays stacked together. In order to readily specify, compare, and evaluate different classes of designs, it can be useful to designate specific symbols for each of the components in a beam-steering lens array. Specific configurations of beam-steering lens arrays can then be described using a sequence of these symbols.

In this work, we use the set of symbols shown in Table 1.

Table 1: Proposed symbols for classifying different beam-steering lens array configurations. Symbols are represented in Unicode and can be copied and pasted as text into any software that supports Unicode.

Symbol*	Meaning
◀	Single-sided lens array with the flat side on the right.
▶	Single-sided lens array with the flat side on the left.
◆	Double-sided lens array
↓	Air-gap between lens arrays supporting a flat, lateral tracking trajectory.
⤸	Air-gap between lens arrays supporting a curved tracking trajectory.
◀▶	A pair of single-sided lens arrays placed back-to-back, with index-matched lubricating oil between them supporting relative lateral translation between the lens arrays.

The symbols from Table 1 can be used to classify both existing and new beam-steering lens array configurations. For instance:

- Lin et al., 2012:[9] ◀⤸▶
- Watson, 1993[14] (for steering of laser beams): ◆↓◆and ◆↓◆◆
- Johnsen et al., 2018:[10] ◆⤸◆and ◀⤸◆⤸◆

*The symbols are represented by the following Unicode[13] code-points: ◀=U+25C0, ▶=U+25B6, ◆=U+25C6, ↓=U+2193, ⤸=U+2938, ◀▶=U+25C0 U+200A U+25B6

3 DESIGN METHOD

We have utilized a design method based on ray-tracing and numerical optimization for designing and comparing different beam-steering lens array configurations. In this section, we describe this design method and specify the conditions for the optimization results reported in this paper.

3.1 Formulation of the optimization problem

We consider three main performance objectives for evaluating the performance of a complete beam-steering lens array:

- Maximizing the efficiency in redirecting sunlight.
- Minimizing the divergence of outgoing sunlight
- Minimizing the cost/complexity

The design of a beam-steering lens array can, therefore, be considered a multi-objective optimization problem. An optimal solution must provide a reasonable trade-off between these objectives. Multi-objective optimization problems can be solved by finding a set of Pareto optimal solutions: solutions where one objective cannot be improved without degrading another objective. In this way, the trade-off between objectives is quantified, allowing a designer to make an informed choice among the set of solutions.[15]

Efficiency and divergence can be quantified as continuous objective values, allowing a multi-objective optimization algorithm to map out the Pareto front between these objectives. Cost/complexity, on the other hand, is difficult to quantify and depends on several different factors. We have, therefore, not tried to quantify complexity directly. Instead, we optimized several different configurations with different levels of complexity.

We formulated the following optimization problem:

$$\min \mathbf{f}(\mathbf{x}, \theta_{max}) = (1 - \overline{\eta}(\mathbf{x}, \theta_{max}), \theta_{max})^T \tag{1}$$

$$\text{such that } g_j(\mathbf{x}) \leq 0, \tag{2}$$

where θ_{max} is the allowed divergence of outgoing sunlight, and $\overline{\eta}(\mathbf{x}, \theta_{max})$ is the average yearly optical efficiency of the optical system $\mathbf{x}$. $g_j(\mathbf{x})$ is a set of inequality constraints, ensuring manufacturability.

3.2 Estimating average optical efficiency

Average optical efficiency can be defined as the fraction of yearly direct irradiation successfully redirected in the desired direction:

$$\overline{\eta}(\mathbf{x}, \theta_{max}) = \frac{E_{out}(\mathbf{x}, \theta_{max})}{E_{in}}, \tag{3}$$

where E_{in} is the yearly direct irradiation received by the beam-steering lens array surface, and $E_{out}(\mathbf{x}, \theta_{max})$ is the yearly irradiation successfully redirected within the permitted exit cone.

This average efficiency can be estimated by integrating across all angles of incidence:

$$\bar{\eta}(\mathbf{x}, \theta_{max}) = \int_0^{\pi} e(\phi) \cdot \eta(\mathbf{x}, \theta_{max}, \phi)\, d\phi, \tag{4}$$

where $e(\phi) = \frac{E_{in,\phi}(\phi)}{E_{in}}$ is the normalized angular distribution of irradiation received by the beam-steering lens array in its installation location. $\eta(\mathbf{x}, \theta_{max}, \phi)$ is the optical efficiency of the beam-steering lens for an optical system $\mathbf{x}$, a maximum divergence of outgoing sunlight θ_{max} and an angle of incidence ϕ.

In this work, we consider the beam-steering lens arrays to have a fixed orientation, tilted towards the equator with an angle equal to the latitude of the installation location as illustrated in Figure 2a. As noted by Ito et al., this orientation gives a peak in irradiation distribution at $22° - 25°$ angle of incidence, irrespective of installation location.[16] We consider the beam-steering lens arrays optimized in this paper to be installed at a latitude of 40°. We simulate the angular distribution of solar irradiation using Meinel and Meinel's air mass attenuation model[17] and assuming that cloud cover is not correlated to time of day or time of year. The resulting normalized irradiation distribution is shown in Figure 2b. When planning a physical realization of such a system, the real meteorological conditions of the desired installation location should be used.

It is worth noting that $\bar{\eta}$ in Equation 3 is defined relative to the irradiation reaching the front surface of the beam-steering lens array as it is mounted in its assumed orientation. Cosine projection loss is therefore not included in this average efficiency, and will give an additional reduction in power compared to a system pointed directly towards the sun. On the other hand, fixed-orientation systems can increase power conversion per land area due to reduced shading between modules, as discussed by Price et al.[18] These effects must be taken into account when comparing tracking-integrated systems to externally tracked systems, but have been considered to be beyond the scope of this work.

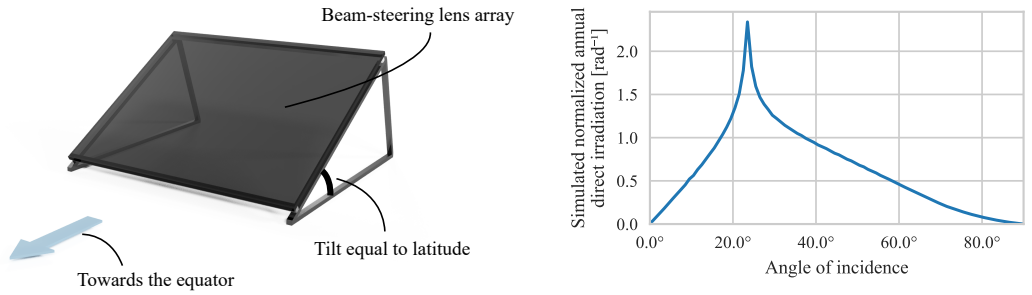

(a) (b)

Figure 2: (a) Assumed orientation of beam-steering lens array during optimization. (b) Simulated angular distribution of normalized yearly direct irradiation on a lens array with the fixed orientation from a, installed at a latitude of 40°

3.3 Numerical optimization

The multi-objective optimization problem in Equation 1 is trivially scalarized by setting a fixed θ_{max}. The Pareto front can then be mapped by repeated optimization of the resulting single-objective optimization problem for different values of θ_{max}.

The scalarized optimization problem was solved using a custom memetic optimization algorithm inspired by Qin et al.'s local search chains.[19] The differential evolution solver from SciPy[20] was extended to optimize the population using local search chains based on SciPy's SLSQP optimization algorithm in addition to the global differential evolution algorithm. The memetic optimization algorithm was run for 1500 iterations for each combination of beam-steering lens array configuration and permitted divergence half-angle, which seemed to give a reasonable trade-off between convergence and computational resources.

The optimization routine was implemented in a Jupyter Notebook[21] and parameterized using Papermill.[22] The optimization workflow was managed using Snakemake,[23] and solved using computational resources from Google Compute Engine. Ray-tracing was performed using a custom sequential three-dimensional ray-tracer, as reported in previous work.[10] Hexagonal lens apertures were used for all simulations to simulate close packing in a lens array. Optimizations were performed across the AM1.5D solar spectrum,[24] and all lenses were assumed to be made from Poly(methyl methacrylate) (PMMA). Reflection losses and chromatic aberration were taken

into account, while absorption losses were not considered.[†] Sunlight was assumed to originate from a uniform solar disc with a 0.27° angular radius. Average efficiency according to Equation 4 was estimated using multi-dimensional numerical integration with a quasi-Monte Carlo method and a low-discrepancy Sobol sequence. Lens surfaces were represented as Forbes' Q^{con} surfaces,[25] with a curvature, a conic constant, and 3 Q^{con} polynomial terms.

Four different configurations were optimized across a range of permitted divergence half-angles from ±0.3° to ±4°: ◀▶⤸◀▶ was optimized to evaluate achievable performance with the most complex configuration with up to 4 air-interfaces. ◀▶↓▶ was optimized to evaluate achievable performance with a simplified and potentially lower-cost system. ◀⤸◆⤸◆ and ◆⤸◆ were optimized for comparison, because they have previously been shown to have good performance for solar tracking.[10]

In each design, the lateral movements of the different lens arrays were constrained to be proportional to each other, allowing linked control, sharing the same mechanical actuator. The aspect ratio of each lens surface was constrained to be 0.7 or less, to prevent excessively curved lenses. Each lens array was constrained not to be thinner than half the lenslet diameter, to prevent too thin lens arrays.

4 RESULTS AND DISCUSSION

Equation 1 was solved using numerical optimization, as described in Section 3.3. The result is shown in Figure 3. Each line represents a specific beam-steering lens array configuration and shows the optimized yearly average efficiency for this configuration as a function of permitted divergence half-angle. Given the non-convex nature of the optimization problem, the optimization algorithm is not guaranteed to find the global optimum. The resulting Pareto front therefore only gives a lower bound on achievable efficiency for a specific configuration and divergence half-angle.

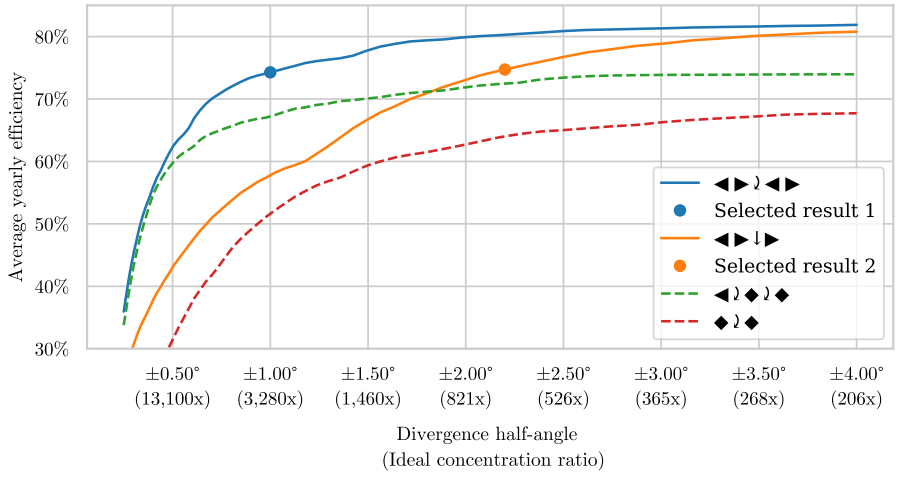

Figure 3: Optimized yearly efficiency as a function of permitted divergence half-angle for different configurations. For reference, the x-axis also shows the corresponding concentration ratio for an ideal concentrator at the given divergence half-angle.

4.1 Selected results

We choose to highlight two results that we believe to be of interest for solar energy applications. The first result is a ◀▶⤸◀▶ configuration optimized for a divergence half-angle of ±1°, which achieves 74.4% average yearly

[†]The beam-steering lens array is a scale-invariant afocal system (as long as it is operated far away from the diffraction limit). Absorption losses depend on the dimensions of the system, which were not specified in these simulations.

efficiency. This configuration, which may be relevant for high concentration applications, such as concentrator photovoltaics (CPV) or solar thermophotovoltaics, is highlighted with a blue circle in the Pareto front in Figure 3. A ray-traced drawing of the system can be seen in Figure 4. Simulated efficiency across the tracking range is shown in Figure 6a and is overlaid with a yearly irradiation distribution in Figure 6b.

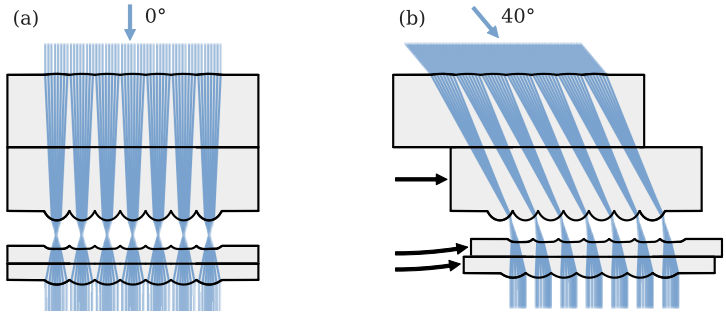

Figure 4: Beam-steering lens array with ◀▶⤸◀▶ configuration optimized for 1° divergence half-angle at (a) 0° angle of incidence and (b) 40° angle of incidence. Tracking motion is indicated by black arrows.

The second highlighted result is a ◀▶↓▶ configuration optimized for ±2.2° divergence half-angle. This configuration offers simpler mechanical implementation at the cost of lower optical performance. Compared to the previous result, the number of single-sided lens arrays is reduced from 4 to 3, and all relative motion is strictly lateral. This result is highlighted with an orange circle in the Pareto front in Figure 3, and a ray-traced drawing of the system can be seen in Figure 5. Simulated efficiency across the tracking range is shown in Figure 6a, and is overlaid with a yearly irradiation distribution in Figure 6b. This configuration may be relevant for medium concentration applications, such as concentrated solar power (CSP), or for solar lighting applications. The sine limit of concentration[26] for an ideal concentrator placed behind this beam-steering lens array is $678x$, which is more than three times the $212x$ ideal concentration ratio for a trough concentrator with single-axis tracking. This indicates that such a simplified beam-steering lens array can be useful for CSP applications despite the relaxed divergence requirements.

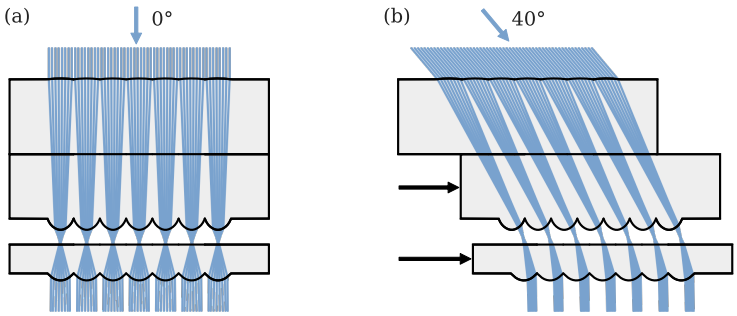

Figure 5: Simplified beam-steering lens array with ◀▶↓▶ configuration optimized for 2.2° divergence half-angle at (a) 0° angle of incidence and (b) 40° angle of incidence. Tracking motion is indicated by black arrows.

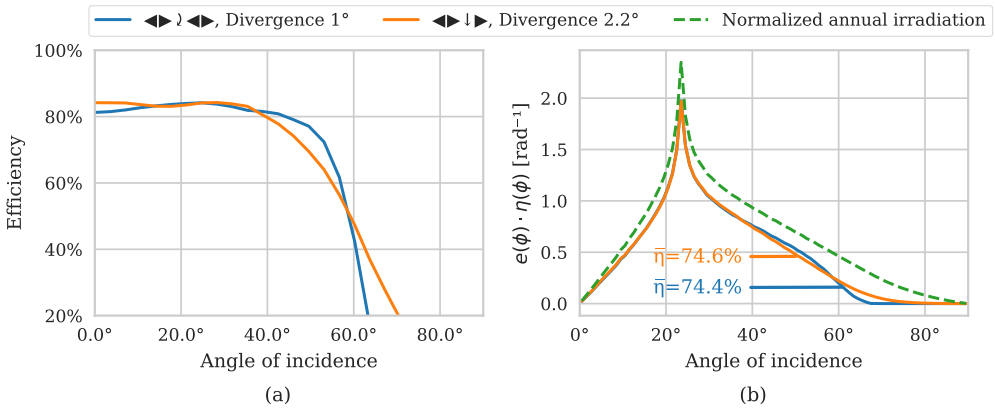

Figure 6: (a) The two selected beam-steering lens arrays have >80% efficiency for ±40°angle of incidence, and a gradual drop-off in efficiency at larger angles of incidence. (b) When the systems are placed in a fixed orientation as described in Section 3.2, this efficiency distribution corresponds to average yearly efficiency of 74.4% for the high concentration design and 74.6% for the simplified design, respectively.

5 CONCLUSIONS

We have introduced a set of symbols for categorizing different beam-steering lens array configurations and developed a numerical approach based on multi-objective optimization for comparing the performance of different configurations depending on application requirements. Using this approach, we have identified new configurations of beam-steering lens arrays that, to the best of our knowledge, outperform previous beam-steering lens arrays reported in the literature. Further work will involve a more extensive search through possible beam-steering lens array configurations, and exploration of the consequences for other installation orientation and locations as well as real-world manufacturing tolerances. The beam-steering lens array configurations reported in this paper may contribute to low-cost tracking-integrated solar energy, and the multi-objective optimization approach may enable further developments in this field. The presented designs are compatible with high-volume manufacturing methods such as injection molding, and future work may also involve extending the concept to Fresnel lenses compatible with roll-to-roll manufacturing processes such as extrusion coating.[27]

REFERENCES

[1] Xie, W. T., Dai, Y. J., Wang, R. Z., and Sumathy, K., "Concentrated solar energy applications using Fresnel lenses: A review," *Renewable and Sustainable Energy Reviews* **15**(6), 2588–2606 (2011).

[2] Winston, R., Minano, J. C., Benitez, P. G., contributions by Narkis Shatz and John C. Bortz, W., and Bortz, J. C., [*Nonimaging Optics*], Elsevier Science (2005).

[3] Apostoleris, H., Stefancich, M., and Chiesa, M., "Tracking-integrated systems for concentrating photovoltaics," *Nature Energy* **1**, 16018 (2016).

[4] Narasimhan, V., Jiang, D., and Park, S.-Y., "Design and optical analyses of an arrayed microfluidic tunable prism panel for enhancing solar energy collection," *Applied Energy* **162**, 450–459 (2016).

[5] DiDomenico, L. D., "Towards doubling solar harvests using wide-angle, broad-band microfluidic beam steering arrays," *Optics Express* **23**(24), A1398–A1417 (2015).

[6] León, N., Ramírez, C., and García, H., "Rotating Prism Array for Solar Tracking," *Energy Procedia* **57**, 265–274 (2014).

[7] Valyukh, S., Valyukh, I., and Chigrinov, V., "Liquid-Crystal Based Light Steering Optical Elements," *Photonics Letters of Poland* **3**(2), 88–90 (2011).

[8] Campbell, R. and Machado, M., "LOW cost CPV = Embedded CPV with internal tracker," in [*2010 35th IEEE Photovoltaic Specialists Conference (PVSC)*], 003003–003007 (2010).
[9] Lin, W., Benitez, P., and Miñano, J. C., "Beam-steering array optics designs with the SMS method," *Proc. SPIE* **8485**, 848505–848505–7 (2012).
[10] Johnsen, H. J. D., Torgersen, J., and Aksnes, A., "Solar tracking using beam-steering lens arrays," *Proc. SPIE* **10758**, 1075805, International Society for Optics and Photonics (2018).
[11] Watson, E., Miller, D., and Barnard, K., "Analysis of fill factor improvement using microlens arrays," *Proc. SPIE* **3276**, 123–134 (1998).
[12] Duparré, J., Radtke, D., and Dannberg, P., "Implementation of field lens arrays in beam-deflecting microlens array telescopes," *Applied Optics* **43**(25), 4854–4861 (2004).
[13] Unicode Consortium, [*The Unicode Standard, Version 12.0*] (2019).
[14] Watson, E. A., "Analysis of beam steering with decentered microlens arrays," *Optical Engineering* **32**(11), 2665–2670 (1993).
[15] Pardalos, P. M., Žilinskas, A., and Žilinskas, J., [*Non-Convex Multi-Objective Optimization*], Springer Optimization and Its Applications, Springer International Publishing (2017).
[16] Ito, A., Sato, D., and Yamada, N., "Optical design and demonstration of microtracking CPV module with bi-convex aspheric lens array," *Optics Express* **26**(18), A879–A891 (2018).
[17] Meinel, A. B. and Meinel, M. P., [*Applied Solar Energy: An Introduction*], Addison-Wesley (1976).
[18] Price, J. S., Sheng, X., Meulblok, B. M., Rogers, J. A., and Giebink, N. C., "Wide-angle planar microtracking for quasi-static microcell concentrating photovoltaics," *Nature Communications* **6**, 6223 (2015).
[19] Qin, A. K., Tang, K., Pan, H., and Xia, S., "Self-adaptive differential evolution with local search chains for real-parameter single-objective optimization," in [*2014 IEEE Congress on Evolutionary Computation (CEC)*], 467–474, IEEE, Beijing, China (2014).
[20] Jones, E., Oliphant, T., Peterson, P., et al., "SciPy: Open source scientific tools for Python," (2001).
[21] Thomas, K., Benjamin, R.-K., Fernando, P., Brian, G., Matthias, B., Jonathan, F., Kyle, K., Jessica, H., Jason, G., Sylvain, C., Paul, I., Damián, A., Safia, A., Carol, W., and Team, J. D., "Jupyter Notebooks – a publishing format for reproducible computational workflows," in [*ELPUB*], 87–90 (2016).
[22] nteract team, "Welcome to papermill — papermill 1.0.1 documentation." https://papermill.readthedocs.io/en/latest/ (2019).
[23] Köster, J. and Rahmann, S., "Snakemake—a scalable bioinformatics workflow engine," *Bioinformatics* **28**(19), 2520–2522 (2012).
[24] Renewable Resource Data Center, "Solar Spectral Irradiance: Air Mass 1.5." https://rredc.nrel.gov/solar/spectra/am1.5/.
[25] Forbes, G. W., "Shape specification for axially symmetric optical surfaces," *Optics express* **15**(8), 5218–5226 (2007).
[26] Winston, R., Jiang, L., and Ricketts, M., "Nonimaging optics: A tutorial," *Advances in Optics and Photonics* **10**(2), 484–511 (2018).
[27] Steinberg, C., Al-Hussainawi, N., Papenheim, M., Mayer, A., Scheer, H.-C., Matschuk, M., and Pranov, H., "Low reflection Fresnel lenses via double imprint combined with vacuum-UV surface hardening," *Journal of Vacuum Science & Technology B* **35**(6), 06G306 (2017).

Paper 4: High-performance stationary solar tracking through multi-objective optimization of beam-steering lens arrays

Research Article | Vol. 28, No. 14 / 6 July 2020 / Optics Express 20503
Optics EXPRESS

High-performance stationary solar tracking through multi-objective optimization of beam-steering lens arrays

HÅKON J. D. JOHNSEN,[1,*] ASTRID AKSNES,[2] AND JAN TORGERSEN[1]

[1]Norwegian University of Science and Technology, Department of Mechanical and Industrial Engineering, Richard Birkelands Vei 2b, Trondheim, Norway
[2]Norwegian University of Science and Technology, Department of Electronic Systems, O.S. Bragstads plass 2b, Trondheim, Norway
[*]hakon.j.d.johnsen@ntnu.no

Abstract: Beam-steering lens arrays enable solar tracking using millimeter-scale relative translation between a set of lens arrays. This may represent a promising alternative to the mechanical bulk of conventional solar trackers, but until now a thorough exploration of possible configurations has not been carried out. We present an approach for designing beam-steering lens arrays based on multi-objective optimization, quantifying the trade-off between beam divergence and optical efficiency. Using this approach, we screen and optimize a large number of beam-steering lens array configurations, and identify new and promising configurations. We present a design capable of redirecting sunlight into a $<2^{\circ}$ divergence half-angle, with 73.4% average yearly efficiency, as well as a simplified design achieving 75.4% efficiency with a $<3.5^{\circ}$ divergence half-angle. These designs indicate the potential of beam-steering lens arrays for enabling low-cost solar tracking for stationary solar concentrators.

1. Introduction

Solar concentrators can provide highly concentrated solar power for applications such as concentrator photovoltaics (CPV), concentrated solar power (CSP), or solar lighting [1]. The concentrators require accurate solar tracking to achieve high concentration [2], which is usually performed by rotating the concentrator to face the sun. Recent work has considered the use of tracking-integrated systems that can track the sun without being rotated by an external solar tracker [3–7].

One approach is the concept of beam-steering, where a tracking-integrated system emits collimated light, which can be concentrated in a separate concentrator [3], as illustrated in Fig. 1(a). This approach allows the design of the concentrator optics to be independent of the design of the tracking optics, and it enables the beam-steering system to be used for different applications. Several beam-steering concepts have been proposed for solar tracking, including electrowetting to change the angle of the interface between two liquids with different refractive indices [8], microfluidic beam-steering arrays [9], rotating prism arrays [10], liquid crystals controlled by electric fields [11], rotating off-axis Fresnel lenses [12], and beam-steering lens arrays [13–15].

A beam-steering lens array consists of a set of lens arrays arranged in an afocal configuration, enabling beam-steering by relative lateral translation between the lens arrays [14], as illustrated in Fig. 1(b). The concept was originally proposed for steering of laser beams [16–18]. In 2012, Lin et al. proposed utilizing the same concept for single-axis solar tracking, while also proposing a design method based on the Simultaneous Multiple Surface (SMS) Method [13]. Johnsen

Paper 4

#396477 https://doi.org/10.1364/OE.396477
Journal © 2020 Received 1 May 2020; revised 18 Jun 2020; accepted 18 Jun 2020; published 25 Jun 2020

Optics EXPRESS

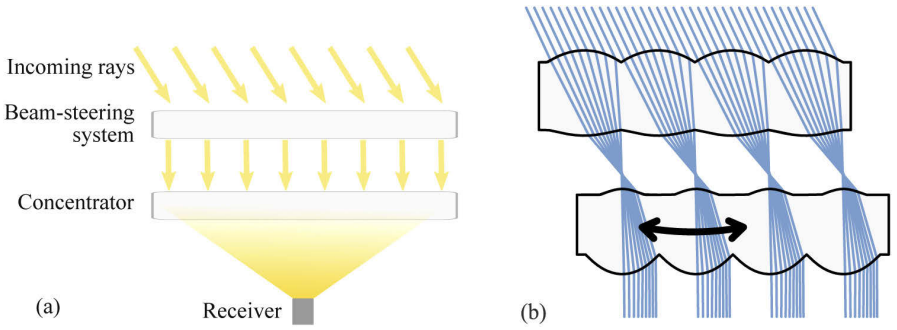

Fig. 1. (a) Conceptual illustration of how a beam-steering system can be combined with conventional concentrator optics. (b) Example of a beam-steering lens array: An afocal stack of lens arrays, which redirects sunlight utilizing relative movement between these lens arrays.

et al. extended the concept to two-axis solar tracking and demonstrated the use of numerical optimization for designing the systems [14,15].

By relying entirely on geometrical optics, beam-steering lens arrays have the benefit that they do not depend on special materials. This can make them compatible with conventional high-volume manufacturing methods such as injection molding or roll-to-roll processing. A successful design may, therefore, have a short path towards commercial implementation. However, the design of a beam-steering lens array requires a careful balancing of the different requirements of the system, such as tracking range, divergence of the outgoing sunlight, and optical efficiency.

In this paper, we numerically investigate the achievable performance of a large number of different beam-steering lens array configurations designed for stationary solar tracking applications. In order to optimize the systems, we propose and use a design method for beam-steering lens arrays based on multi-objective optimization. Section 2 contains a description of the concepts and requirements of beam-steering lens arrays. Section 3 introduces the optimization method and the optimization parameters selected in this work, including a classification scheme used to generate the different optimized configurations. In Section 4, we present the results of the numerical optimization, which are further discussed in Section 5.

2. Beam-steering lens arrays

Figure 2 shows the basic paraxial working principle of a basic beam-steering lens array with a pair of lens arrays stacked in an afocal configuration. The lens arrays are separated by their combined focal lengths $f_1 + f_2$. The system can track incoming sunlight at an angle ϕ by translating the last lens array a distance Δx such that it is always aligned with the image of the sun from the first lens array:

$$\Delta x = f_1 \tan \phi. \tag{1}$$

In order for all rays to reach the correct lenslet in the array L_2, the second focal length must be smaller than the first. This leads to an angular magnification factor M:

$$M = \frac{f_1}{f_2} = 1 + 2\frac{f_1}{d} \tan \phi_{max}, \tag{2}$$

where ϕ_{max} is the highest supported angle of incidence for the beam-steering lens array.

Sunlight has an inherent divergence half-angle of approximately $\theta = 0.27°$ [19], which is magnified by this angular magnification factor M after passing through a beam-steering lens array.

Optics EXPRESS

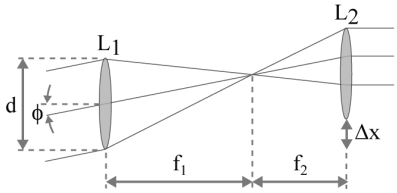

Fig. 2. Paraxial working principle of a simple beam-steering lens array.

The resulting divergence half-angle limits the maximum achievable concentration of a system with the configuration from Fig. 1(a) according to the fundamental limit to solar concentration for 2-axis concentration in air [2]:

$$C_{max} = \frac{1}{(\sin\theta)^2} \tag{3}$$

To allow high concentration ratios, it is therefore desirable that the angular magnification of the system is low. This leads to a trade-off between the tracking range ϕ_{max}, and divergence angle θ for this simple paraxial model of a beam-steering lens array.

It has been shown that this magnification factor can be eliminated in laser beam-steering systems by introducing an additional paraxial field lens to the system, where all three lens arrays have the same focal length f [17]. This shows the importance of design choices such as the number and order of surfaces when designing a beam-steering lens array. We call this the configuration of the system, which is a topic of investigation in this work.

While utilizing the same underlying principle, there are significant differences between earlier systems for steering of laser beams [16–18] and a system designed for solar tracking:

- In solar tracking, the beam-steering system receives sunlight from varying directions and emits it in a fixed direction. The earlier proposed laser systems [16–18] work in reverse, receiving the beam from a fixed direction and emitting in a variable direction.
- In laser systems, the lens arrays usually work in the diffractive regime, and additional phase-shifting optics are required to enable continuous beam-steering [17]. For solar tracking covering larger areas, the individual lenslets can be made large enough that the geometrical optical approximation is appropriate, and the separate lenslets can be considered individually.
- The steering range used in previously proposed laser systems is 5° to 15° [18,20,21], allowing design considerations based mainly on the paraxial approximation presented in this section. For stationary solar tracking, much larger steering angles are required, and the simple paraxial approximation presented in this section is no longer sufficient.
- In solar tracking, the system must be able to handle broadband sunlight, requiring chromatic aberration to be taken into account.

Based on these differences, we believe that a design method based on numerical optimization will be best able to handle the complexities and requirements of solar tracking applications.

3. Design method

We have utilized a numerical design method based on ray-tracing and numerical multi-objective optimization to design the beam-steering lens array systems. Numerical optimization is routinely used to design optical systems, and several studies of imaging optical systems have shown how the design space can be further explored by the use of multi-objective optimization algorithms,

Optics EXPRESS

identifying the trade-off between a set of competing system objectives [22–24]. In this section, we describe our design method, demonstrating how multi-objective optimization can also be utilized to design nonimaging optical system, and we specify the conditions for the results reported later in the paper.

3.1. Formulation of the optimization problem

We consider three main performance objectives for evaluating the performance of a complete beam-steering lens array:

- Maximizing the efficiency in redirecting sunlight.
- Minimizing the divergence of outgoing sunlight
- Minimizing the cost/complexity of the resulting system

The design of a beam-steering lens array can be considered a multi-objective optimization problem. An optimized solution must provide a reasonable trade-off between these objectives. Multi-objective optimization problems can be solved by finding a set of Pareto optimal solutions: solutions where the performance in one objective cannot be improved without degrading performance in another objective. In this way, the trade-off between objectives is quantified, allowing a designer to make an informed choice among the set of solutions [25].

Efficiency and divergence can be quantified as continuous objective functions, allowing a multi-objective optimization algorithm to map out the Pareto front between these objectives. Cost/complexity, on the other hand, is difficult to quantify and depends on several factors. Rather than quantify complexity directly, we consider cost/complexity to be influenced by the *configuration* of the beam-steering lens array – the sequence of surfaces and type of relative movements between them. We have chosen to optimize a broad set of configurations, enabling the comparison of different configurations with varying complexity, and allowing the selection of a configuration with the appropriate level of complexity for a specific use case. Cost/complexity can also be influenced by a number of other factors, including material selection, manufacturing tolerances, and optimization constraints for manufacturability - all of which are kept constant in the present work and may be considered more thoroughly in future work.

We formulated the following optimization problem:

$$\min \mathbf{f}\left(\mathbf{x}, \theta_{max}\right) = \left(-\overline{\eta}\left(\mathbf{x}, \theta_{max}\right), \theta_{max}\right) \tag{4}$$

$$\text{such that } g_j\left(\mathbf{x}\right) \leq 0, \tag{5}$$

where θ_{max} is the allowed divergence of outgoing sunlight, $\mathbf{x}$ is a set of free variables specifying the optical system (as listed in Table 2). $\overline{\eta}\left(\mathbf{x}, \theta_{max}\right)$ is the average yearly optical efficiency of the optical system subject to θ_{max}, as described in Section 3.2. The two components of $\mathbf{f}$ represent the two objectives: Maximizing the average yearly efficiency (minimizing $-\bar{\eta}$), while also minimizing the allowed divergence (minimizing θ_{max}). $g_j\left(\mathbf{x}\right)$ is a set of inequality constraints as listed in Table 3, ensuring manufacturability.

3.2. Average yearly efficiency

The metric of average yearly efficiency is inspired by the work from Ito et al., who elegantly showed that such a metric could be used to design a tracking-integrated system [26]. We define the average yearly optical efficiency as the fraction of yearly direct irradiation successfully redirected in the desired direction:

$$\overline{\eta}\left(\mathbf{x}, \theta_{max}\right) = \frac{E_{out}\left(\mathbf{x}, \theta_{max}\right)}{E_{in}}, \tag{6}$$

where E_{in} is the yearly direct irradiation received by the beam-steering lens array surface, and $E_{out}\left(\mathbf{x}, \theta_{max}\right)$ is the yearly irradiation successfully redirected within the permitted exit cone $\pm\theta_{max}$.

Optics EXPRESS

This average efficiency can be estimated by integrating across all angles of incidence ϕ:

$$\bar{\eta}(\mathbf{x}, \theta_{max}) = \int_0^{\pi} e(\phi) \times \eta(\mathbf{x}, \theta_{max}, \phi)\, d\phi, \tag{7}$$

where $e(\phi) = \frac{E_{in,\phi}(\phi)}{E_{in}}$ is the normalized angular distribution of irradiation received by the beam-steering lens array in its installed location. $\eta(\mathbf{x}, \theta_{max}, \phi)$ is the optical efficiency of the beam-steering lens for an optical system $\mathbf{x}$, a maximum divergence of outgoing sunlight θ_{max} and an angle of incidence ϕ.

In this work, we consider the beam-steering lens arrays to have a fixed orientation, tilted towards the equator with an angle equal to the latitude of the installation location, as illustrated in Fig. 3(a). As noted by Ito et al., this orientation gives a peak in irradiation distribution at $22° - 25°$ angle of incidence, irrespective of installation location [26]. We consider the beam-steering lens arrays optimized in this paper to be installed at a latitude of 40°. The location of 40° was chosen as an example to demonstrate the principle. However, as demonstrated by Schuster [27], this angular distribution is virtually independent of installation latitude when the panel is tilted according to installation latitude. We simulate the angular distribution of solar irradiation using Meinel and Meinel's air mass attenuation model [28] and for simplicity assume that cloud cover is not correlated to time of day or time of year. The resulting normalized irradiation distribution is shown in Fig. 3(b).

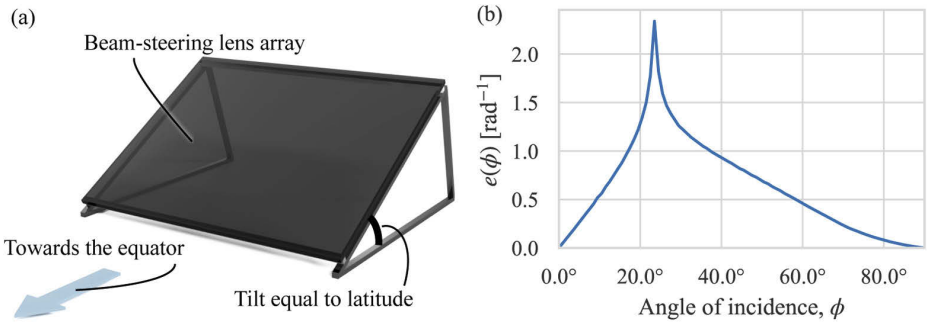

Fig. 3. (a) Assumed orientation of beam-steering lens array during optimization. (b) Simulated angular distribution of normalized yearly direct irradiation on a lens array with the fixed orientation from a, installed at a latitude of 40°.

With this formulation, the location of the installation location, weather data, and orientation of the beam-steering lens array are all contained in the normalized angular distribution of irradiation, $e(\phi)$, as shown in Eq. (7). The same formulation can therefore be used for optimizing beam-steering lens arrays with the details of a planned installation, by using the appropriate distribution $e(\phi)$. This may include real-world weather data, as well as other orientations, for instance being oriented east or west, or being mounted on single-axis external trackers.

It is worth noting that $\bar{\eta}$ in Eq. (6) is defined relative to the irradiation reaching the front surface of the beam-steering lens array while it is mounted in its chosen orientation. The cosine projection loss is therefore not included in the average efficiency, and will give an additional reduction in intensity compared to a system pointed directly towards the sun. On the other hand, fixed-orientation systems can increase power conversion per land area due to reduced shading between modules, as discussed by Price et al. [29]. These effects must be taken into account when comparing tracking-integrated systems to externally tracked systems, but have been considered to be beyond the scope of this work. Here, the aim is to compare different stationary systems that all share the same cosine projection loss.

Optics EXPRESS

3.3. Classifying different configurations

Previously proposed beam-steering lens array designs have utilized both single-sided [13] and double-sided [14] lens arrays, with relative lateral [30] or curved [13] tracking motion, and with both two [13], and three [31] lens arrays stacked together. In order to readily specify, compare, and evaluate different classes of designs, it can be useful to designate specific symbols for each of the components in a beam-steering lens array. Specific configurations of beam-steering lens arrays can then be described using a sequence of these symbols.

In this work, we use the set of symbols shown in Table 1.

The symbols from Table 1 can be used to classify both existing and new beam-steering lens array configurations. For instance:

- The example beam-steering lens array in Fig. 1: ◆⤸◆
- Lin et al., 2012 [13]: ◄⤸►
- Watson, 1993 [17] (for steering of laser beams): ◆↓◆ and ◆↓◆▤◆
- Johnsen et al., 2018 [14]: ◆⤸◆ and ◄⤸◆⤸◆

Table 1. Proposed symbols for classifying different beam-steering lens array configurations.

Symbol[a]	Meaning
◄	Single-sided lens array with the flat side on the right.
►	Single-sided lens array with the flat side on the left.
◆	Double-sided lens array
◄►	A pair of single-sided lens arrays placed back-to-back, with index-matched lubricating oil between them supporting relative lateral translation between the lens arrays.
↓	Air-gap between lens arrays supporting a flat, lateral tracking trajectory.
⤸	Air-gap between lens arrays supporting a curved tracking trajectory.
▤	Air-gap between two surfaces, but no relative movement between the surfaces.

[a]The symbols are represented by the following Unicode [32] code-points: ◄=U+25C0, ►=U+25B6, ◆=U+25C6, ↓=U+2193, ⤸=U+2938, ◄►=U+25C0 U+200A U+25B6, ▤=U+25A4

3.4. Selecting configurations

Using the presented code for classifying beam-steering lens arrays, we have performed a comprehensive optimization of all possible combinations of the symbols in Table 1 with a maximum of 1 air-gap. This leads to a total of 52 configurations, of which 40 contains at least 1 movable surface. These configurations cover the range from complex configurations such as ◄►⤸◄►, to simple configurations such as ◄►. Optimizing across this span can therefore give good insight into the trade-off between minimizing complexity and maximizing system performance.

3.5. Numerical optimization

The multi-objective optimization problem in Eq. (4) was solved using a memetic version of the MOEA/D-DE [33] multi-objective optimization algorithm. This algorithm decomposes the multi-objective problem into a set of scalarized sub-problems that are solved cooperatively.

Optics EXPRESS

We created the scalarized sub-problems by setting θ_{max} in Eq. (4) to fixed values in the range $0.5° \leq \theta_{max} \leq 5°$, which we assume to encompass the region of interest between high-accuracy and low-accuracy tracking. The MOEA/D implementation from Pymoo [34] was extended with the differential evolution strategy and the diversity preservation scheme proposed in the MOEA/D-DE algorithm [33]. The algorithm was then further extended to augment the global differential evolution with local searches based on SciPy's [35] implementation of the SLSQP optimization algorithm [36], as shown in Fig. 4. The resulting memetic optimization algorithm was run until convergence, with a limit of 10 000 iterations for each beam-steering lens array configuration.

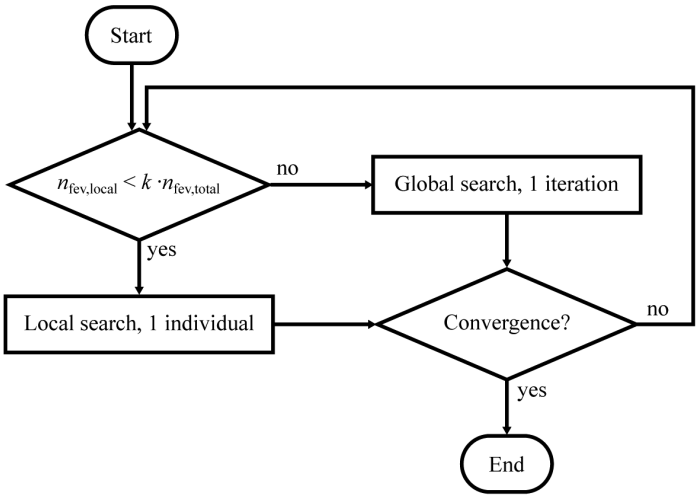

Fig. 4. The global MOEA/D-DE optimization algorithm is combined with the SLSQP local optimization algorithm to form a hybrid optimization algorithm. The choice between local and global search is based on the number of objective function evaluations in the local search, $n_{fev,local}$ compared to the total number of objective function evaluations, $n_{fev,total}$. We used $k = 0.5$, which means that 50% of the search effort is dedicated to the local searches.

The optimization workflow was managed using Snakemake [37]. Ray-tracing was performed using a custom sequential three-dimensional ray-tracer, as reported in previous work [14]. Hexagonal lens apertures were used for all simulations to simulate close packing in a lens array. Optimizations were performed across the AM1.5D solar spectrum [38], and all lenses were assumed to be made from Poly(methyl methacrylate) (PMMA). Reflection losses and chromatic aberration were taken into account, while absorption losses were not considered. The beam-steering lens array is a scale-invariant afocal system (as long as it is operated far away from the diffraction limit). Absorption losses depend on the dimensions of the system, which were not specified in these simulations. Reflection losses were estimated according to Fresnel's equations, taking the average of R_p and R_s and assuming that the light stays approximately unpolarized throughout the system. The angular distribution of sunlight was modeled using Buie's sunshape distribution model [39], assuming a circumsolar radiation of 5%. Average efficiency, according to Eq. (7), was estimated using multi-dimensional numerical integration with a quasi-Monte Carlo method implemented using a low-discrepancy Sobol sequence. Lens surfaces were represented as 8th order Forbes' Q^{con} surfaces [40], and the full set of free variables that was optimized is listed in Table 2. The lens arrays were optimized for as-built performance by assuming uniformly distributed positioning errors of $\pm 0.0025 \cdot T$ where T is the total thickness of the system, and assuming uniformly distributed slope errors in the surfaces of ±8 mrad, as listed in Table 3. If the

Optics EXPRESS

beam-steering lens array design is scaled to have a thickness of 20mm, this would correspond to a positioning error of 50 μm. In the ray-optical regime, errors such as curvature error, thickness error, surface waviness, or tracking error, all have the effect of changing the position and slope at the point where a ray intercepts a surface [2]. All these errors are therefore combined into the chosen error distribution for slope and position error. These errors were integrated into the quasi-Monte Carlo integration of Eq. (7) by sampling from these error distributions each time a ray crosses a surface, and this approach is further discussed in Section 5.2.

Table 2. List of free variables during optimization of the beam-steering lens arrays

Every surface	
R	Radius of curvature
k	Conic constant
a_1, a_2, a_3	Aspherical Q^{con} coefficients
t	Thickness
For the whole system	
c_1, c_2, c_3, c_4	Polynomial coefficients representing tracking motion
Every tracking motion (every ◄►, ↓, and ⤸)	
d	Proportionality constant for tracking motion
Every curved tracking motion (every ⤸)	
R_t	Radius of curvature of tracking geometry
k_t	Conic constant for tracking geometry
$a_{t,1}, a_{t,2}$	Q^{con} polynomial representing tracking geometry

In addition to assuming a fixed distribution of positioning and slope errors, the effect of these errors was further investigated by optimizing the ◄►↓◄► configuration for a set of different error distributions.

In each design, the lateral movements of the different lens arrays were constrained to be proportional to each other, allowing linked control, sharing the same mechanical actuator. The aspect ratio of each lens surface was constrained to be 0.5 or less, to prevent excessively curved lenses. Each lens array was constrained not to be thinner than half the lenslet diameter, to prevent too thin lens arrays, and also to be no thicker than 3 times the lenslet diameter, as summarized in Table 3.

These assumptions and constraints were chosen as an example of fairly permissive constraints, to explore a broad design space and get an overview of the performance of different configurations of beam-steering lens arrays. When planning a physical realization of such a system, these constraints would be modified according to the requirements of the chosen fabrication process.

Optics EXPRESS

Table 3. Manufacturing errors and manufacturing constraints assumed during optimization.

Assumed manufacturing errors (uniform distributions, T is total system thickness)	
Position error	$\pm 0.0025 \cdot T$
Slope error	±8mrad
Constraints (D is lenslet diameter)	
Lens thickness (thinnest point)	$>0.5 \cdot D$
Lens thickness (thickest point)	$<3 \cdot D$
Air gap thickness (thinnest point)	>0
Air gap thickness (thickest point)	$<2 \cdot D$
Lens aspect ratio	<0.5

4. Optimization results

The result of the numerical optimization is shown in Fig. 5. Each line represents a specific beam-steering lens array configuration, and each point along the line represents a specific design optimized for the particular trade-off between efficiency and divergence half-angle. Given the non-convex nature of the optimization problem, the optimization algorithm is not guaranteed to find the global optimum. The resulting Pareto front therefore only gives a lower bound on achievable efficiency for a specific configuration and divergence half-angle.

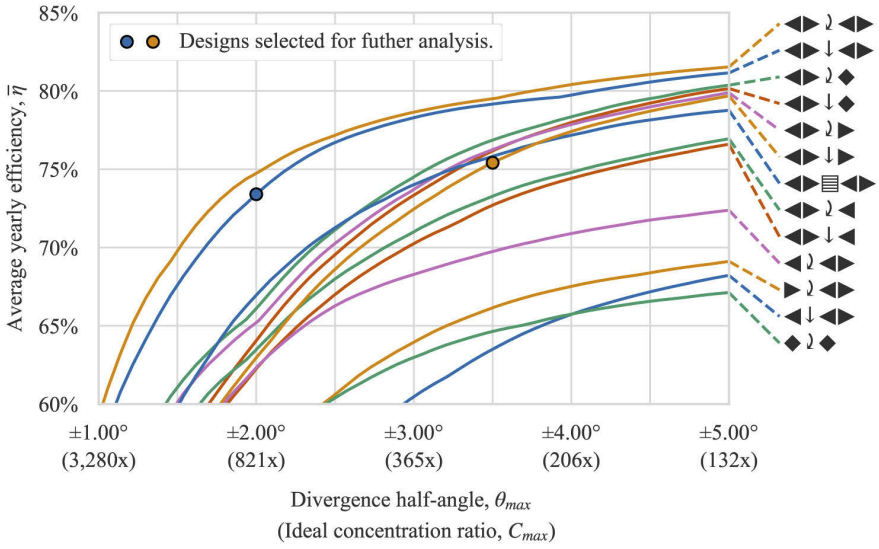

Fig. 5. Set of the best performing optimized configurations, mapping out the trade-off between efficiency and divergence half-angle. The value in brackets below the divergence half angle represents the ideal geometric concentration at this divergence half-angle, according to Eq. (3).

Due to the number of optimized configurations, only the best-performing configurations are shown in Fig. 5. The full set is available in Fig. 11.

Optics EXPRESS

4.1. Selected results

Each point along the lines in Fig. 5 represents a separate beam-steering lens array design. We report on two of those designs in more detail, representing different trade-offs between efficiency, divergence, and complexity. The first result is a ◄►↓◄► configuration optimized for a divergence half-angle of ±2°, which achieves 73.4% average yearly efficiency. This represents a configuration with high complexity, low divergence, and high efficiency. The result is highlighted with a blue circle in the Pareto fronts in Fig. 5, and a ray-traced drawing of the system can be seen in Fig. 6. Simulated efficiency across the tracking range is shown in Fig. 8(a) and is overlaid with a yearly irradiation distribution in Fig. 8(b).

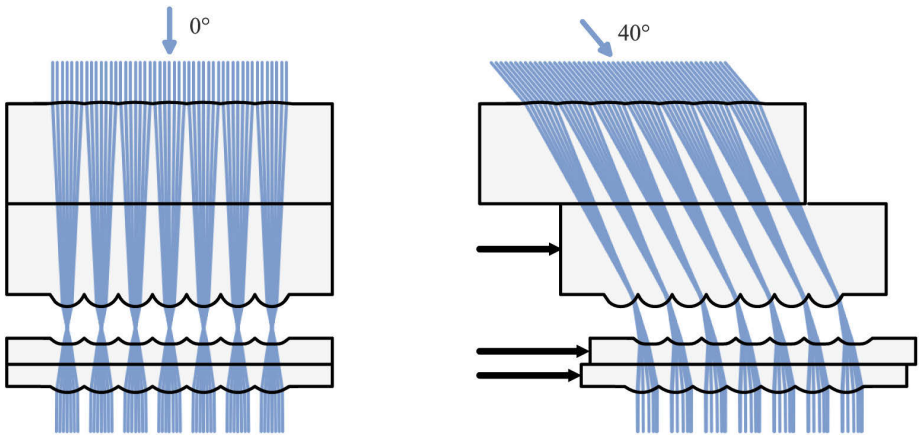

Fig. 6. Beam-steering lens array with ◄►↓◄► configuration optimized for 2° divergence half-angle (● in Fig. 5), drawn at 0° and 40° angles of incidence respectively. The black arrows indicate tracking motion. The drawing shows a 2 -dimensional slice of the optimized system, which consists of hexagonally packed three-dimensional lens arrays.

The second result is a ◄►↓► configuration optimized for ±3.5° divergence half-angle, which achieves 75.4% average yearly efficiency. This is an example of a system where a lower mechanical complexity is traded for a higher permitted divergence half-angle. The result is highlighted with a brown circle in the Pareto front in Fig. 5, and a ray-traced drawing of the system can be seen in Fig. 7. Simulated efficiency across the tracking range is shown in Fig. 8(a), and is overlaid with a yearly irradiation distribution in Fig. 8(b).

A ray-traced 3D model of the two selected designs is shown in Fig. 9. Zemax OpticStudio models are available as we show in Code 1 (Ref. [41]), and a comparison between the Zemax OpticStudio models and the internal ray-tracer models are included in Appendix C.

4.2. Influence of position and slope errors

To investigate the influence of position and slope errors on the optimization results, the ◄►↓◄► design was optimized for a set of error distributions with magnitudes different from the ones described in Table 3. The Pareto fronts for the different error distributions is shown in Fig. 10(a), while a tolerance analysis of selected designs is shown in Fig. 10(b). In addition, all configurations were also optimized for nominal performance assuming no errors, and the resulting Pareto fronts are included in Fig. 12 in Appendix B.

Optics EXPRESS

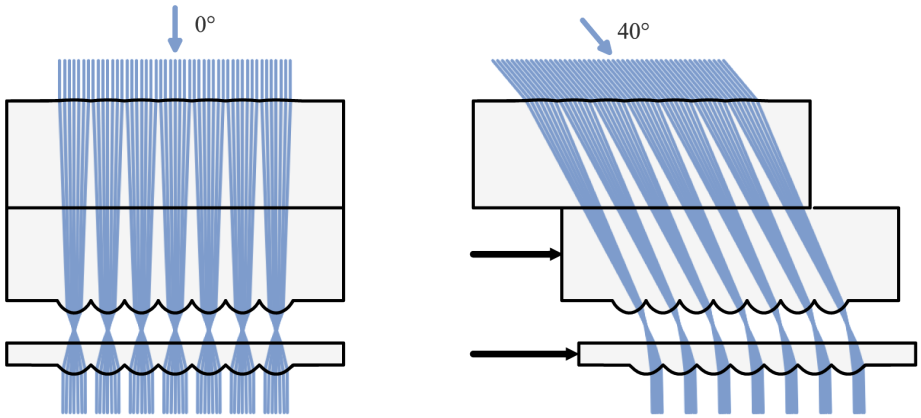

Fig. 7. Simplified beam-steering lens array with ◀▶↓▶ configuration optimized for 3.5° divergence half-angle (● in Fig. 5), drawn at 0° and 40° angles of incidence respectively. The black arrows indicate tracking motion. The drawing shows a 2-dimensional slice of the optimized system, which consists of hexagonally packed three-dimensional lens arrays.

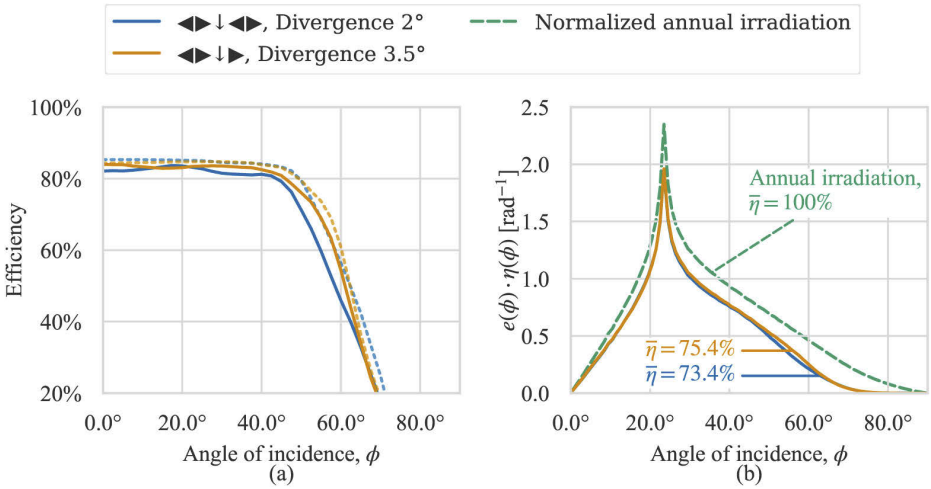

Fig. 8. (a) The two selected beam-steering lens arrays have >80% efficiency for ±40°angle of incidence, and a gradual drop-off in efficiency at larger angles of incidence. The dashed curves show nominal performance, while the continuous curves show expected performance with the chosen set of error distributions. (b) When the systems are placed in a fixed orientation as described in Section 3.2, this efficiency distribution corresponds to average yearly efficiency of 73.5% for the high concentration design and 75.6% for the simplified design, respectively.

Optics EXPRESS

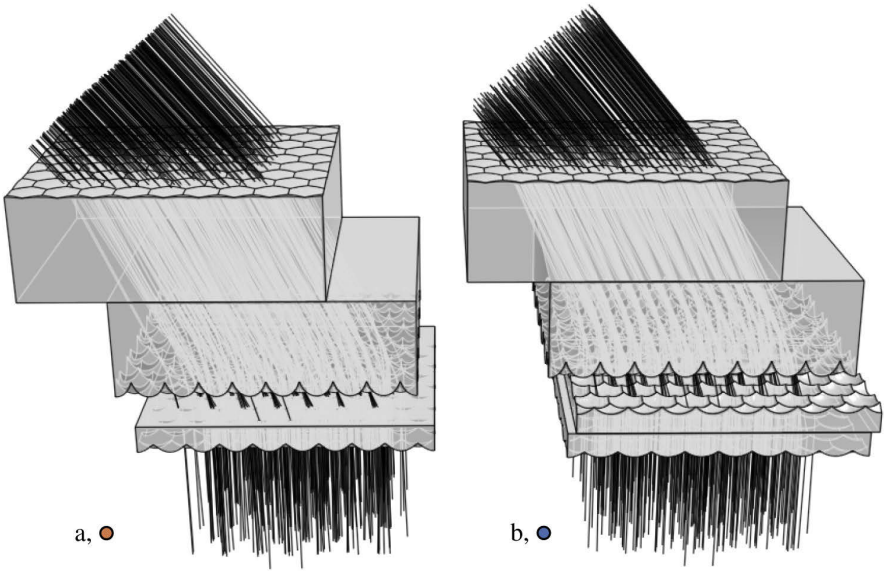

Fig. 9. Ray-traced 3D-model of the two selected beam-steering lens arrays, both shown at a 40° angle of incidence. (a) ◄►↓► configuration optimized for a permitted divergence of 3.5°, (b) ◄►↓◄► configuration optimized for a permitted divergence of 2.0°.

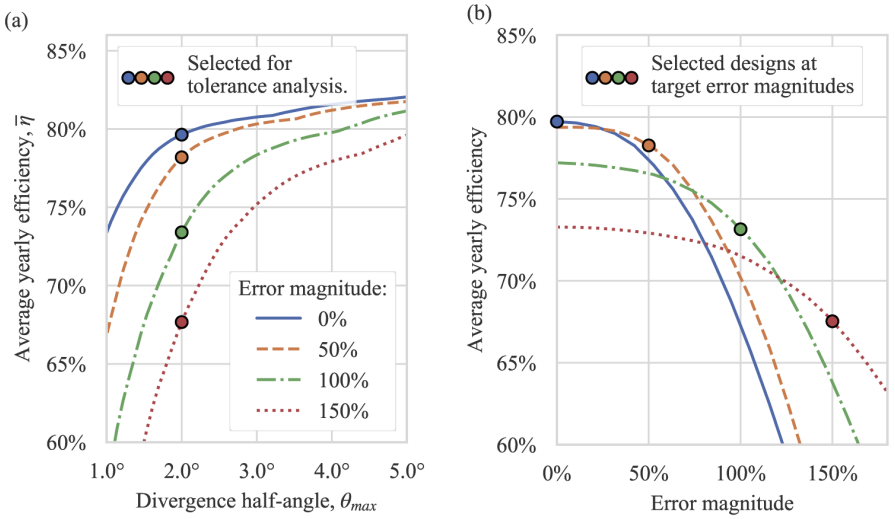

Fig. 10. (a) Optimized Pareto fronts for the ◄►↓◄► configuration, assuming different scaled versions of the error distributions in Table 3. 100% corresponds to the values reported in the table. The achievable performance is strongly influenced by the scale of manufacturing errors, as can be seen by the large changes to the Pareto fronts. (b) The selected designs from *a* are simulated at different error distributions to see how sensitive they are to errors. The system optimized for nominal performance has the highest performance at zero manufacturing errors, but is also the most sensitive to such errors.

Optics EXPRESS

5. Discussion

Stationary solar tracking requires beam-steering lens arrays with a wide dual-axis tracking range, making it difficult to rely on paraxial models and experience from conventional optical design to choose the ideal configuration. The use of numerical multi-objective optimization has enabled screening of many different configurations, to identify designs that are promising for future implementations of this concept.

The optimization results show that fairly complex optical systems are required to achieve high efficiency and low divergence for stationary solar tracking. The complex ◀▶⤸◀▶ and ◀▶↓◀▶ configurations outperform all the other configurations in Fig. 5 across the entire Pareto front.

At higher permitted divergence half-angles, some additional systems achieve relatively high efficiency, more specifically the class of systems starting with a ◀▶-pair of single-sided lens arrays.

Simpler configurations with only 1 moving surface, such as ◆⤸◆ or ◀▶ do not have the required degrees of freedom to enable high-efficiency stationary solar tracking. As seen in Fig. 5, the ◆⤸◆ configuration only achieves 67% average yearly efficiency when divergence half-angle is permitted to be as high as ±5.00°.

The selected results presented in Section 4.1 represent two different prioritizations of the different objectives, and they represent designs that we believe might be of interest for solar energy applications. The high-complexity ◀▶↓◀▶ design in Fig. 6 redirects sunlight into a narrow cone of ±2° divergence. It may therefore be relevant for high concentration applications, such as concentrator photovoltaics (CPV) or high-temperature concentrated solar power (CSP) applications. Figure 5 shows how even higher performance can be achieved with a ◀▶⤸◀▶ configuration, but the additional complexity in implementing a curved tracking trajectory might not be worth the relatively minor improvements to performance.

The selected ◀▶↓▶ design offers a simpler mechanical implementation with 3 lens arrays instead of 4. This reduced complexity comes at the cost of increased permitted divergence half-angle. The permitted divergence angle of ±3.5° represents a geometric concentration limit of 268x according to Eq. (3), which is still 26% higher than the $\frac{1}{sin(0.27°)} \approx 212$ concentration limit of conventional linear trough concentrators with single-axis tracking [2]. We therefore believe that this design might be of interest for low- to medium temperature CSP applications.

The beam-steering lens arrays demonstrated here emit collimated and redirected sunlight. To be used in CSP or CPV applications, these devices must be combined with a solar concentrator, for instance in the configuration illustrated in Fig. 1(a). An investigation into the best way to add such a concentrator, as well as a comparison of the resulting performance compared to other tracking-integrated solar concentrators, will be of interest for future development of this concept.

5.1. Optimizing for as-built performance

As described in Section 3.5, the systems were optimized for as-built performance by estimating the expected efficiency under the influence of manufacturing errors. Optimizing the systems for as-built performance is important because a system optimized for nominal performance can be very sensitive to manufacturing errors, while a system with slightly lower nominal performance may exhibit significantly lower sensitivity to surface errors [42]. We consider optimization for as-built performance to be especially important in the type of screening performed in this work, in order to not unrealistically favor highly complex configurations that may turn out to require very strict manufacturing tolerances. This effect is demonstrated in the tolerance analysis in Fig. 10(b): The system optimized for nominal performance is more sensitive to errors than systems optimized for as-built performance.

The optimization results are strongly affected by the chosen error distributions, as seen in Fig. 10(a), where the same configuration has been optimized for different error distributions. The distributions in this work were chosen as an example to demonstrate how the systems can

be optimized while taking manufacturing errors into account, and as a common ground for comparing the different beam-steering lens array configurations. When planning a real-world implementation of a beam-steering lens array, these error distributions should be updated to more accurately match selected manufacturing tolerances of the chosen lens molding process and system assembly.

Due to the strong influence of the error distributions, it can be difficult to compare the results in Fig. 5 with other related work optimized for different tolerances, or for nominal performance. For this reason, we have also included Pareto fronts optimized for nominal performance, available in Fig. 12 in Appendix B. The nominal results in Fig. 12 can be useful for comparing the beam-steering lens array configurations in this work against other alternatives optimized for nominal performance. However, we expect the nominal designs to be too sensitive to manufacturing errors to be used as a basis a physical beam-steering lens array, and therefore keep them outside the main body of the paper.

5.2. Implementation

There is no universally accepted way to optimize an optical system for reduced sensitivity to manufacturing errors, and different optical design software packages have implemented different heuristics to try to achieve this goal [42]. The task is especially challenging in conventional optical design, where the design of each individual system is of interest. In these designs, tolerance analysis is typically performed by sampling each surface error from the manufacturing tolerances, before applying an error compensation such as a refocus and simulating the resulting performance of the whole system. In the case of a beam-steering lens array, on the other hand, the object of interest is the combined average performance of the full set of lenses in the lens arrays, each subject to their own set of errors. We have therefore chosen to directly integrate the error distributions into the objective function by including them in the quasi-Monte Carlo integration of Eq. (7). In this way, each ray traced through the system is subject to a unique set of manufacturing errors sampled from the error distribution. This approach enables fast calculation of the average performance of a system subject to the selected error distributions, allowing the estimate to be directly used during optimization.

Unlike conventional tolerance analysis, our approach does not enable the use of compensators. The estimate might, therefore, be too pessimistic when estimating the influence of lateral positioning errors, which can likely be partially compensated for by the closed-loop tracking system in a physical realization of a beam-steering lens array. When planning a real-world implementation of a beam-steering lens array, the resulting design should therefore also be subjected to conventional tolerance analysis to more accurately validate the predicted as-built performance.

5.3. Multi-objective optimization

The use of a multi-objective optimization algorithm has enabled a comprehensive screening a large number of configurations of beam-steering lens arrays for stationary solar tracking, without having to make an upfront decision for the trade-off between permitted divergence angle and efficiency.

The permitted divergence angle is related to the achievable concentration ratio through Eq. (3). The trade-off curves in Fig. 5 are therefore a representation of the efficiency-versus-concentration curves known from Nonimaging Optics [2], and the objective function in Eq. (4) can be considered a special case of the overall problem in Nonimaging Optics of simultaneously optimizing both efficiency and concentration. The use of multi-objective optimization algorithms may, therefore, be of general interest to several problems in the field of Nonimaging Optics, and may constitute a topic of further future investigation beyond the topic of beam-steering lens array design.

Optics EXPRESS

6. Conclusions

We have performed a thorough screening of beam-steering lens array configurations in order to identify the most promising configurations for stationary solar tracking applications. This was enabled by using a set of symbols to specify and generate each configuration, and optimizing each configuration using multi-objective numerical optimization. The multi-objective optimization approach has enabled the optimization of beam-steering lens arrays without having to make an up-front decision for the trade-off between efficiency and divergence. The approach also enables the handling of manufacturing constraints and expected manufacturing errors, and may be of interest for other design problems in the field of nonimaging optics.

From this screening, we have identified beam-steering lens array designs capable of high efficiency full-day stationary solar tracking, and we specifically picked out two designs that might be candidates for solar energy applications. The first design has relatively high mechanical complexity with 4 optical surfaces, and can be suitable for high-concentration applications, achieving 73.4% average yearly efficiency in redirecting sunlight into a $<2^\circ$ divergence half-angle. The second system has lower complexity, with 3 optical surfaces, and may be suitable for low-concentration applications. It achieves 75.4% average yearly efficiency in redirecting sunlight into a $<3.5^\circ$ divergence half-angle. These reported configurations may contribute to the development of low-cost tracking-integrated solar energy, and further the development of tracking-integrated solar concentrators.

Optics EXPRESS

Appendix A Full optimization results

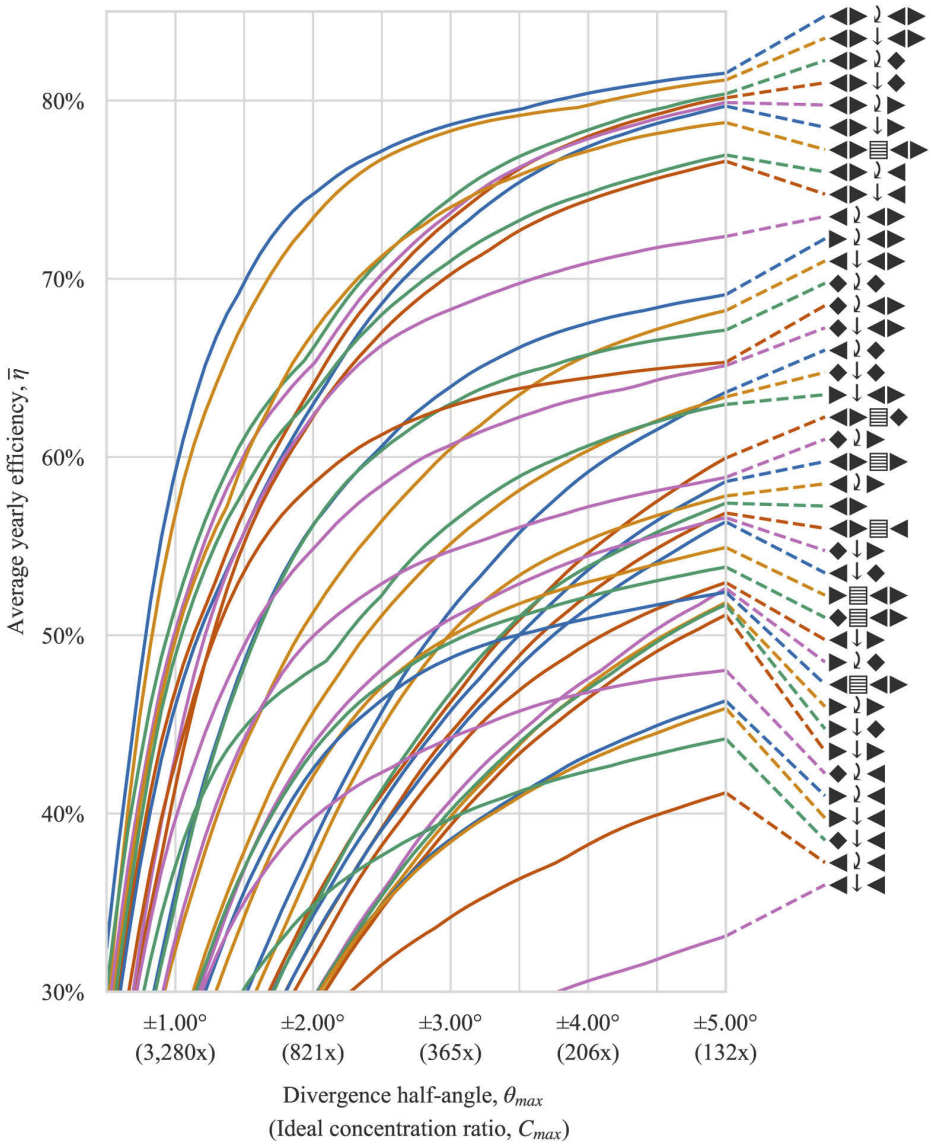

Fig. 11. Full set of trade-off curves for different configurations of beam-steering lens arrays optimized as described in Section 3.5.

Optics EXPRESS

Appendix B Full optimization results optimized for nominal performance

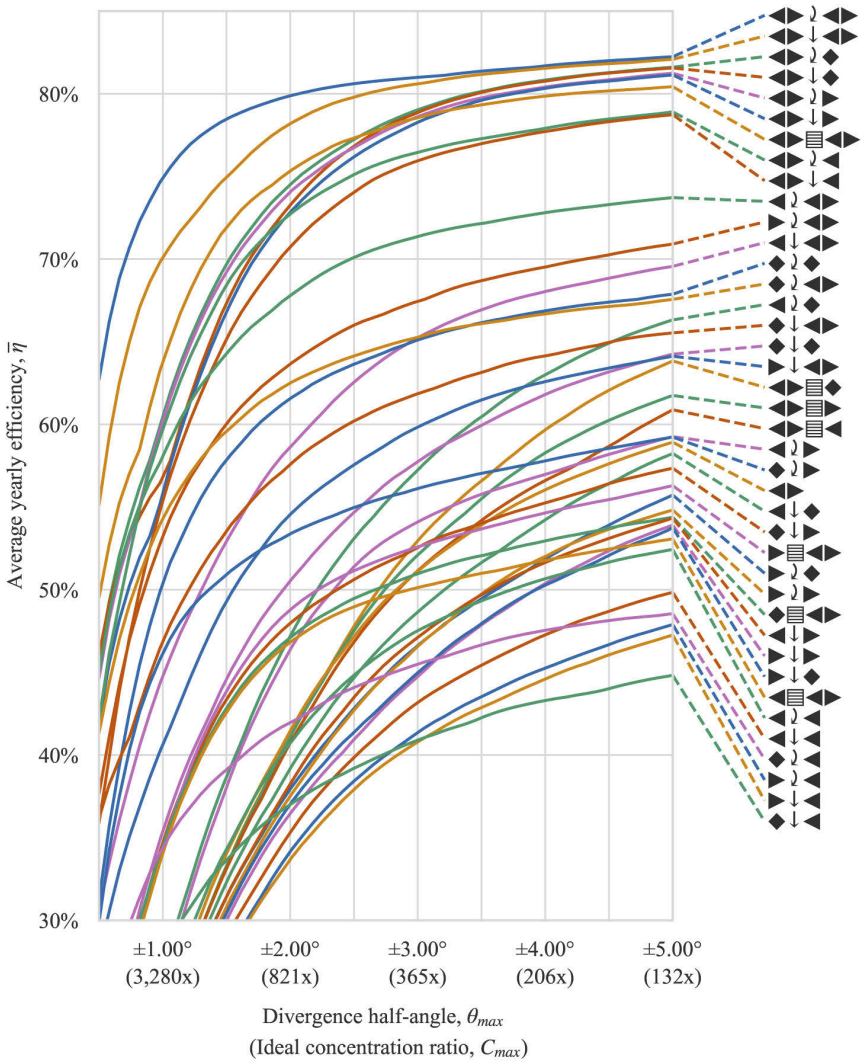

Fig. 12. Full set of trade-off curves for different configurations of beam-steering lens arrays optimized as described in Section 3.5, but assuming nominal performance instead of as-built performance.

Appendix C Details on Zemax OpticStudio model

Zemax OpticStudio models of the two selected beam-steering lens array designs is available in the supplementary materials Code 1 (Ref. [41]). These models are used to document and verify the designs, and also used to create the 3D models in Fig. 9. However, due to limitations in Zemax OpticStudio, the models do not capture the full complexity of the Python ray-tracer used during optimization.

Optics EXPRESS

The Zemax OpticStudio model includes a Merit Function used to evaluate optical efficiency at the discrete set of angle of incidence. This merit function is used to verify the performance of the beam-steering lens arrays, as shown in Fig. 13. However, the merit function does not implement the design method described in Section 3, and is not suitable for optimization using the built-in optimization algorithms in Zemax OpticStudio, which do not support multi-objective optimization.

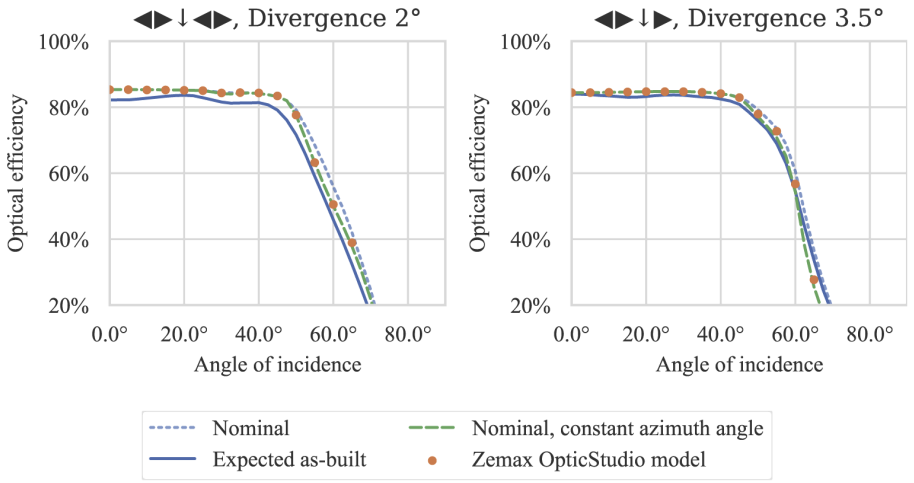

Fig. 13. Comparing internal Python model and Zemax OpticStdio model of the selected beam-steering lens array designs. The Zemax OpticStudio model assumes nominal performance and constant azimuth angle, and the simulated efficiencies agree well with the internal Python model when these assumptions are replicated.

The efficiency estimate from Zemax OpticStudio contains the following set of simplifications compared to the Python model:

- Tracking motion is represented at a set of discrete angles of incidence using the multi-configuration functionality in Zemax OpticStudio. During optimization, tracking motion is represented as a continuous function of angle of incidence.
- The builtin PMMA material model in Zemax OpticStudio is only defined between 365nm and 1060nm, and the AM1.5D solar spectrum is therefore clipped to this range. During optimization, the whole AM1.5D spectrum is used.
- For simplicity, the Zemax OpticStudio model only demonstrates solar tracking across 1 axis – in other words, with a constant azimuth angle. Since lenslets are packed hexagonally and thus not completely rotationally symmetric, tracking performance is not fully uniform across different azimuth angles. During optimization, the azimuth angle is included as an integration dimension in the multi-dimensional quasi-Monte Carlo integration of Eq. (7).
- The Zemax OpticStudio model estimates nominal system performance, not as-built performance, as discussed in Section 5.1.
- During optimization, the lenslet surfaces are represented using 8th order Forbes' Q^{con} surfaces [40]. When creating the Zemax OpticStudio models, this representation is converted to an even polynomial representation, in order to be represented as Zemax OpticStudio's "Hexagonal Lenslet Array" object type.

Optics EXPRESS

- The Zemax OpticStudio system is modeled as a lens array with 9 by 9 lenslets, and the source is modeled as a rectangular source aimed towards this array. There might therefore be small edge-effects, where some of the lenslets are only partially illuminated. During optimization, an infinite array of lenslets is assumed.

Acknowledgments

Portions of this work were presented at the *SPIE Optical Engineering + Applications* conference in 2019, paper number 111200B [15], and at the *SPIE Optical Engineering + Applications* conference in 2018, paper number 1075805 [14].

Disclosures

The authors declare no conflicts of interest.

References

1. W. T. Xie, Y. J. Dai, R. Z. Wang, and K. Sumathy, "Concentrated solar energy applications using Fresnel lenses: A review," Renewable Sustainable Energy Rev. **15**(6), 2588–2606 (2011).
2. R. Winston, J. C. Minano, P. G. Benitez, W. N. Shatz John, C. Bortz, and J. C. Bortz, *Nonimaging Optics* (Elsevier Science, 2005).
3. H. Apostoleris, M. Stefancich, and M. Chiesa, "Tracking-integrated systems for concentrating photovoltaics," Nat. Energy **1**(4), 16018 (2016).
4. F. Duerr, Y. Meuret, and H. Thienpont, "Tracking integration in concentrating photovoltaics using laterally moving optics," Opt. Express **19**(S3), A207–A218 (2011).
5. F. Duerr, Y. Meuret, and H. Thienpont, "Tailored free-form optics with movement to integrate tracking in concentrating photovoltaics," Opt. Express **21**(S3), A401–A411 (2013).
6. A. J. Grede, J. S. Price, and N. C. Giebink, "Fundamental and practical limits of planar tracking solar concentrators," Opt. Express **24**(26), A1635–A1646 (2016).
7. P. Kotsidas, V. Modi, and J. M. Gordon, "Nominally stationary high-concentration solar optics by gradient-index lenses," Opt. Express **19**(3), 2325–2334 (2011).
8. V. Narasimhan, D. Jiang, and S.-Y. Park, "Design and optical analyses of an arrayed microfluidic tunable prism panel for enhancing solar energy collection," Appl. Energy **162**, 450–459 (2016).
9. L. D. DiDomenico, "Towards doubling solar harvests using wide-angle, broad-band microfluidic beam steering arrays," Opt. Express **23**(24), A1398–A1417 (2015).
10. N. León, C. Ramírez, and H. García, "Rotating Prism Array for Solar Tracking," Energy Procedia **57**, 265–274 (2014).
11. S. Valyukh, I. Valyukh, and V. Chigrinov, "Liquid-Crystal Based Light Steering Optical Elements," Photonics Lett. Pol. **3**(2), 88–90 (2011).
12. R. Campbell and M. Machado, "LOW cost CPV = Embedded CPV with internal tracker," in *2010 35th IEEE Photovoltaic Specialists Conference*, (IEEE, 2010), pp. 003003–003007.
13. W. Lin, P. Benitez, and J. C. Miñano, "Beam-steering array optics designs with the SMS method," Proc. SPIE **8485**, 848505 (2012).
14. H. J. D. Johnsen, J. Torgersen, and A. Aksnes, "Solar tracking using beam-steering lens arrays," Proc. SPIE **10758**, 4 (2018).
15. H. J. D. Johnsen, A. Aksnes, and J. Torgersen, "Pushing the limits of beam-steering lens arrays," Proc. SPIE **11120**, 10 (2019).
16. K. M. Flood, B. Cassarly, C. Sigg, and J. Finlan, "Continuous wide angle beam steering using translation of binary microlens arrays and a liquid crystal phased array," Proc. SPIE **1211**, 296–304 (1990).
17. E. A. Watson, "Analysis of beam steering with decentered microlens arrays," Proc. SPIE **32**(11), 2665–2670 (1993).
18. A. Akatay, C. Ataman, and H. Urey, "High-resolution beam steering using microlens arrays," Opt. Lett. **31**(19), 2861–2863 (2006).
19. S. A. Kalogirou, *Solar Energy Engineering: Processes and Systems* (Academic, 2013).
20. J. Bourderionnet, M. Rungenhagen, D. Dolfi, and H. D. Tholl, "Continuous laser beam steering with micro-optical arrays: Experimental results," Proc. SPIE **7113**, 71130Z (2008).
21. J. Xiang, N. Wu, J. Zhang, and L. Wu, "Design of driving and control system based on Voice Coil Actuation for linear motion of micro-lens array," Proc. SPIE **7133**, 713330 (2009).
22. I. Ono, S. Kobayashi, and K. Yoshida, "Global and multi-objective optimization for lens design by real-coded genetic algorithms," Proc. SPIE **3482**, 110–121 (1998).
23. Bráulio Fonseca Carneiro de Albuquerque, F. L. de Sousa and A. S. Montes, "Fonseca Carneiro de Albuquerque Multi-objective approach for the automatic design of optical systems," Opt. Express **24**(6), 6619–6643 (2016).

Optics EXPRESS

24. C. C. Olson, "Automated design of optical architectures using novel encoding methods and a multi-objective optimization framework," Proc. SPIE **11105**, 11 (2019).
25. P. M. Pardalos, A. Žilinskas, and J. Žilinskas, *Non-Convex Multi-Objective Optimization, Springer Optimization and Its Applications* (Springer International Publishing, 2017).
26. A. Ito, D. Sato, and N. Yamada, "Optical design and demonstration of microtracking CPV module with bi-convex aspheric lens array," Opt. Express **26**(18), A879–A891 (2018).
27. C. S. Schuster, "The quest for the optimum angular-tilt of terrestrial solar panels or their angle-resolved annual insolation," Renewable Energy **152**, 1186–1191 (2020).
28. A. B. Meinel and M. P. Meinel, *Applied Solar Energy: An Introduction* (Addison-Wesley, 1976).
29. J. S. Price, X. Sheng, B. M. Meulblok, J. A. Rogers, and N. C. Giebink, "Wide-angle planar microtracking for quasi-static microcell concentrating photovoltaics," Nat. Commun. **6**(1), 6223 (2015).
30. E. Watson, D. Miller, and K. Barnard, "Analysis of fill factor improvement using microlens arrays," Proc. SPIE **3276**, 123–134 (1998).
31. J. Duparré, D. Radtke, and P. Dannberg, "Implementation of field lens arrays in beam-deflecting microlens array telescopes," Appl. Opt. **43**(25), 4854–4861 (2004).
32. Unicode Consortium, The Unicode Standard, Version 12.0 (2019).
33. H. Li and Q. Zhang, "Multiobjective Optimization Problems With Complicated Pareto Sets, MOEA/D and NSGA-II," IEEE Trans. Evol. Computat. **13**(2), 284–302 (2009).
34. J. Blank and K. Deb, "Pymoo: Multi-Objective Optimization in Python," IEEE Access **8**, 89497–89509 (2020).
35. P. Virtanen, R. Gommers, T. E. Oliphant, M. Haberland, T. Reddy, D. Cournapeau, E. Burovski, P. Peterson, W. Weckesser, J. Bright, S. J. van der Walt, M. Brett, J. Wilson, K. J. Millman, N. Mayorov, A. R. J. Nelson, E. Jones, R. Kern, E. Larson, C. J. Carey, İ. Polat, Y. Feng, E. W. Moore, J. VanderPlas, D. Laxalde, J. Perktold, R. Cimrman, I. Henriksen, E. A. Quintero, C. R. Harris, A. M. Archibald, A. H. Ribeiro, F. Pedregosa, P. van Mulbregt, and S. . Contributors, "SciPy 1.0: Fundamental algorithms for scientific computing in Python," Nat. Methods **17**(3), 261–272 (2020).
36. D. Kraft, "A software package for sequential quadratic programming," Tech. Rep. DFVLR-FB 88-28, DLR German Aerospace Center – Institute for Flight Mechanics (Koln Germany, 1988).
37. J. Köster and S. Rahmann, "Snakemake—a scalable bioinformatics workflow engine," Bioinformatics **28**(19), 2520–2522 (2012).
38. Renewable Resource Data Center, Solar Spectral Irradiance: Air Mass 1.5, https://rredc.nrel.gov/solar/spectra/am1.5/.
39. D. Buie, A. G. Monger, and C. J. Dey, "Sunshape distributions for terrestrial solar simulations," Sol. Energy **74**(2), 113–122 (2003).
40. G. W. Forbes, "Shape specification for axially symmetric optical surfaces," Opt. Express **15**(8), 5218–5226 (2007).
41. H. J. D. Johnsen, A. Aksnes, and J. Torgersen, "Zemax OpticStudio Models of Beam-Steering Lens Arrays, figshare," (2020). https://doi.org/10.6084/m9.figshare.12505784
42. K. E. Moore, "Optimization for as-built performance," Proc. SPIE **10925**, 1 (2019).

Paper 5: Beyond the 2D limit: Étendue-squeezing line-focus solar concentrators

Beyond the 2D limit: Étendue-squeezing line-focus solar concentrators

HÅKON J. D. JOHNSEN[1,*], ASTRID AKSNES[2], AND JAN TORGERSEN[1]

[1] Norwegian University of Science and Technology, Department of Mechanical and Industrial Engineering, Richard Birkelands Vei 2b, Trondheim, Norway
[2] Norwegian University of Science and Technology, Department of Electronic Systems, O.S. Bragstads plass 2b, Trondheim, Norway
[*] Corresponding author: hakon.j.d.johnsen@ntnu.no

Compiled November 15, 2020

Line-focus solar concentrators are commonly designed by extruding a two-dimensional concentrator in the third dimension. For concentration in air, these concentrators are, by the nature of their design, limited by the two-dimensional solar concentration limit of 212x. This limit is orders of magnitude lower than the 45 000x concentration limit for three-dimensional solar concentrators. Through the use of étendue-squeezing, we conceptually show that it is possible to design line-focus solar concentrators beyond this 2D limit. This allows a concentrator to benefit from a line-focus suitable for heat-extraction through a tubular receiver, while reaching concentration ratios and acceptance angles previously unseen for line-focus concentrators. We show two design examples, achieving a simulated 75x concentration and 218x concentration ratio respectively, with a $\pm 1^\circ$ acceptance angle. For comparison, the 2D concentration limit is 57x at this acceptance angle. Étendue-squeezing line-focus solar concentrators, combined with recent developments in tracking-integration, may enable the development of a new class concentrated solar power (CSP) system.

http://dx.doi.org/10.1364/ao.XX.XXXXXX

Solar concentrators are essential for efficient utilization of solar thermal energy, and have a fundamental concentration limit in air of

$$C_{max} = \frac{1}{(\sin \theta_{max})^2} \tag{1}$$

where θ_{max} is the acceptance angle of the concentrator, which must at least be wide enough for the $\theta \approx 0.27^\circ$ divergence half-angle of sunlight. This leads to a solar concentration limit in air of approximately 45 000x[1]. To approach the limit, the concentrator must concentrate sunlight in three dimensions, which traditionally means concentrating to a point-like focus. The high fundamental concentration limit enables point-focus solar concentrators to be designed with large acceptance angles and non-ideal optics, and still achieve sufficient concentration for many applications. In the remainder of this paper we will be considering the condition $\theta_{max} = 1^\circ$, where the increased acceptance angle represents an increased tolerance to tracking- and surface errors. At this increased acceptance angle, the two-dimensional concentration limit is $3\,283x$.

Solar concentrators can also be built to concentrate sunlight to a line-focus. Such a line-focus is suitable for heat extraction through tubular receivers, and can also be designed to benefit from a simplified one-axis tracking motion. Line-focus concentrators are commonly designed by extruding two-dimensional concentrator geometries, which limits the concentration in air to the 2D concentration limit[1]:

$$C_{max,2D} = \frac{1}{\sin \theta_{max}}. \tag{2}$$

For a solar divergence half-angle of $\theta = 0.27^\circ$, the limit is approximately 212x, and with the 1° acceptance angle considered in this paper it is reduced to $57x$. The 2D and 3D limits in Eqs. 1-2 are plotted against acceptance angle in Figure 1.

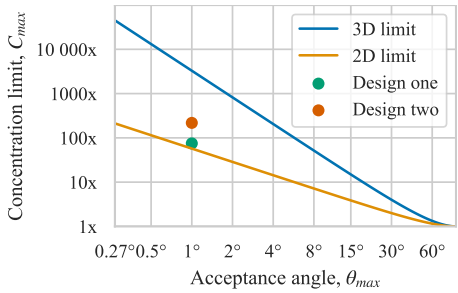

Fig. 1. Concentration limits versus acceptance angle, as given by Eqs. 1-2, shown on a log-log scale. The line-focus concentrators demonstrated in this work, represented by the symbols ● and ●, have concentration ratios beyond the 2D concentration limit.

It has previously been shown that the concentration ratio of linear primary concentrators can be boosted beyond the 2D concentration limit by introducing secondary concentrators close to the line-focus, reaching concentration ratios of 300x with one-axis polar tracking[2], or >1000x with two-axis tracking[3, 4].

However, these secondary concentrators achieve their increased concentration ratio by breaking the line-focus into a set of small point- or line-foci, missing the benefit of a true line-focus for tubular receivers (as further illustrated in Fig. S3 of the Supplemental Document). It has also been shown that the 2D limit can be surpassed using nominally linear concentrators where the translational symmetry is broken by ridges in the concentrator, but these have focused on relatively large acceptance angles suitable for stationary solar concentration[5–7].

We show that the common approach of extruding a two-dimensional concentrator is not the only way to design a line-focus concentrator, and demonstrate a method to directly construct a 3D concentrator that concentrates to a line-focus. Thus, it is possible to benefit from the high concentration of 3D concentrators while maintaining the practical benefits for heat-extraction through tubular receivers placed along a line-focus. The use of such a high-concentration line-focus concentrator would require two-axis tracking, but this does not necessarily mean that it needs to be mounted on a two-axis external solar tracker. Instead, tracking across the secondary axis may be implemented without physical rotation of the concentrator, similar to what has previously been demonstrated with tracking-integrated solar concentrators for concentrator photovoltaics (CPV) applications[8].

An afocal pair of lens surfaces can be used to compress an optical beam in one axis, while expanding it in the other axis, as illustrated in Figure 2a. If the ratio of compression and expansion is 1:N where N is an integer, the lens pairs can be tessellated in such a way that they fill the front and back surfaces of a lens array, as shown in Figure 2b [9]. This is known as an étendue-squeezing lens array, as introduced in José Blen's 2007 thesis[10], and is an example of the more general concept of étendue-squeezing[11]. The étendue-squeezing lens array trades angular extent along one axis against angular extent along the other axis by a factor N[9]. It has been demonstrated for applications such as changing the aspect ratio of the collimated beam from an LED source[9].

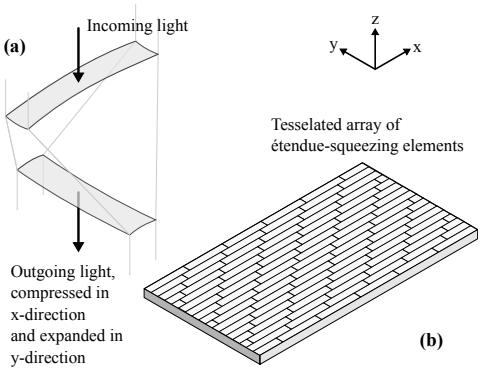

Fig. 2. (a) Principle of étendue-squeezing using an afocal lens pair. (b) The lens-pairs can be tessellated into a complete étendue-squeezing lens array.

By adjusting the lens geometry, the étendue-squeezing lens array can be used to create a solar concentrator with a line-focus: Instead of emitting the collimated beam, as shown in Fig. 2, each lens-pair can be optimized to redirect the sunlight towards a shared focal line. The principle, as well as a complete such solar concentrator, are shown in Figure 3. Such a concentrator thus becomes a combination of a linear Fresnel lens — redirecting the sunlight towards a shared focal line, and an étendue-squeezing lens array — reducing angular extent in the y-direction to permit higher concentration ratios. As shown in the design examples below, this principle enables the concentrator to utilize two-axis tracking and bypass the 2D concentration limit.

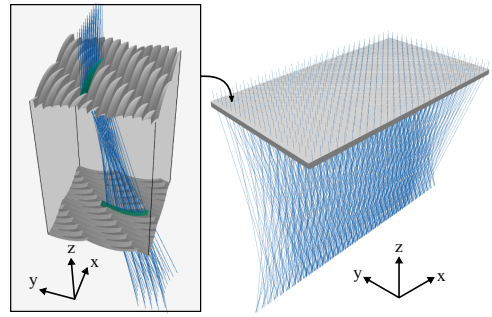

Fig. 3. A solar concentrator utilizing étendue-squeezing, consisting of an array of tessellated étendue-squeezing lens pairs. Each lens-pair squeezes the beam in the x-direction and expands it in the y-direction, while redirecting the sunlight towards the common focal line. The cutout shows one such lens-pair highlighted in green, and demonstrates how the lens-pairs are tessellated into a complete double-sided lens array.

To demonstrate the principle, we used numerical optimization to create two line-focus solar concentrators: One concentrator consists of only a double-sided lens array, and one concentrator uses an additional secondary reflector. Both designs were constructed with an étendue squeezing factor of $N = 7$ (the ratio of the short to the long side of the individual rectangular facets is 1:7). The factor 7 was chosen as an example, with the aim of being high enough to allow for significant concentration boost, while low enough to allow for practical implementation. Each individual lens-pair was numerically optimized according to its position in the concentrator, using a custom Python ray-tracer. Optimization was performed using a memetic optimization algorithm combining the SLSQP and Differential Evolution algorithms from the Scipy library[12]. The optimization was performed in two stages: In the first stage, a small subset of the lens pairs were optimized to identify a realistic geometric concentration ratio where efficiency on the order of 80% could be expected. In the second stage, all lens pairs were independently optimized for maximum efficiency at the geometric concentration ratio chosen from the first stage. The freeform front- and back- surfaces were represented as 6th order Legendre polynomials, chosen for being orthogonal in sag on the rectangular lens aperture[13]. Due to the problem's symmetry, only Legendre terms symmetric in the x-direction were allowed to be non-zero during optimization. After optimization, the lens pairs were tessellated and combined into a Zemax OpticStudio model to verify and evaluate the complete system. These Zemax OpticStudio models are available in the supplementary material as we show in Code 1 (Ref. [14]). The lens arrays are assumed to be made from PMMA, and illuminated using the AM1.5D spectrum and a top-hat $\pm 1^\circ$ angular distribution. This angular distribution was

chosen as an example, to demonstrate the possibility of designing for high tolerance to tracking errors. Reflection losses and chromatic aberration are taken into account. For simplicity, volume absorption and surface scattering losses were not included in the simulation of these design examples. For simplicity, the absorbing surface is assumed to be planar. The optimization of concentrator performance with tubular receivers is left for future work, and may involve the adaptation of techniques previously developed for high-concentration 2D concentrators for tubular receivers[15].

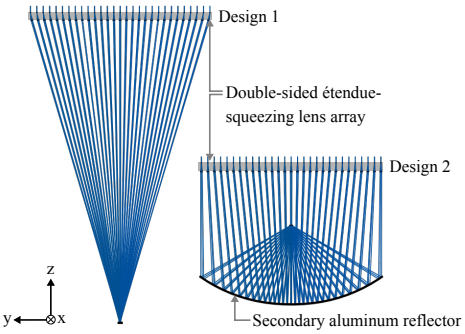

Fig. 4. Ray-traced drawing of the two design examples. Only a subset of the lens-pairs are drawn and traced, to reduce clutter in the drawing. In reality, the lens-pairs are tessellated to fill the entire front and back surfaces of the lens array, as shown in Fig. 3.

The first design example is a double-sided lens array, for operation similar to a linear Fresnel lens. A ray-traced 3D model of the optimized concentrator is shown in Fig. 3, and a 2D drawing is shown in Fig. 4. The concentrator is optimized for a 95x geometric concentration ratio under $\pm 1^\circ$ illumination, and achieves 79.1% efficiency at these conditions. This leads to an effective optical concentration of $C_{eff} = 0.791 \cdot 95 \approx 75.1$. The resulting concentrator has an optimized numerical aperture of $NA = 0.32$ ($f/1.47$). The intensity across the focal line of the of the concentrator is shown in Fig. 5, and the angular acceptance is shown in Fig. 6. Further details about the compression of angular extent performed by this concentrator is shown in Fig. S1 of the Supplemental Document. This concentrator demonstrates that it is possible to surpass the 2D concentration limit, but the concentration ratio of this example design is still only about 31% higher than the 2D limit. The low numerical aperture of the resulting concentrator indicates that the concentration can be increased by a high numerical aperture secondary concentrator, leading us to the next design example.

The second design example combines the étendue-squeezing lens array with a reflective secondary concentrator assumed to be made from aluminum. The geometry of this reflective secondary is designed so that the resulting concentrator is approximately aplanatic, a condition that has previously been shown to generate concentrators with performance very close to the fundamental concentration limit[16, 17]. The numerical aperture of the resulting concentrator was $NA = 0.89$, chosen to be relatively close to 1 for high concentration, while having a more practical geometry than a concentrator fully reaching $NA = 1$. Optimized

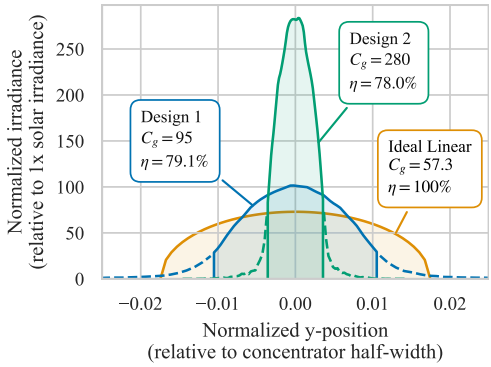

Fig. 5. Intensity profile across the focal line for the two concentrators, under 1 sun AM1.5D illumination with a $\pm 1^\circ$ top-hat angular distribution. The solid lines represent the intensity within the selected geometric concentration ratios. The non-uniform intensity profile of the ideal linear concentrator is caused by the circular $\pm 1^\circ$ angular distribution of the illumination, as further discussed in the Supplemental Document.

for a geometric concentration ratio of 280x, this concentrator achieves 78.0% efficiency under $\pm 1^\circ$illumination. This leads to an effective optical concentration of $C_{eff} = 0.780 \cdot 280 \approx 218$. The intensity across the focal line of the concentrator shown in Fig. 5 and the angular acceptance of the concentrator is shown in Fig. 6.

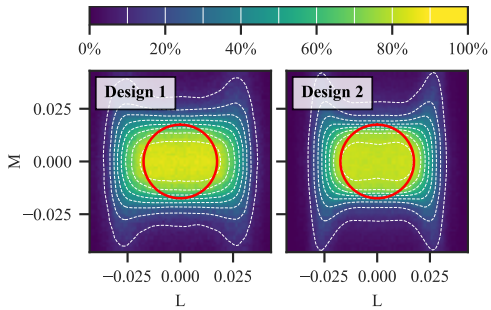

Fig. 6. Optical efficiency of the concentrators as a function of incidence angle, shown as contour plots in direction cosine space. L and M are direction cosines along the x- and y-axis, respectively. The concentrators are optimized for maximum efficiency under a $\pm 1^\circ$ top-hat angular distribution, which is illustrated by the red circles.

The presented design examples have modeled efficiencies of 79.1% and 78.0%, respectively. The losses arise from reflection losses in the lens array, geometric losses from shading of neighboring elements in the lens array, absorption losses in the reflector, and finally, a non-unity intercept factor. Volume absorption losses, surface scattering losses, and losses due to manufacturing tolerances were not included in these simulations. The relative magnitude of each loss was measured by selectively disabling loss mechanisms while simulating the system, and are summarized in Table 1.

Table 1. Relative magnitude of different losses in the designs

	Design 1	Design 2
Lens array reflection loss	7.8%	7.6%
Lens array geometric loss	3.2%	2.6%
Reflector absorption loss	-	5.4%
Intercept loss	11.4%	8.3%
Complete efficiency	79.1%	78.0%

A consequence of the decreased angular extent along the y-axis in these concentrators is an increased angular extent along the x-axis. This angular extent leads to a gradual reduction in intensity at the ends of the line-focus, as illustrated in Fig. 7. The effect can be eliminated by using edge reflectors, or the concentrator modules can be placed in long enough solar collector assemblies that such edge effects become negligible — similar to how conventional parabolic trough solar concentrators are organized in long solar collector assemblies.

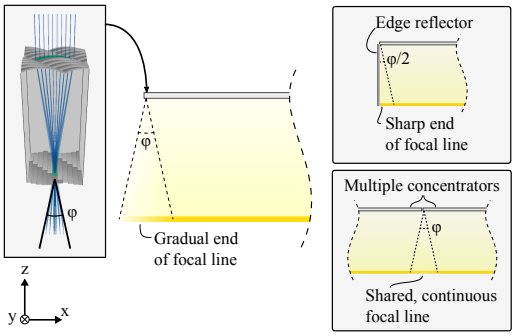

Fig. 7. The étendue-squeezing lens pairs increase the angular extent of the light along the x-direction, which introduces a softening at the ends of the focal line. This effect can be circumvented by creating a long assembly of concentrators sharing the same focal line, or by using an edge reflector.

Both of the presented design examples demonstrate the possibility of utilizing étendue-squeezing to go beyond the 2D concentration limit, as plotted in Fig. 1. This may represent a new class of solar concentrator, achieving the high concentration and high acceptance angle of three-dimensional concentrators, while maintaining the linear and modular geometry of line-focus solar concentrators. The combination of such concentrators with tracking-integration to achieve the required two-axis solar tracking without needing to rotate the concentrator across two axes will be of interest for future research. One potential approach for such tracking integration is beam-steering lens arrays[18], which can perform one (or two) axis tracking using millimeter-scale lateral translation and emit collimated sunlight for concentration by an étendue-squeezing concentrator. The presented design examples are chosen to demonstrate the concentration abilities of étendue-squeezing solar concentrators. Still, they are not necessarily the most economical and practical way to implement an étendue-squeezing concentrator. Further research is needed to identify designs that show a good trade-off between efficiency, concentration and manufacturability.

In summary, we have shown through two design examples how étendue-squeezing can be used to design line-focus concentrators not limited by the 2D concentration limit. To the best of our knowledge, this type of concentrator has not previously been reported in the literature, and the possibility of such concentrators has not previously been appreciated. We have further proposed how developments in tracking-integration can be used to circumvent the need for two-axis tracking of these concentrators. If a manufacturable and practical étendue-squeezing solar concentrator can be combined with tracking integration, this may constitute a promising path towards a new class of concentrated solar power, combining the high concentration of heliostats with the modular nature of parabolic trough concentrators.

ACKNOWLEDGMENTS

Portions of this work were presented at the *SPIE Optical Engineering + Applications* conference in 2020, paper number 1149509[19].

DISCLOSURES

The authors declare no conflicts of interest.

See Supplement 1 for supporting content.

REFERENCES

1. R. Winston, J. C. Minano, P. G. Benitez, W. contributions by Narkis Shatz and John C. Bortz, and J. C. Bortz, *Nonimaging Optics* (Elsevier Science, 2005).
2. M. Brunotte, A. Goetzberger, and U. Blieske, Sol. Energy **56**, 285 (1996).
3. T. Cooper, G. Ambrosetti, A. Pedretti, and A. Steinfeld, Appl. Opt. **52**, 8586 (2013).
4. B. Wheelwright, R. Angel, and B. Coughenour, "Freeform lens design to achieve 1000X solar concentration with a parabolic trough reflector," in *Classical Optics 2014*, (Optical Society of America, 2014), p. ITh1A.2.
5. M. Rönnelid and B. Karlsson, Appl. Opt. **37**, 5222 (1998).
6. J. C. Bortz, N. E. Shatz, and R. Winston, Proc. SPIE **4446**, 201 (2001).
7. J. Nilsson, R. Leutz, and B. Karlsson, Sol. Energy Mater. Sol. Cells **91**, 525 (2007).
8. H. Apostoleris, M. Stefancich, and M. Chiesa, Nat. Energy **1**, 16018 (2016).
9. P. Benítez, J. C. Miñano, and J. Blen, "Squeezing the Étendue," in *Illumination Engineering*, (John Wiley & Sons, Ltd, 2013), pp. 71–99.
10. J. Blen, "Design of multiple free-form optical surfaces in three dimensions," Ph.D. thesis, Universidad Politécnica de Madrid (2007).
11. P. Benítez, J. Miñano *et al.*, "étendue squeezing optics: Beating the angle-space compromise of symmetrical systems," in *International Nonimaging Optics Workshop*, (2005).
12. E. Jones, T. Oliphant, P. Peterson *et al.*, "SciPy: Open source scientific tools for Python," http://www.scipy.org/ (2001).
13. M. I. Nikolic, P. Benítez, B. A. Narasimhan, D. Grabovickic, J. Liu, and J. C. Miñano, Opt. Eng. **55**, 071204 (2016).
14. H. J. D. Johnsen, A. Aksnes, and J. Torgersen, "Zemax OpticStudio Models of Étendue-Squeezing Solar Concentrators," figshare (2020).
15. P. Benítez, R. García, and J. C. Miñano, Appl. Opt. **36**, 7119 (1997).
16. J. M. Gordon, Opt. Express **18**, A41 (2010).
17. E. T. A. Gomes, N. Fraidenraich, O. C. Vilela, C. A. A. Oliveira, and J. M. Gordon, Sol. Energy **191**, 697 (2019).
18. H. J. D. Johnsen, A. Aksnes, and J. Torgersen, Opt. Express (2020).
19. H. J. D. Johnsen, A. Aksnes, and J. Torgersen, Proc. SPIE **11495**, 1149509 (2020).

Beyond the 2D limit: Étendue-squeezing line-focus solar concentrators: supplemental document

1. TRANSFORMATION OF ANGULAR EXTENT

The presented étendue-squeezing concentrators compress the angular extent of the light along the y-axis, while also shifting it so that the light is redirected towards the common focal line. To show this transformation, we plot how radiance in direction cosine space is modified by the concentrator, as shown in Fig. S1. The transformation in angular extent from position a to position a′ shows how the angular extent is reduced along the y-axis (M-component in the figure), while the angular extent along the x-axis is increased (L-component in the figure). The angular extent along the x-axis was not penalized in the optimization, and the optimization algorithm has therefore selected a design where this angular extent is magnified by a large factor. This leads to the observed reduction in radiance.

At point b-b′ in the concentrator, we observe how the concentrator performs the combined action of compressing the angular extent along the y-axis while also shifting it in the y-direction, so that the light is redirected to the common focal line.

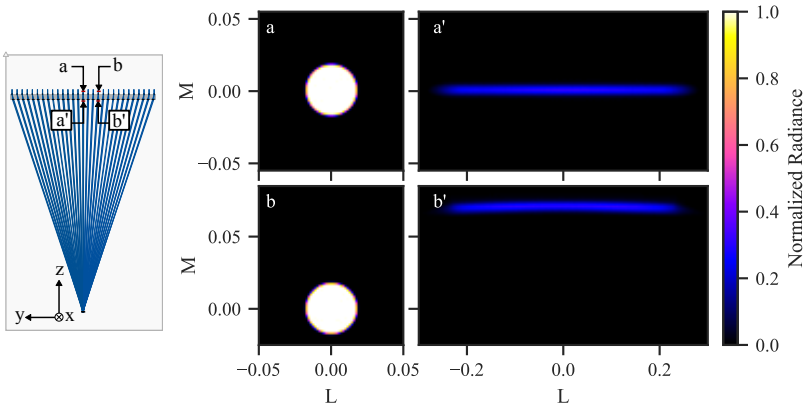

Fig. S1. Transformation of angular extent as light passes through the étendue-squeezing concentrator, shown as radiance in direction cosine space. Note that scale of the y-axis has been compressed in the a′ and b′ plots to prevent the figure from becoming too wide.

2. INTENSITY DISTRIBUTION OF THE IDEAL 2D CONCENTRATOR

Fig. 5 of the main paper shows the intensity distribution across the focal line for the two étendue-squeezing concentrators compared to an ideal linear concentrator. While this ideal linear concentrator may be expected to have a uniform intensity distribution exactly at the 2D concentration limit, this is not the case when it is evaluated under the same conditions as the étendue-squeezing concentrators. Therefore, the real intensity distribution of an ideal imaging linear concentrator under these same conditions is used to provide a fair comparison. A brief

explanation of the non-uniformity of this concentrator is included here, while a more thorough discussion is left for other work.

If an ideal concentrator is illuminated with uniform radiance over its full acceptance angle and full aperture, it achieves a uniform intensity distribution exactly reaching the thermodynamic concentration limit[1]. However, if the radiance is not uniform, the concentrated intensity profile may also be non-uniform.

An ideal reflective linear concentrator designed for an acceptance angle of θ_{max} accepts all rays where the projected angle θ_p in the 2D plane of the concentrator (the y-z plane in the coordinate system in Fig. S2a) is less than θ_{max}[1, 2]. This angular acceptance region takes the shape of an ellipse in direction cosine space, with a major radius of 1 and a minor radius of θ_{max}[1, 2], as illustrated in Fig. S2b. When evaluating the concentrators in this paper, we use a rotationally symmetric angular distribution with a radius θ_{max}, which represents subjecting the concentrator to two-axis solar tracking. This angular distribution does not fill the full angular acceptance of the ideal linear concentrator, despite using the same value of θ_{max}, as illustrated in Fig. S2, and the intensity profile is therefore no longer necessarily uniform. The amount of non-uniformity depends on the type of ideal concentrator. For simplicity we have used the extreme case of an ideal imaging concentrator where the y-position of each ray on the focal line only depends on the ray's projected angle of incidence in the y-z plane, θ_p.

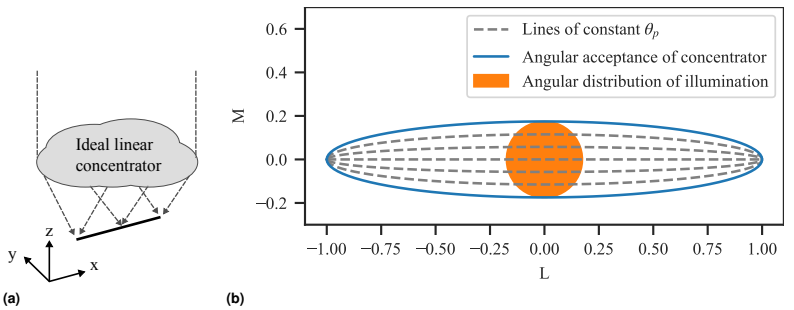

Fig. S2. (a) Coordinate system assumed for the ideal linear concentrator. (b) Illustration of geometry mismatch between angular acceptance of an ideal linear concentrator, compared to the circular angular distribution used to generate Fig. 5 of the main paper. L is direction cosine along the length of the linear concentrator and M is direction cosine across its width. This plot shows the case when $\theta_{max} = 10^\circ$ in order to make the region large enough to be clearly visible, but the same geometry applies when $\theta_{max} = 1^\circ$ as in the main paper. The lines of constant projected angle θ_p shows how different projected angles receive illumination with different angular extent allong the x-axis, leading to the nonuniform intensity profile for an ideal imaging concentrator.

3. MOTIVATION FOR A FULL LINE-FOCUS IN CONCENTRATED SOLAR POWER APPLICATIONS

This paper reports on a way to design a three-dimensional concentrator that concentrates sunlight to a continuous line-focus while going beyond the 2D concentration limit commonly associated with such concentrators. Fig. S3 conceptually shows how this continuous line-focus compares to the previously explored approach of going beyond the 2D limit by using secondary concentrators to break the line-focus from a parabolic trough into several smaller point-foci[3–5]. For concentrated solar power (CSP) applications, where the thermal energy may be extracted through tubular recievers, the continuous line-focus permits the use of a narrower tubular receiver, leading to lower heat losses. Alternatively, it may permit the use of larger acceptance angles while concentrated towards the same receiver size.

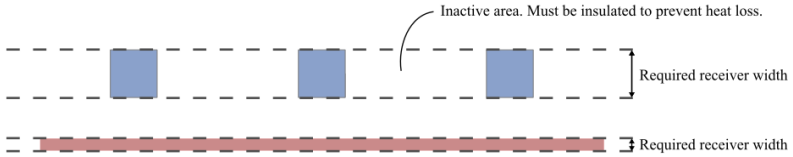

Fig. S3. Conceptual comparison between several point foci and one line-focus. The combined area of the blue point-foci is identical to that of the red line-focus, but the red line-focus is better for extracting heat through a tubular receiver.

REFERENCES

1. R. Winston, J. C. Minano, P. G. Benitez, W. contributions by Narkis Shatz and John C. Bortz, and J. C. Bortz, *Nonimaging Optics* (Elsevier Science, 2005).
2. R. Winston and W. Zhang, "Pushing concentration of stationary solar concentrators to the limit," Opt. Express **18**, A64–A72 (2010).
3. M. Brunotte, A. Goetzberger, and U. Blieske, "Two-stage concentrator permitting concentration factors up to 300x with one-axis tracking," Sol. Energy **56**, 285–300 (1996).
4. T. Cooper, G. Ambrosetti, A. Pedretti, and A. Steinfeld, "Theory and design of line-to-point focus solar concentrators with tracking secondary optics," Appl. Opt. **52**, 8586–8616 (2013).
5. B. Wheelwright, R. Angel, and B. Coughenour, "Freeform lens design to achieve 1000X solar concentration with a parabolic trough reflector," in *Classical Optics 2014*, (Optical Society of America, 2014), p. ITh1A.2.

ISBN 978-82-471-9743-1 (printed ver.)
ISBN 978-82-471-9791-2 (electronic ver.)
ISSN 1503-8181 (printed ver.)
ISSN 2703-8084 (online ver.)

NTNU
Norwegian University of
Science and Technology